FINAL REPORT

Targeted Improvements in the Fire INventory from NCAR (FINN) Model for Texas Air Quality Planning

AQRP Project 14-011

Prepared for:

David Sullivan
Texas Air Quality Research Program
The University of Texas at Austin

and

Jim MacKay
Texas Commission on Environmental Quality

Prepared by:

Elena McDonald-Buller (Principal Investigator), Yosuke Kimura
Center for Energy and Environmental Resources
The University of Texas at Austin

Christine Wiedinmyer (Co-Principal Investigator)
National Center for Atmospheric Research

and

Chris Emery (Co-Principal Investigator), Zhen Liu, Greg Yarwood
Ramboll Environ

QA Requirements: Audits of Data Quality: 10% Required

December 2015

ACKNOWLEDGMENTS

The authors thank Kevin Sampson from the National Center for Atmospheric Research for his assistance with the development of the FINN burned area algorithm and ArcGIS processor.

The preparation of this report is based on work supported by the State of Texas through the Air Quality Research Program administered by The University of Texas at Austin by means of a Grant from the Texas Commission on Environmental Quality.

Executive Summary

The Fire INventory from NCAR (FINN) is a global fire emissions model that estimates daily emissions of trace gases and particles from open biomass burning. It is widely used in global and regional modeling studies. The overall objective of this project was to conduct targeted improvements to the FINN model that would benefit the global and regional air quality management and research communities, with a special focus on needs for Texas. The project produced FINN emissions estimates for fire events in 2012 (Figure ES1) to support air quality modeling efforts of the Texas Commission on Environmental Quality (TCEQ).

Figure ES1. Annual total MODIS Active Fire detection counts in 2012 (detection confidence estimate $\geq$ 20%).

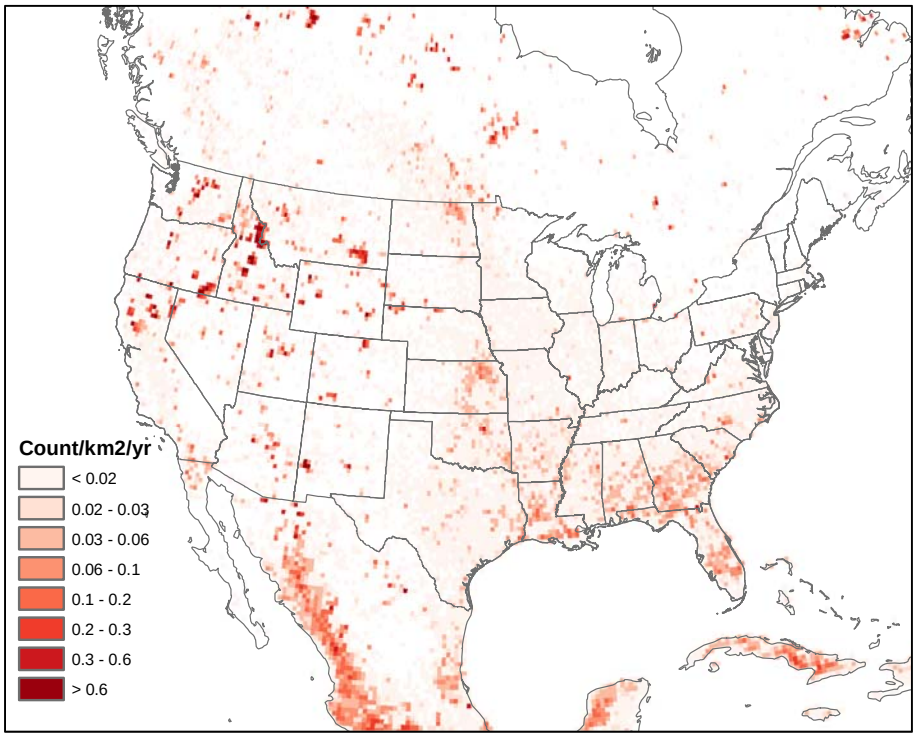

A new algorithm for estimating area burned from satellite-derived fire detections was developed and incorporated into FINN to address a known under prediction bias for area burned. Improvements in the area burned estimation were accompanied by better spatial resolution in the characterization of land cover, new fuel loading data with greater spatial resolution for the United States, and incorporation of the new Vegetation Continuous Fields (VCF) Collection 5 product from the Moderate Resolution Imaging Spectroradiometer (MODIS) for estimating bare and vegetative cover. Crop-specific emission factors and fuel loadings developed by McCarty (2011) have been added to FINN as an option for users that have a land cover data resource that distinguishes major crop types typically found in the United States. Collectively, these modifications increased carbon monoxide (CO) emissions in TCEQ's photochemical modeling domain by 42% relative to the earlier version of FINN, primarily due to

increases in the area burned estimates. These modifications form the basis of the next generation of the FINN model, FINN v.2.

In the FINN emissions model, land cover and land use are used to assign emission factors and fuel loadings and, consequently, these input data are critical for the estimation of fire emissions. The MODIS Land Cover Type product has been used as the default resource for land cover characterization in FINN, but new global, U.S. national, and Texas regional products are now available alternatives. Annual FINN emissions estimates during 2012 were generated for seven land cover data products alone or in combination:

- Three simulations were conducted with global databases including the MODIS Land Cover Type (LCT), United Nations Global Land Cover (GLC-SHARE), and European Space Agency (ESA) Climate Change Initiative.
- Two simulations utilized a combination of U.S. national databases, including the U.S. Forest Service Fuel Characteristic Classification System (FCCS) with and without the U.S. Department of Agriculture National Agricultural Statistical Service Cropland Data Layer (CDL), and the MODIS LCT product outside of the U.S.
- Two simulations were conducted using a Texas (TCEQ) regional land cover product (Popescu et al., 2011) with and without the CDL, the FCCS in the remainder of the continental U.S., and MODIS LCT elsewhere.

Annual emissions estimates for CO, nitrogen oxides (NO_x), and fine particulate matter ($PM_{2.5}$) were compared between the simulations for six geographic regions: Texas, the Lower Mississippi Valley, Southeastern U.S., Great Plains, Western U.S. and Mexico (Figure ES2). Differences between simulations highlighted the complex sensitivity of emissions estimates from the FINN model to various land cover inputs and associated fuel loadings and emission factors. Within Texas, the global-scale ESA and GLC-SHARE products produced higher emissions estimates than the MODIS LCT product during 2012; the Texas regional product (with or without the CDL) produced emission estimates were 10% to 19% greater than the MODIS LCT product. Characterization of croplands had minimal effects on annual emissions estimates in Texas.

The Emission Processing System (EPS) underwent extensive updates to produce a new version (EPS v3.22) for the TCEQ as well as to accommodate use of the new area burned algorithm in FINN. CAMx simulations for a June 2012 episode obtained from the TCEP were performed with three different FINN outputs driven by different land cover products: the MODIS LCT, ESA, and Texas regional product with the Cropland Data Layer. In addition, a CAMx simulation for which all fire emissions were removed ("No Fire" case) was also conducted for comparison purposes.

In early June of 2012, northwestern Mexico (Sierra Madre Occidental) exhibited high fire activity, which affected simulated ozone levels in the region as well as within downwind areas of the U.S. Fire activity in the Rocky Mountains of the western U.S. was pronounced later in the month. Regardless of the land cover product used for the fire emissions estimates, the median contribution of fire events to MDA8 ozone concentrations in Texas throughout the month of June was approximately 2 ppb (Figure ES3, which shows the contribution of all fires to the selected regions of interest). This contribution was likely associated with fires in northwestern Mexico that occurred every day for the initial two-thirds of the month. The maximum contribution of fires on predicted MDA8 ozone concentrations in Texas exceeded 40 ppb during the episode period. Differences in predicted MDA8 ozone concentrations in Texas ranged from -10 ppb to +21 ppb between the simulations that used FINN emissions estimates derived with

the ESA or MODIS LCT products and from -18 ppb to +33 ppb between the simulations using the FINN emissions derived from the TCEQ_CDL or MODIS_LCT products.

Figure ES2. Annual FINN emissions estimates for (a) CO, (b) NO_x, (c) $PM_{2.5}$ by geographic region (Texas, the Lower Mississippi Valley, Southeastern U.S., Great Plains, Western U.S. and Mexico). FINN estimates are shown using different land cover inputs: MODIS LCT, GLC-SHARE, ESA, and TCEQ and TCEQ_CDL (Texas and Lower Mississippi Valley) or FCCS and FCCS_CDL data products (Southeastern U.S. and Western U.S.). Note difference in scale for the Western U.S and Mexico.

(a)

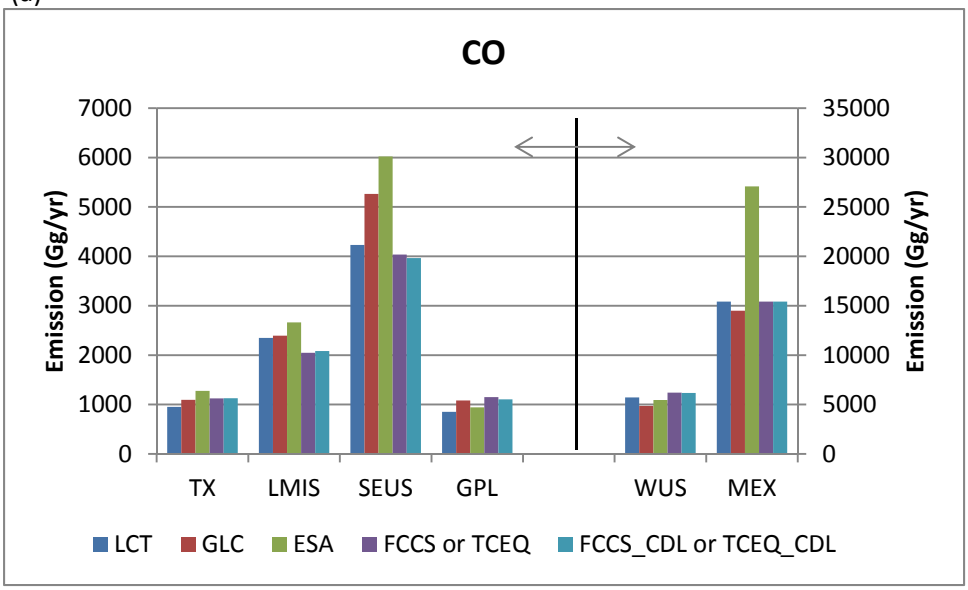

(b)

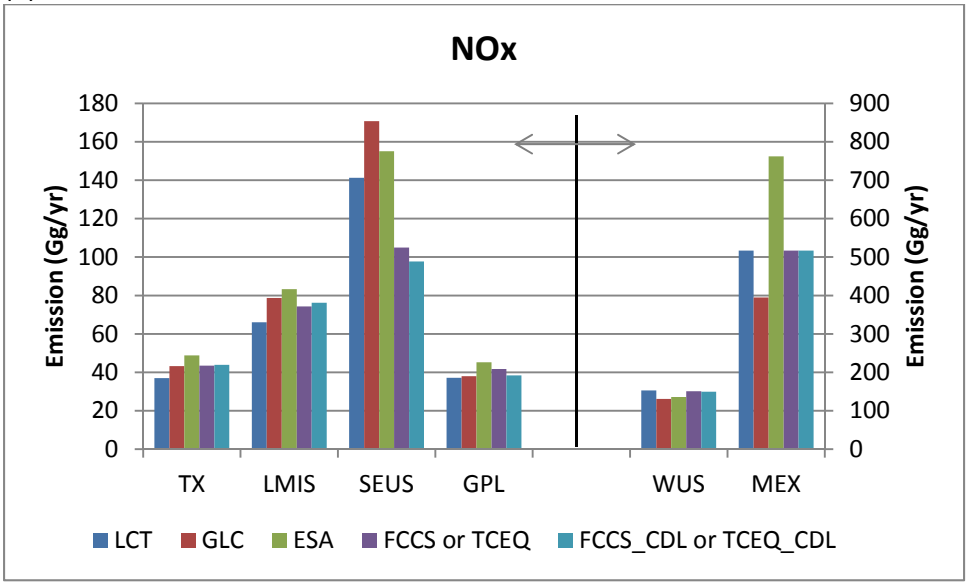

(c)

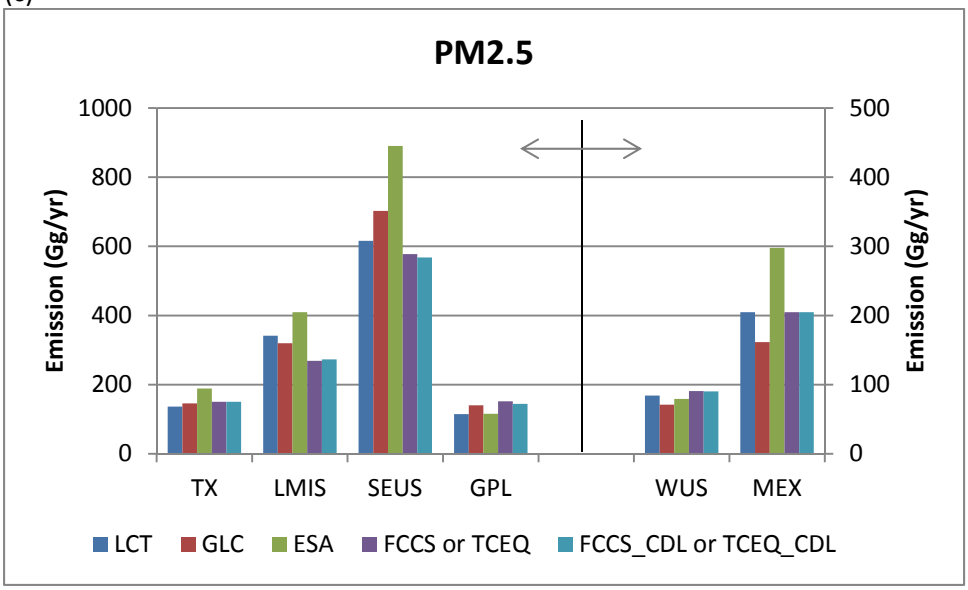

The project activities also resulted in the development and implementation of an approach for partitioning FINN NO_x emissions estimates into aged NO_z forms (i.e., nitrogen dioxide [NO_2], nitric acid [HNO_3], peroxyacetyl nitrate [PAN], C3 and higher peroxyacyl nitrates, and organic nitrates) to account for rapid NO_x oxidation in fire plumes. A CAMx simulation was conducted based on FINN emissions estimates driven by the TCEQ_CDL land cover scenario with NO_x partitioning implemented during EPS processing. Results from this simulation were compared to a similar CAMx simulation (TCEQ_CDL) without NO_x partitioning. Median differences in predicted MDA8 ozone concentrations between the simulations were within -0.5ppb for the six geographic regions, including Texas.

At this time, we recommend use of the following combination of land cover products in FINN to support Texas air quality modeling activities: the Texas regional land cover product with the Cropland Data Layer (TCEQ_CDL), the U.S. Forest Service Fuel Characteristic Classification System (FCCS) in the remainder of the continental U.S., and MODIS Land Cover Type (MODIS_LCT) product elsewhere. This combination provides the greatest spatial resolution and specificity in land cover and fuel loadings for the Texas regional domain and continental U.S. However, we note the importance of understanding the range of FINN emissions estimates that can be obtained with different land cover products and the strong need for *in situ* evaluation of fuel loadings. Future work should focus on validation of land cover and, in particular, fuel loadings in the United States. The algorithm in EPS that partitions NO_x into aged NO_z forms should reflect the evolution of scientific understanding; our initial approach is implemented as an option in EPS v3.22. Reconciliation of fire detection between varying satellite and ground-based incident resources remains an on-going need; and evaluation of the Visible Infrared Imaging Radiometer Suite (VIIRS) products, the latest of the series of earth observing detectors, should be considered in the future.

Figure ES3. Contribution of all fire events to MDA8 ozone concentrations in each geographic region during June 2012. The box represents 25th to 75th percentiles with a vertical line showing the median. Whisker stretches to the minimum and maximum values. The concentration axis uses inverse hyperbolic sine transformation ($\sinh^{-1} x \equiv \ln(x + \sqrt{1 + x^2})$) to facilitate interpretation.

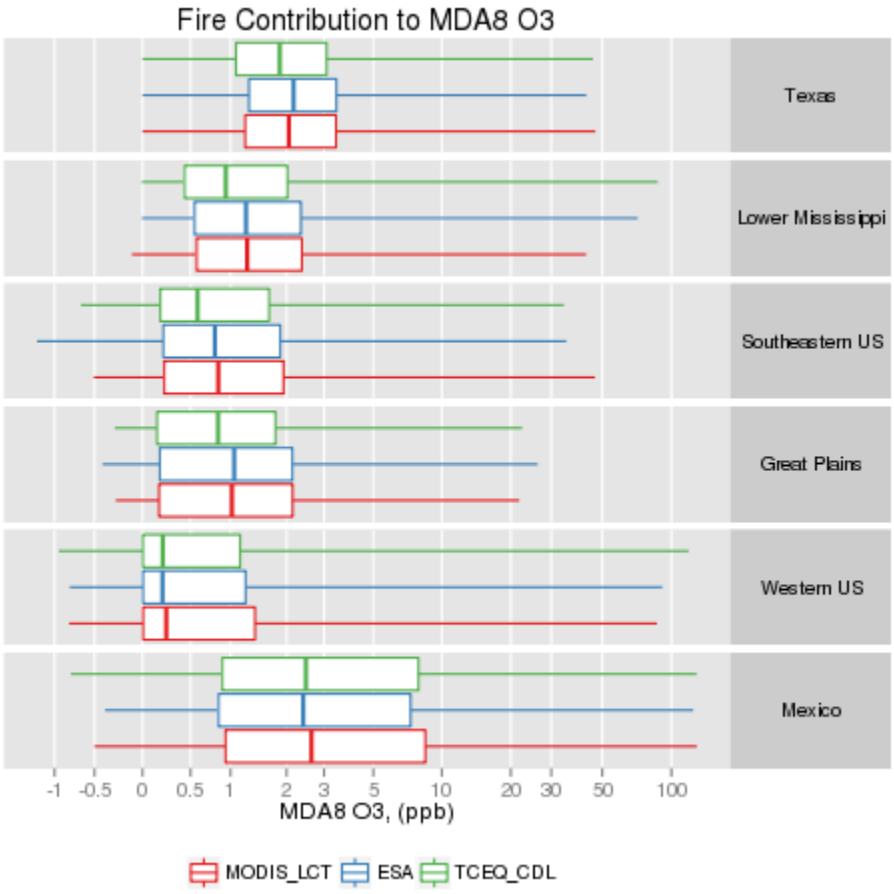

Table of Contents

Executive Summary 3
Table of Contents 8
List of Figures 10
List of Tables 13
List of Acronyms 15
1. Introduction 19
1.1 Technical Context and Motivation 19
1.2 Objectives 20
1.3 Fire Climatology and 2012 Activity 20
1.4 Report Overview 20
1.5 References 24
2. FINN Configuration and Default Data Resources 26
2.1 Fire Detection and Area Burned 26
2.2 Land Use/Land Cover Classification 27
2.3 Fuel Loadings 28
2.4 Fraction of Biomass Burned 28
2.5 Emission Factors 29
2.6 Chemical Speciation Profiles 29
2.7 References 30
3. Targeted Improvements in Burned Area Characterization and Emission Factors 32
3.1 Burned Area Characterization 32
3.1.1. Fire Identification 32
3.1.2 Estimation of Burned Area 34
3.1.3. Land Cover Analysis 35
3.2 Emission Factors 39
3.3 Implications for Emissions Estimates 40
3.4 References 41
4. Land Cover and Fuel Loading Data Resources: Emissions Estimates and Regional Air Quality 42
4.1 Global Land Use/Land Cover Data Resources 42
4.1.1 Global Land Cover-SHARE (GLC-SHARE) 42
4.1.2 ESA Climate Change Initiative (ESA-CCI) 42
4.2 U.S. National Products 45
4.2.1 U.S. Forest Service Fuel Characteristic Classification System (FCCS) 45
4.2.2 USDA National Agricultural Statistical Service Cropland Data Layer (CDL) 45

4.3 TCEQ Regional Land Cover Product 47
4.4 Intercomparison of Fuel Loading Estimates 49
4.4 References 49
5. Fire Emissions Estimates and Implications for Air Quality Predictions 51
5.1 Scenarios 51
5.2 Annual Emissions Estimates 51
5.3 CO Emissions by Land Cover Class 55
5.4 Contributions of Croplands to Monthly CO Emissions Estimates 61
5.5 Implications for Regional Air Quality 64
5.5.1 CAMx Configuration 64
5.5.2 Regional Air Quality Predictions 71
5.6 References 79
6. Partitioning of NO_x Emissions to NO_z in Fire Plumes 80
6.1 Predicted Effects on Air Quality 84
6.2 References 86
7. Data Quality Assurance 88
7.1 FINN Code 88
7.2 Land Cover Rasters and Fuel Loading 88
7.3 ArcGIS Preprocessor 88
7.4 FINN Output 89
7.5 EPS3 Processors 89
8. Conclusions and Recommendations 91
Appendix 93
A.1 MODIS LCT mapping and fuel loadings 93
A.2 GLC mapping and fuel loadings 94
A.3 ESA mapping and fuel loadings 95
A.4 FCCS mapping and fuel loadings 97
A.5 FCCS_CDL mappings and fuel loadings 110
A.6 TCEQ mapping and loadings 112
A.7 TCEQ_CDL mappings and fuel loadings 113

List of Figures

Figure 1. Geographic regions of focus for the study 21

Figure 2. Predicted 12-year monthly mean CO emissions (columns; error bars show maximum and minimum values) and 2012 estimates (black line) by region for (a) Texas, (b) the Lower Mississippi Valley, (c) Southeastern U.S., (d) Great Plains, (e) Western U.S. and (f) Mexico. 22

Figure 3. MODIS mean FRP (Megawatts) during 2000-2013. This product provides a measure of fire intensity. Source: http://svs.gsfc.nasa.gov/cgi-bin/details.cgi?aid=4093 27

Figure 4. Annual total MODIS Rapid Response fire detection counts in 2012 (detection confidence estimate > 20%)..... 34

Figure 5. Illustration of burned area estimation algorithm. (a) MODIS Active Fire detections on June 27, 2012 in southern Montana, (b) corresponding $1km^2$ "fire squares, (c) "detection rectangles" determined from the scan and track sizes of the pixel, (d) "fire polygon" used with the MODIS VCF product as the basis for the burned area estimate and (e) fire subdivisions for land cover analysis within the burned area..... 36

Figure 6. MODIS VCF version 051 percent cover for year 2012 (a) tree cover (b) non-tree vegetation, and (c) non-vegetated. 38

Figure 7. Effects of FINN modifications on CO emissions estimates for the national RPO modeling domain. 40

Figure 8. Land cover representations in the (a) MODIS LCT, (b) GLC-SHARE, and (c) ESA-CCI global products mapped to FINN categories. Note that these databases do not specify crop types. 44

Figure 9. Land cover representations in the (a) FCCS and (b) FCCS_CDL products mapped to FINN categories. 46

Figure 10. (a) The TCEQ dataset developed by Popescu et al. (2011) and (b) the TCEQ and (c) TCEQ_CDL data product mapped to FINN categories. 48

Figure 11. Fuel loadings for tree and herbaceous fuels by land cover product (MODIS LCT, ESA, TCEQ); values are averaged for 2012 fire events by FINN land cover class within six geographic regions shown in Figure 1. 50

Figure 12. Annual emissions estimates for (a) CO, (b) NOx, (c) $PM_{2.5}$ by region (see Figure 1). Estimates are shown for the MODIS LCT, GLC-SHARE, ESA, and TCEQ and TCEQ_CDL (Texas and Lower Mississippi Valley) or FCCS and FCCS_CDL data products (Southeastern U.S. and Western U.S.). Note difference in scale for the Western U.S and Mexico and that emissions for Mexico reflect those for the entire country, i.e., beyond the boundaries of the 12-km CAMx domain described below. 53

Figure 13. Annual CO emissions estimates by land cover class in each data product for (a) Texas, (b) the Lower Mississippi Valley, (c) Southeastern U.S., (d) Great Plains, (e) Western U.S, and (f) Mexico. Note difference in scale in each plot. 57

Figure 14. Monthly CO emissions estimates by land cover class for selected land cover scenarios: (a) TCEQ_CDL scenario for the Lower Mississippi Valley and (b) FCCS_CDL scenario for the Great Plains. The top plot in each shows all FINN land cover types whereas the bottom plot shows only crops. 62

Figure 15. CAMx 36km/12km/4km nested modeling grids. (Source: http://www.tceq.texas.gov/airquality/airmod/data). 65

Figure 16. Diurnal distribution of fire emissions applied in the EPS3/TMPRL module. ... 69

Figure 17. Diurnal profile of the vertical distribution of the fire plumes (red) and the fraction of hourly emissions allocated to CAMx vertical layer 1 (green) in each of the five fire classes defined by daily area burned within each fire complex. 70

Figure 18. Contribution of fire events to predicted MDA8 ozone concentration for selected days (a) June 4th, (b) June 28th. The contribution was determined as the difference in predicted MDA8 ozone concentrations between the MODIS LCT and "No Fire" scenarios by grid cell. 72

Figure 19. Contribution of fire events to MDA8 ozone concentrations in Texas by each geographic emission region during June 2012. The box represents 25th to 75th percentiles with a vertical line showing the median. Whisker stretches to the minimum and maximum values. Values represent predictions for 36-km resolution grid cells regardless of location. The concentration axis uses inverse hyperbolic sine transformation ($\sinh - 1\mathrm{x} \equiv \ln(\mathrm{x} + 1 + \mathrm{x}2)$ to facilitate interpretation. 73

Figure 20. Predicted difference in MDA8 ozone concentrations between the ESA and MODIS LCT products (left) and TCEQ_CDL and MODIS LCT products (right) on (a) June 4, 2012 and (b) June 28, 2012. 75

Figure 21. Differences in MDA8 ozone concentrations between the ESA or TCEQ_CDL scenarios and the MODIS LCT scenario. The box represents 25th to 75th percentiles with a vertical line showing the median. Whisker stretches to the minimum and maximum values. The concentration axis uses inverse hyperbolic sine transformation ($\sinh - 1\mathrm{x} \equiv \ln(\mathrm{x} + 1 + \mathrm{x}2)$ to facilitate interpretation. 76

Figure 22. NO_x emissions estimates for June 2012 within the CAMx modeling domain: (a) by region of interest and (b) domain-wide total. 77

Figure 23. Scatter plot of MDA8 O3 concentration between the (a) ESA versus MODIS LCT scenarios and (b) TCEQ_CDL versus MODIS LCT scenarios. Values represent predictions for 36-km resolution grid cells regardless of location. 78

Figure 24. Hourly temporal profiles used in the EPS3 TMPRL module to partition total daily NO_x from each fire into hourly NO_2, PAN, PANX, HNO_3 and NTR/NTR2 as a function

of four vegetation types: (a) tropical forest; (b) temperate forest; (c) savannah/grassland; (d) boreal forest. 83

Figure 25. Fire contribution to MDA8 ozone in Texas from TCEQ_CDL cases with and without NOx to NOz partitioning. The box represents 25th to 75th percentiles with a vertical line showing the median. Whisker stretches to the minimum and maximum values. The concentration axis uses inverse hyperbolic sine transformation ($\sinh -1\mathrm{x} \equiv \ln(\mathrm{x} + 1 + \mathrm{x}2)$ to facilitate interpretation. 85

Figure 26. Distributions of differences in MDA8 ozone concentrations in Texas between the TCEQ CDL simulations with and without NOx partitioning by geographic region during June 2012. The box represents 25th to 75th percentiles with a vertical line showing the median. Whisker stretches to the minimum and maximum values. The concentration axis uses inverse hyperbolic sine transformation ($\sinh -1\mathrm{x} \equiv \ln(\mathrm{x} + 1 + \mathrm{x}2)$ to facilitate interpretation. 86

List of Tables

Table 1. Fuel loadings (g/m^2) assigned in the FINN framework (Wiedinmyer et al., 2011). Values for North America are shown with gray background. 28

Table 2. FINN v.1.5 emission factors (g/m^2) by land cover type for carbon monoxide (CO), oxides of nitrogen (NO_x), non-methane organic compounds (NMOC), ammonia (NH_3), sulfur dioxide (SO_2), particulate matter ($PM_{2.5}$ and PM_{10}), organic carbon (OC), black carbon (BC). 29

Table 3. Chemical speciation factors for the conversion of NMOC emissions (kg/day) to MOZART-4 chemical species (moles/day) for generic land cover class in the default configuration of FINN (Source: Wiedinmyer et al, 2011). Reference Emmons et al. (2010) for description of lumped species. 30

Table 4. Summary of FINN v.2 emission factors (g/m^2) by land cover type. *Note that the Akagi et al reference refers to the emission factors reported by Akagi et al 2011 and all updates (from May 2014 and February 2015) posted at http://bai.acom.ucar.edu/Data/fire/. Note that a land cover code of "7" is not used in FINNv2.* 39

Table 5. Mapping between GLC-SHARE and FINN (ref. Table 4) for selected land cover categories. 42

Table 6. Mapping between ESA-CCI and FINN (ref. Table 4) for selected land cover categories. 43

Table 7. Contingency table of fire records between the MODIS LCT and ESA land cover products: (a) count of subdivided burned area polygons and (b) differences in CO emission estimated ($E_{ESA} – E_{MODIS}$) in Gg/yr. Land cover is identified according to FINN categories. 60

Table 8. Contingency table of fire records between the MODIS LCT and TCEQ land cover products: (a) count of subdivided burned area polygons and (b) differences in CO emission estimated ($E_{TCEQ} – E_{MODIS}$) in Gg/yr. Land cover is identified according to FINN categories. 61

Table 9. Model configuration and default input data developed by TCEQ for the 2012 CAMx modeling episode (Source: http://www.tceq.texas.gov/airquality/airmod/data/tx2012) 65

Table 10. Mapping between WRF and CAMx model vertical layer structures for the May-June 2012 modeling database. The WRF domain extends to ~20 km (50 hPa) with 43 layers. http://www.tceq.texas.gov/airquality/airmod/rider8/modeling/domain. 66

Table 11. Mapping of MOZART-4 species to CAMx CB6r2 species. Note that FPRM, PSO4, and PNO3 are allocated using default WRAP profiles for agricultural burning (applied to shrubs, grasslands, and agricultural burning) and for wildfires (applied to all forest fires). 67

Table 12. Noontime, nighttime and daily average partition of total NO_x into five NO_y compounds based on the Aerosol Simulation Program (ASP) modeling results of Lonsdale et al. (2014) for four vegetation types. Also shown is the mapping between ASP and CB6 species. 81

Table 13. Mapping of 4 ASP vegetation types of Lonsdale et al. (2014) to the 9 FINNv2 land cover types to support the speciation of daily NOx emissions in the FIRESPEC pre-processor..... 82

List of Acronyms

AQRP	Air Quality Research Program
ASP	Aerosol Simulation Program
AVHRR	Advanced Very High Resolution Radiometer
CAMx	Continuous Air Quality Model with Extension
CB	Carbon-Bond mechanism
CB05	Carbon-Bond mechanism Version 05
CB6	Carbon-Bond mechanism Version 6
CB6r2	Carbon-Bond mechanism Version 6 Revision 2
CDL	Cropland Data Layer
CHMSPL	CHeMical SPLit module
CMG	Climate Modeling Grid
CO	Carbon Monoxide
CONUS	Contiguous United States
ECV	Essential Climate Variables
EPS	Emission Processing System
ESA	European Space Agency
ESA-CCI	ESA Climate Change Initiative
ESA SAR	ESA Synthetic Aperture Radar
FAO	Food and Agriculture Organization
FB	Fraction of Biomass Burned
FCCS	Fuel Characteristic Classification System
FETS	Fire Emissions Tracking System
FINN	Fire INventory from NCAR
FIRESPEC	FIRESPEC software
FPRM	Fine Other Primary (diameter≤2.5 μm) Particulate Matter
FRP	Fire Radiative Power
GLC-SHARE	Global Land Cover-SHARE

GOES	Geostationary Operational Environmental Satellite
GPL	Great Plains
GROUPPTS	GROUPPTS software
HNO3	Nitric Acid
HMS	Hazard Mapping System
IDL	Interactive Data Language
IGBP	International Geosphere-Biosphere Programme
LANDFIRE	Landscape Fire and Resource Management Planning Tools
LMIS	Lower Mississippi
MDA8	Maximum Daily 8-hour Average
MERIS	MEdium-spectral Resolution, Imaging Spectrometer
MEX	Mexico
MODIS	Moderate Resolution Imaging Spectroradiometer
MODIS LCT	MODIS Land Cover Type
MOZART-4	Model for OZone and Related chemical Tracers Version 4
MTBS	Monitoring Trends in Burn Severity
NAAQS	National Ambient Air Quality Standard
NAB	North American Background
NASA	National Aeronautics and Space Administrations
NASS	National Agricultural Statistical Service
NCAR	National Center for Atmospheric Research
NEI	National Emissions Inventory
NIFC	National Interagency Fire Center
NLCD	National Land Cover Dataset
NMOC	Non-Methane Organic Compounds
NO2	Nitrogen Dioxide
NOAA	National Oceanic and Atmospheric Administration
NOx	Nitrogen Oxides

NOy	Compounds with Odd Nitrogen
NOz	Oxidized NOx
NPP	Suomi National Polar-orbiting Partnership
NTR	Organic Nitrates
NTR2	Multi-functional Organic Nitrates
PAN	Peroxyacetyl Nitrate
PANX	C3 and higher Peroxyacyl Nitrate
PM2.5	Particulate Matter up to 2.5 micrometer
PNO3	Particulate Nitrate
PREFIR	PREprocessor for point FIRe source emissions module
PSO4	Particulate Sulfate
PSTFIR	PoST processor for FIRe source emissions module
PTSMRG	PTSMRG software
RPO	Regional Planning Orginzations
RSAC	Remote Sensing Applications Center
SAPRC99	Statewide Air Pollution Research Center mechanism Version 99
SEUS	Southeastern US
SMARTFIRE	SmartFire Fire Information System
SPOT VEGETATION	Satellite Pour l'Observation de la Terre Vegetation
TCEQ	Texas Commission on Environmental Quality
TMPRL	TeMPoRaL allocation module
TPWD	Texas Parks and Wildlife Department
TX	Texas
UN	United Nations
UNFCCC	UN Framework Convention on Climate Change
USDA	United States Department of Agriculture
USFS	United States Forest Service
USGS	United States Geological Survey

VCF	Vegetation Continuous Fields
VIIRS	Visible Infrared Imaging Radiometer Suite
VOC	Volatile Organic Compound
WFEIS	Wildland Fire Emissions Information System
WRAP	Western Regional Air Partnership
WRF	Weather Research and Forecasting model
WUS	Western US

1. Introduction

Wildland fires and open burning can be substantial sources of ozone precursors and particulate matter. The influence of fire events on air quality in Texas has been well documented by observational and modeling studies (e.g., Junquera er al., 2005; Morris et al., 2006; McMillan et al., 2010; Villanueva-Fierro et al., 2009; Kemball-Cook et al., 2014). Accurate characterization of fire events in Texas, other states, and neighboring countries is necessary for understanding their influence on measured ambient concentrations, for providing a weight of evidence for exceptional event exclusions if necessary, and for conducting air quality modeling for planning and attainment demonstrations. On a national basis, wildfires are among the natural emission sources that contribute to North American Background (NAB) ozone, which would occur in the U.S. in the absence of all North American anthropogenic emissions (McDonald-Buller et al., 2011; Zhang et al., 2011; Emery et al., 2012). NAB has historically informed federal policy decisions on setting the National Ambient Air Quality Standard (NAAQS) for ozone (EPA, 2013; 2014). The National Climate Assessment (Melillo et al., 2014) indicates an increase in the number of days with temperatures exceeding 100°F, the number of warm nights above 80°F, and the number of consecutive dry days in the future as well as changes in water availability in Texas over the next several decades. These changes may have profound and complex impacts on fire events. Texas is not alone in facing these potential challenges. Projected changes in climate suggest that fire frequency in the western U.S. may increase (Westerling et al., 2011; Westerling et al., 2006). Westerling and Bryant (2008) use downscaled climate model output to estimate fire probability across the state of California. In all cases, the probability of fires across the state was expected to increase, resulting in increased pollutant emissions (Hurteau et al., 2014). As more stringent federal standards for ozone are defined and implemented, emissions of precursors from regional and longer-range sources such as fires that can contribute to background concentrations will become increasingly important for understanding the relative effectiveness of local and regional emissions control programs in Texas and throughout United States.

1.1 Technical Context and Motivation

The Fire INventory from the National Center for Atmospheric Research (FINN; Wiedinmyer et al., 2011) is a global fire emissions model that generates inputs for air quality models at a resolution of approximately 1 km^2. FINN estimates daily emissions of trace gases and particles from open biomass burning, including wildfires, agricultural fires, and prescribed burning (but not biofuel use or trash burning). FINN is especially applicable for global and regional modeling studies and has been widely used (e.g., Tsao et al, 2011; Lin et al., 2012; Jiang et al., 2012; Young et al., 2012; Loughner et al., 2014); it offers high spatial and temporal resolution necessary for capturing daily variations in emissions and chemistry, consistency across geopolitical boundaries, and chemical speciation profiles for volatile organic compound (VOC) emissions for the GEOS-Chem, SAPRC99, and MOZART-4 mechanisms. Mappings from MOZART-4 to the Comprehensive Air Quality Model with Extensions (CAMx) Carbon Bond (i.e., CB05 and CB6) mechanisms are also available, and a specific profile for the CB6r2 mechanism is under development. FINN v.1 was released in 2010 and updated in 2011. FINN v. 1.5 was released in 2014.

During the 2012-2013 fiscal year of the Air Quality Research Program (AQRP), Project #12-018 evaluated the sensitivity of FINNv1 emissions estimates to the variability in input parameters and investigated the effects on modeled air quality using CAMx. Sensitivity studies used different input data sources for land cover, emission factors, fire detection, burned area, and fuel loading in FINN. The project found that variability in fire emissions is season- and region-dependent in the United States, and differences in emissions estimates due to varying input data resources could exceed a factor of two. The use of the different estimates of fire emissions had substantial impacts on CAMx predictions of ozone and fine particulate matter concentrations in Texas and other regions of the United States. It has been recognized that the extensive efforts for land cover characterization within and surrounding Texas had not been leveraged for fire emissions modeling, and better characterization and constraints were needed for agricultural areas with high fire activity. AQRP Project #12-018 and other studies (i.e., Pfister et al. 2011) also indicated that FINN tended to underpredict area burned particularly for large wildfires.

1.2 Objectives

The overall objective of this AQRP project (#14-011) was to conduct targeted improvements to the FINN model that would benefit the global and regional air quality management and research communities, with a special focus on needs for Texas. Specific objectives included developing a new approach for estimating area burned from satellite-derived fire detections, characterizing and incorporating inputs for specific crop types, developing an initial approach for partitioning NO_x into aged NO_z forms to account for rapid NO_x oxidation in fire plumes, and applying alternative land cover representations from emerging global, U.S. national, and Texas regional land cover products. The project focuses on FINN estimates and regional air quality predictions for fire events in 2012 to support TCEQ air quality modeling efforts.

1.3 Fire Climatology and 2012 Activity

Figure 1 shows regions of the United States that were the geographic focus for FINN emission estimates in this study. Figure 2 shows predicted 12-year (2002-2014) mean monthly carbon monoxide (CO) emissions from FINN v.1.5 and 2012 estimates for the regions; it indicates particularly high fire activity in the Western United States during August and September of 2012 relative to the 12-year mean.

1.4 Report Overview

This report is organized into the following sections: Section 2 provides an overview of the default configuration of the FINN model. Descriptions of the burned area algorithm and new emission factors for croplands are presented in Section 3, along with an assessment of algorithm modifications on FINN emission estimates. Section 4 describes the land cover data resources (global, U.S. national, regional) investigated for the project. Section 5 describes the fire emission estimates and their effects on CAMx air quality predictions. Section 6 describes the NO_x-NO_z partitioning approach and impacts on CAMx predictions. Section 7 provides an overview of data quality assurance. Section 8 provides conclusions and recommendations for future work.

Figure 1. Geographic regions of focus for the study.

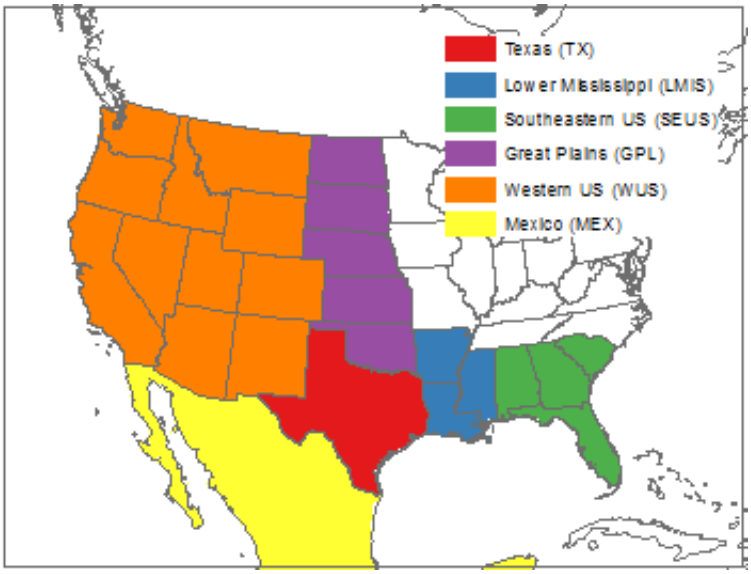

Figure 2. Predicted 12-year monthly mean CO emissions (columns; error bars show maximum and minimum values) and 2012 estimates (black line) by region for (a) Texas, (b) the Lower Mississippi Valley, (c) Southeastern U.S., (d) Great Plains, (e) Western U.S. and (f) Mexico.

(a)

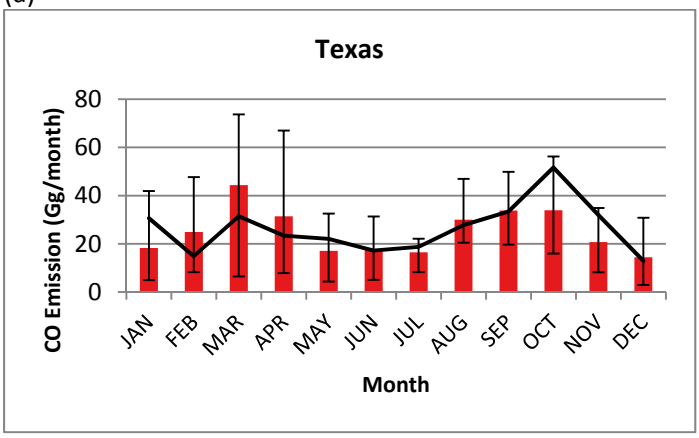

(b)

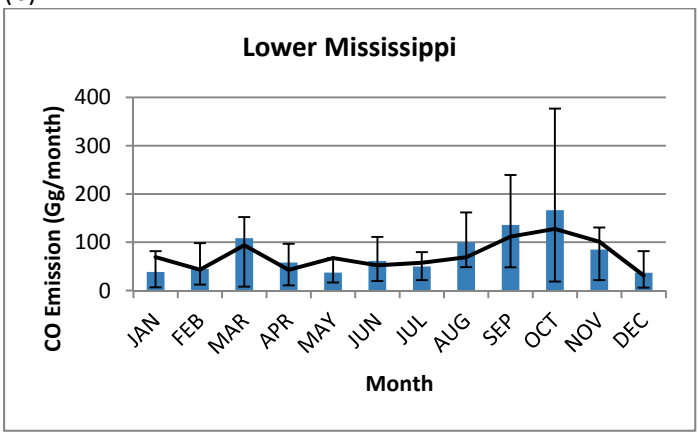

(c)

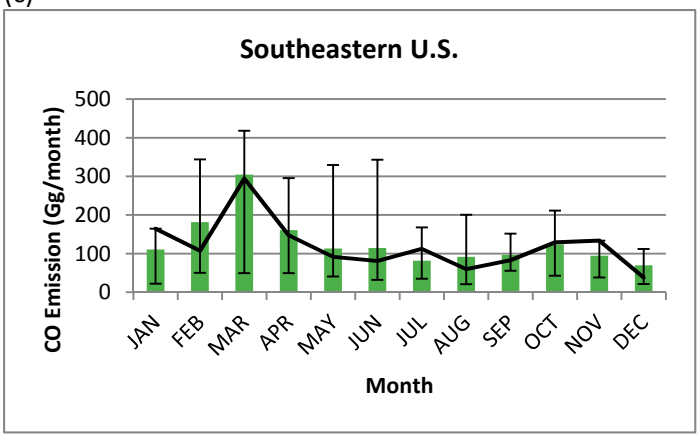

(d)

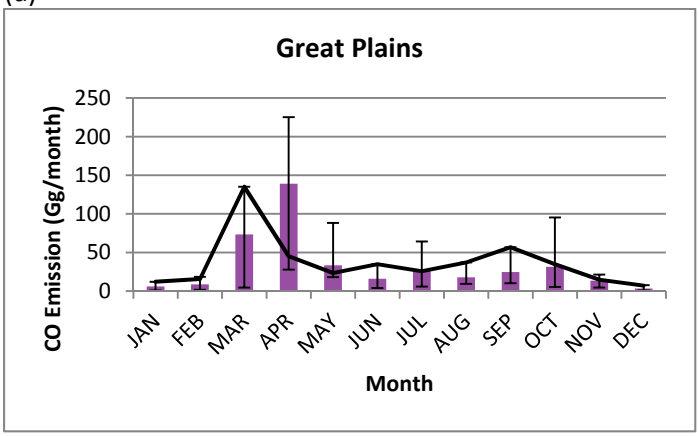
Great Plains
CO Emission (Gg/month)
250
200
150
100
50
0
JAN
FEB
MAR
APR
MAY
JUN
JUL
AUG
SEP
OCT
NOV
DEC
Month

(e)

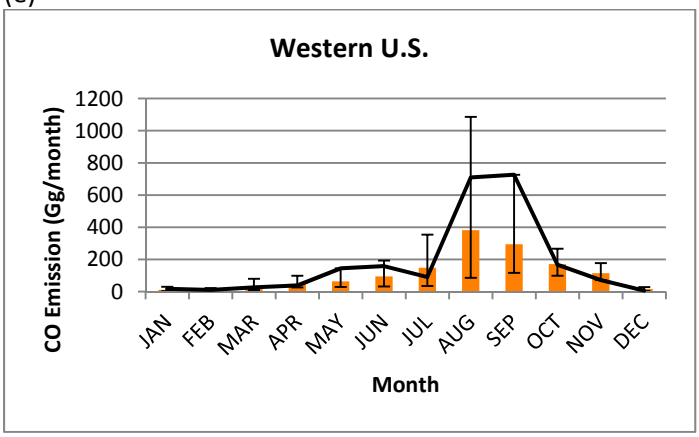
Western U.S.
CO Emission (Gg/month)
1200
1000
800
600
400
200
0
JAN
FEB
MAR
APR
MAY
JUN
JUL
AUG
SEP
OCT
NOV
DEC
Month

(f)

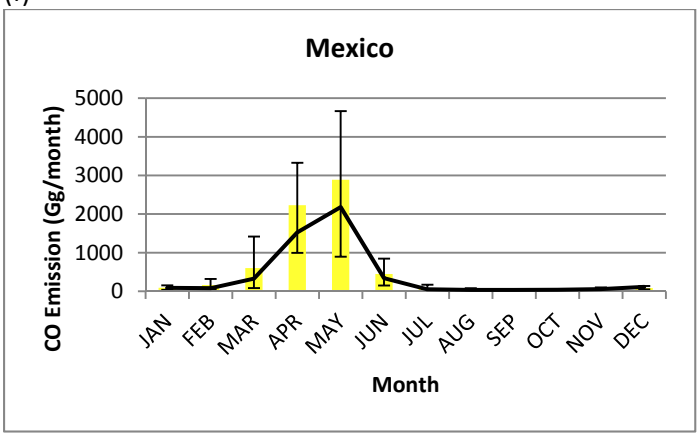
Mexico
CO Emission (Gg/month)
5000
4000
3000
2000
1000
0
JAN
FEB
MAR
APR
MAY
JUN
JUL
AUG
SEP
OCT
NOV
DEC
Month

1.5 References

Emery, C., J. Jung, N. Downey, J. Johnson, M. Jimenez, G. Yarwood, R. Morris. Regional and global modeling estimates of policy relevant background ozone over the United States. *Atmospheric Environment*, 47, 206-217, 2012.

EPA, 2013. Integrated Science Assessment of Ozone and Related Photochemical Oxidants. Prepared by the US Environmental Protection Agency (EPA/600/R-10/076F). http://cfpub.epa.gov/ncea/isa/recordisplay.cfm?deid=247492.

EPA, 2014 Policy Assessment for the Review of the Ozone NAAQS. Prepared by the US Environmental Protection Agency (EPA-452/R-14-006). http://www.epa.gov/ttn/naaqs/standards/ozone/s_o3_2008_pa.html

Hurteau, M.D., A. L. Westerling, C. Wiedinmyer , B. P. Bryant. Projected effects of climate and development of California wildfire emissions through 2011, *Environmental Science & Technology,* 48(4), 2298–2304, 2014.

Jiang, X., C. Wiedinmyer, A. G. Carlton. Aerosols from Fires: An examination of the effects on ozone photochemistry in the Western United States, *Environmental Science & Technology*, 46, 11878−11886, 2012.

Junquera, V., M.M. Russell, W. Vizuete, Y. Kimura, D. Allen. Wildfires in Eastern Texas in August and September 2000: Emissions, aircraft measurements, and impact on photochemistry, *Atmospheric Environment*, 39(27), 4983-4996, 2005.

Kemball-Cook, S., T. Pavlovic, J. Johnson, L. Parker, D.J. Rasmussen, J. Zagunis, L. Ma, G. Yarwood. Analysis of Wildfire Impacts on High Ozone Days in Houston, Beaumont, and Dallas-Fort Worth during 2012 and 2013. Final report for WO582-11-10365-FY14-19, prepared for the Texas Commission on Environmental Quality, Austin, TX, by ENVIRON International Corporation, Novato, CA (July 2014).

Lin, M., A. M. Fiore, L. W. Horowitz, O. R. Cooper, V. Naik, J. Holloway, B. J. Johnson, A. M. Middlebrook, S. J. Oltmans, I. B. Pollack, T. B. Ryerson, J. X. Warner, C. Wiedinmyer, J. Wilson, B. Wyman. Transport of Asian ozone pollution into surface air over the Western United States in spring, *Journal of Geophysical Research*, 117, D00V07, 2012.

Loughner, C.P., M. Tzortziou, M. Follette -Cook, K. E. Pickering , D. Goldberg , C. Satam, A. Weinheimer, J. H. Crawford, D. J. Knapp, D. D. Montzka, G. S. Diskin, R. R. Dickerson. Impact of bay-breeze circulations on surface air quality and boundary layer export, *Journal of Applied Meteorology and Climatology*, 53, 1697-1713, 2014.

McDonald-Buller, E.C., D.T. Allen, N. Brown, D.J. Jacob, D. Jaffe, C.E. Kolb, A.S. Lefohn, S. Oltmans, D.D. Parrish, G. Yarwood, L. Zhang. Establishing Policy Relevant Background (PRB) ozone concentrations in the United States. *Environmental Science & Technology*, 45 (22), 9484–9497, 2011.

McMillan, W.W., R.B. Pierce, L.C. Sparling, G. Osterman, K. McCann, M.L. Fischer, B. Rappengluck, R. Newson, D. Turner, C. Kittaka, K. Evans, S. Biraud, B. Lefer, A. Andrews, S. Oltmans, 2010. An observational and modeling strategy to invetigate the impact of remote sources on local air quality: A Houston, Texas, case study from the Second Texas Air Quality Study (TexAQS II), *Journal of Geophysical Research*, 115, D01301.

Melillo, J.M., T.C. Richmond, G.W. Yohe. Climate Change Impacts in the United States. *Third National Climate Assessment*, 2014.

Morris, G.A., S. Hersey, A.M. Thompson, S. Pawson, J. E. Nielsen, P.R. Colarco, W.W. McMillan, A. Stohl, S. Turquety, J. Warner, B.J. Johnson, T. L. Kucsera, D. E. Larko, S.J. Oltmans, and J.C. Witte. Alaskan and Canadian forest fires exacerbate ozone pollution over Houston, Texas on 19 and 20 July 2004, *Journal of Geophysical Research*, 111, D24S03, 2006.

Tsao, C-C., J. E. Campbell, M. Mena-Carrasco, S. N. Spak, G. R. Carmichael, Y. Chen. Increased estimates of air-pollution emissions from Brazilian sugar-cane ethanol, Nature Climate Change, 2, 53-57, 2011.

Villanueva-Fierro, I., C.J. Popp, R.W. Dixon, R.S. Martin, J.S. Gafney, N.A. Marley, J.M. Harris, 2009. Ground-level chemical analysis of air transported from the 1998 Mexican-Central American fires to the Southwestern USA, *Revista Internacional de Contaminacion Ambiental*, 25(1), 23-32, 2009.

Westerling, A. L. and B.P. Bryant. Climate change and wildfire in California. *Climatic Change*, 87, S231-S249, 2008.

Westerling, A. L., M.G., Turner, E.A.H. Smithwick, W.H. Romme, M.G. Ryan. Continued warming could transform greater Yellowstone fire regimes by mid-21st century. Proceedings of the National Academy of Sciences, 108, 13165-13170, 2011.

Westerling, A. L., H.G. Hidalgo, D.R. Cayan, T.W. Swetnam. Warming and Earlier Spring Increase Western U.S. Forest Wildfire Activity. *Science*, 313, 940-943, 2006.

Wiedinmyer, C., S. K. Akagi, R. J. Yokelson, L. K. Emmons, J. A. Al-Saadi, J. J. Orlando, and A. J. Soja. The Fire INventory from NCAR (FINN): A high resolution global model to estimate the emissions from open burning, *Geoscientific Model Development*, 4(3), 625-641, 2011.

Young, P.J., L. K. Emmons, J. M. Roberts, J.-F. Lamarque, C. Wiedinmyer, P. Veres, T. C. VandenBoer. Isocyanic acid in a global chemistry transport model: Tropospheric distribution, budget, and identification of regions with potential health impacts, Journal of Geophysical Research, 117, D10308, 2012.

Zhang, L., Jacob, D.J., Downey, N.V., Wood, D.A., Blewitt, D., Carouge, C.C., van Donkelaar, A., Jones, D.B.A., Murray, L.T., Wang, Y. Improved estimate of the policy-relevant background ozone in the United States using the GEOS-Chem global model with 1/2°×2/3° horizontal resolution over North America, *Atmospheric Environment*, 45, 6769-6776, 2011.

2. FINN Configuration and Default Data Resources

FINN and its framework have been described in detail by Wiedinmyer et al. (2011) and are summarized here to provide a context for the improvements undertaken in this project. Emissions in FINN are estimated as:

$$E_i = A\,(x,t) * B(x) * FB * ef_i$$

where E_i is the mass emission of species *i* (kg/day), $A(x,t)$ is the area burned at time *t* and location *x* (km^2/day), $B(x)$ is the biomass (fuel) loading at location *x* (g/m^2), FB is the fraction of biomass burned, and ef_i is the emission factor of species *i* (g/kg biomass burned). All biomass terms are on a dry weight basis. The FINN methodology has been developed such that the inputs and parameterizations are flexible and can be changed. The default data sources for FINN v.1 and v1.5 are described below.

2.1 Fire Detection and Area Burned

Global observations from the Moderate Resolution Imaging Spectroradiometer (MODIS) instrument on-board NASA's Terra and Aqua satellites have been used as the default for fire detection in FINN. MODIS hot spot observations are obtained from the National Aeronautics and Space Administrations (NASA's) data portal (https://firms.modaps.eosdis.nasa.gov/download/); this database provides daily fire detections with a nominal horizontal resolution of ~1 km^2 and include the location, overpass time (UTC), and confidence of the detection. Among the uncertainties with daily fire detections, double counting of fires within a day is possible because observations from both the Terra and Aqua satellites are applied. Wiedinmyer et al. (2011) addressed this issue for their global assessment by removing duplicate fire detections for a single day that fell within a 1-km^2 radius of another fire detection, according to the approach of Al-Saadi et al. (2008). Consequently, for each 1-km^2 hot spot, there is a constraint of one fire per day, but fires that occur the following day at the same location are counted again. MODIS satellite observations do not provide daily global coverage at latitudes between approximately 30° N and 30°S, due to the observational swath path; this area includes portions of southern Texas. The FINN model accounts for this limitation as described by Wiedinmyer et al. (2011).

An upper limit of 1 km^2 for area burned has been assumed in the FINN default configuration, except for fires located in grasslands and savannas, which have been assigned a burned area of 0.75 km^2 (Wiedinmyer et al., 2006; Al-Saadi et al., 2008). The burned area is scaled by the percent bare cover using the MODIS Vegetation Continuous Fields (VCF) product. The assumption of an upper limit for burned area has been a recognized limitation in FINN.

Figure 3 shows the MODIS Climate Modeling Grid (CMG) mean Fire Radiative Power (FRP) (http://svs.gsfc.nasa.gov/cgi-bin/details.cgi?aid=4093) during 2000-2013. Although not used for FINN emission estimates, this product provides information on the measured radiant heat output of detected fires. Many lower intensity fires are prescribed fires for either agricultural or ecosystem management purposes. Most intense fires occur in the western United States, where lightning and human activity ignite blazes that rapidly become uncontained; emissions from

these fires, which spread over large areas, can be subject to underestimation from the assumptions of the FINN burned area algorithm.

Figure 3. MODIS mean FRP (Megawatts) during 2000-2013. This product provides a measure of fire intensity. Source: http://svs.gsfc.nasa.gov/cgi-bin/details.cgi?aid=4093

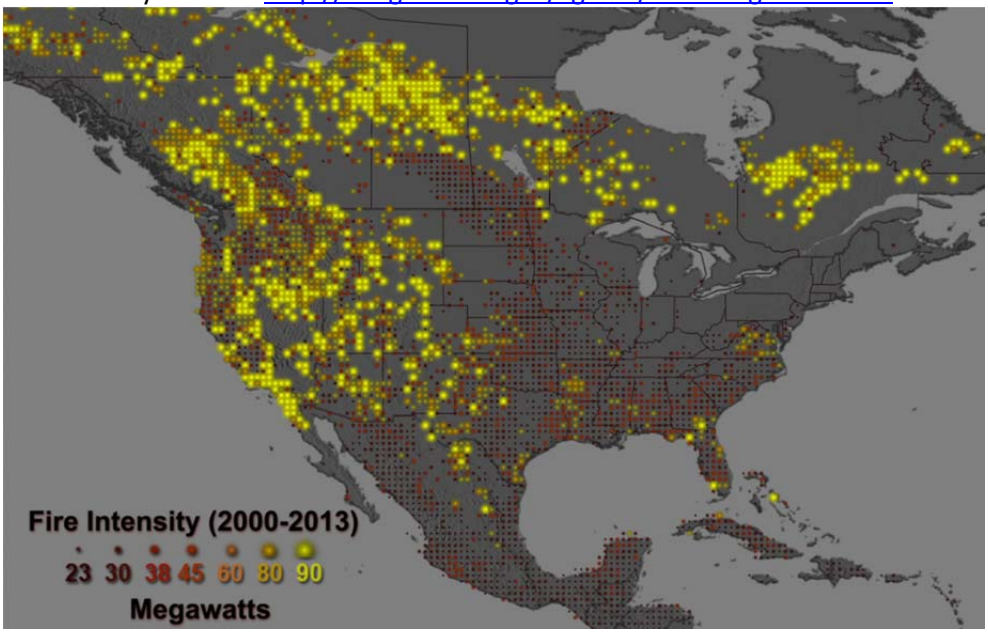

2.2 Land Use/Land Cover Classification

Vegetation type associated with each fire pixel has been based on the MODIS Land Cover Type (LCT) product. The LCT product has a spatial resolution of 1 km^2. Each fire pixel is assigned to one of seventeen land use/land cover classifications defined by the International Geosphere Biosphere Programme (IGBP). The MODIS LCT product for 2009 has been used as the default in .ersions 1 and 1.5. The MODIS VCF product is used to identify the density of the vegetation at each active fire location. The VCF product has a spatial resolution of 500m and provides proportional estimates of woody vegetation, herbaceous vegetation, and bare ground cover. VCF data are scaled to 1-km spatial resolution to match the fire detection and LCT datasets. Wiedinmyer et al. (2011) describe the assignment of vegetation coverage between the LCT and VCF products in greater detail. The VCF Collection 4 version 3 product has been used to date as the default input to FINN v.1 and v. 1.5.

Global land cover classifications from the MODIS LCT product have been mapped to generic categories with associated fuel loadings and emission factors: grasslands and savanna, shrublands and woody savannas, tropical forest, temperate forest, boreal forest, and croplands. In FINN v.1, evergreen needleleaf, deciduous, and mixed forests were assigned based on the latitude. Points at latitude greater than 50°N were identified as boreal; forest land classes at lower latitudes were identified as temperate. Additional data were included for temperate evergreen forests in a more recent release of emission factors from Yokelson et al. (2013) and Akagi et al (2013), available from http://bai.acd.ucar.edu/Data/fire/. Consequently, in FINN v.1.5, needleleaf forests were assigned emissions factors based on latitude: those forests

located at latitudes greater than 50°N were assigned emissions factors for boreal forests. In contrast, those at latitudes less than 50°N were assigned emission factors for temperate evergreen forests. Not only were evergreen forests assigned new emission factors based on their latitude, they were also assigned the corresponding fuel loading of forests in that region. Therefore, temperate evergreen forests were assigned the fuel loading of temperate forest rather than boreal forest (10, 492 kg/m^2 versus 25,000 g/m^2 from Table 1 below).

2.3 Fuel Loadings

In the default FINN framework, fuel loadings for five of the six land cover classification are assigned to world regions based on the work of Hoelzemann et al. (2004) unless otherwise noted. Croplands are assigned the same fuel loading as grasslands for each world region.

Table 1. Fuel loadings (g/m^2) assigned in the FINN framework (Wiedinmyer et al., 2011). Values for North America are shown with gray background.

Global Region	Tropical Forest	Temperate Forest	Boreal Forest	Woody Savanna and Shrublands	Savanna and Grasslands
North America	*28,076*[b]	*10,492*	*25,000*[a]	*5,705*	*976*
Central America	20,260	11,000[a]		2,224	418
South America	25,659	7,400[a]		3,077	552
Northern Africa	25,366	3,497		2,501	318
Southern Africa	25,295	6,100		2,483	360
Western Europe	28,076[b]	7,120	6,228	4,523	1,321
Eastern Europe	28,076[b]	11,386	8,146	7,752	1,612
North Central Asia	6,181[c]	20,807	25,000[a]	11,009	2,170
Near East	6,181[c]	10,316		2,946	655
East Asia	6,181[c]	7,865		4,292	722
Southern Asia	27,969	14,629		5,028	1,445
Oceania	16,376	11,696[d]		1,271	245

[a] Akagi et al. [2010] and references therein
[b] A tropical forest class was added for North America and Europe in the LCT product
[c] All Asia assigned equal tropical forest values
[d] Taken as the average of tropical and temperate forest for Oceania

2.4 Fraction of Biomass Burned

The fraction of biomass burned (FB) has been determined as a function of tree cover by default in FINN based on the approach of Ito and Penner (2004). For areas with $\geq$ 60% tree cover in the VCF product, FB is 0.3 for the woody fuel and 0.9 for the herbaceous cover. For areas < 40% tree cover, no woody fuel is assumed to burn and the FB is 0.98 for the herbaceous cover. For fires in areas with 40% - 60% tree cover, the FB is 0.3 for woody fuels and is calculated as the following

for herbaceous fuels: $\mathrm{FB} = \exp(-0.13 \times fraction\ of\ tree\ cover)$. The fraction of tree cover and fuel loading by land cover type are used to determine the amount of woody fuel available in each global region; herbaceous fuel loading is assumed to be identical to that of grasslands in each global region.

2.5 Emission Factors

Emission factors for each FINN land cover type are shown in Table 2 and described by Wiedinmyer et al. (2011).

Table 2. FINN v.1.5 emission factors (g/m^2) by land cover type for carbon monoxide (CO), oxides of nitrogen (NO_x), non-methane organic compounds (NMOC), ammonia (NH_3), sulfur dioxide (SO_2), particulate matter ($PM_{2.5}$ and PM_{10}), organic carbon (OC), black carbon (BC).

FINN Land Cover	**Emissions Factor (g/m^2)**								
	CO	NO_x	NMOC	NH_3	SO_2	$PM_{2.5}$	PM_{10}	OC	BC
Savanna and Grassland	59	2.8	9.3	0.49	0.48	5.4	7.1	2.6	0.37
Shrubland and Woody Savanna	68	3.9	4.8	1.2	0.68	9.3	11.4	6.6	0.5
Tropical Forest	92	2.6	26	1.3	0.4	9.1	18.5	4.7	0.52
Temperate Forest	122	1.04	28.5	2.47	1.1	15	17	7.6	0.56
Boreal Forest	127	0.90	29.3	2.7	0.4	15.3	18.5	7.8	0.2
Temperate Evergreen Forest	88	1.92	23.5	0.84	1.1	12.9	17	7.6	0.56
Cropland (generic)	111	3.5	57	2.3	0.4	5.8	7	3.3	0.69

2.6 Chemical Speciation Profiles

Regional and global-scale air quality models require the use of simplified chemical mechanisms. Chemical speciation factors are available within FINN to convert total emissions of NMOCs to moles of emitted individual organic compounds or lumped species for the GEOS-Chem (Bey et al., 2001; http://www.geos-chem.org/), MOZART-4 (Emmons et al., 2010a), and SAPRC99 (Carter et al., 2000) chemical mechanisms (Wiedinmyer et al., 2011). The chemical speciation profile for MOZART-4 is shown in Table 3; MOZART-4 has been used with processing algorithms developed by Ramboll Environ to obtain profiles for the CB05 and CB6 mechanisms used in CAMx. NCAR is currently incorporating CB6r2 speciation profiles directly into FINN.

Table 3. Chemical speciation factors for the conversion of NMOC emissions (kg/day) to MOZART-4 chemical species (moles/day) for generic land cover class in the default configuration of FINN (Source: Wiedinmyer et al, 2011). Reference Emmons et al. (2010) for description of lumped species.

	Generic Land Cover Type					
MOZART 4 Species	Savanna/ Grasslands	Tropical Forest	Temperate Forest	Agriculture	Boreal Forest	Shrublands
BIGALD	0.02	0.01	0.01	0.01	0.01	0.02
BIGALK	0.20	0.13	0.11	0.09	0.16	0.42
BIGENE	0.45	0.52	0.22	0.37	0.35	0.63
$C_{10}H_{16}$	0.01	0.04	0.03	0.00	0.04	0.01
C_2H_4	2.27	1.38	1.11	1.08	1.62	2.30
C_2H_5OH	0.02	0.01	0.01	0.01	0.01	0.02
C_2H_6	0.82	0.82	0.29	0.43	1.63	1.01
C_3H_6	0.43	0.56	0.26	0.38	0.76	0.77
C_3H_8	0.18	0.10	0.10	0.08	0.13	0.37
CH_2O	2.12	2.08	1.33	1.84	1.46	2.23
CH_3CHO	1.03	1.27	0.38	3.05	0.67	0.96
CH_3CN	0.21	0.36	0.12	0.55	0.13	0.41
CH_3COCH_3	0.22	0.39	0.20	0.83	0.20	0.71
CH_3COCHO	0.81	0.37	0.17	0.19	0.28	0.86
CH_3COOH	2.08	1.87	0.53	2.19	1.80	1.24
CH_3OH	1.92	2.60	1.51	2.11	2.50	2.49
CRESOL	0.44	0.17	0.07	0.60	0.85	0.00
GLYALD	0.50	0.79	0.28	1.68	0.25	1.39
HCN	1.01	0.56	0.51	0.33	2.49	1.29
HYAC	1.01	0.55	8.03	0.00	0.77	0.00
ISOP	0.05	0.07	0.03	0.60	0.14	0.03
MACR	0.00	0.08	0.00	0.00	0.00	0.00
MEK	1.31	0.85	0.41	0.79	1.64	1.16
MVK	0.00	0.20	0.00	0.00	0.00	0.00
NO	0.38	0.74	0.26	0.09	0.70	0.74
TOLUENE	1.16	2.06	0.61	1.07	1.30	1.32
HCOOH	0.65	0.44	0.26	0.90	0.57	0.16
C_2H_2	0.72	0.36	0.14	0.21	0.20	0.55

2.7 References

Al-Saadi, J., et al. Intercomparison of near-real-time biomass burning emissions estimates constrained by satellite fire data, *Journal of Applied Remote Sensing*, 2, 2008

Akagi, S. K., R.J. Yokelson, I.R. Burling, S. Meinardi, I. Simpson, D.R. Blake, G.R. McMeeking, A. Sullivan, T. Lee, S. Kreidenweis, S. Urbanski, J. Reardon, D.W. T. Griffith, T.J. Johnson, D.R. Weise. Measurements of reactive trace gases and variable O_3 formation rates in some South Carolina biomass burning plumes, *Atmospheric Chemistry and Physics*, 13, 1141-1165, 2013.

Bey, I., D. J. Jacob, R.M. Yantosca, J.A. Logan, B. Field, A. M. Fiore, Q. Li, H. Liu, L. J. Mickley, M. Schultz. Global modeling of tropospheric chemistry with assimilated meteorology: Model description and evaluation, *Journal of Geophysical Research*, 106, 23073–23096, 2001

Carter, W. P. L., Implementation of the SAPRC-99 Chemical Mechanism into the Models-3 Framework, US EPA, 2000.

Emmons, L. K., et al. Impact of Mexico City emissions on regional air quality from MOZART-4 simulations, *Atmospheric Chemistry and Physics*, 10(13), 6195-6212, 2010.

Hoelzemann, J.J., M.G. Schultz, G.P. Brasseur, C. Granier, and M. Simon. Global Wildland Fire Emission Model (GWEM): Evaluating the use of global area burnt satellite data, *Journal of Geophysical Research*, 109, D14S04, 2004.

Ito, A., Penner, J. E. Global estimates of biomass burning emissions based on satellite imagery for the year 2000, *Journal of Geophysical Research*, 109, D14S05, 2004.

Pfister, G.G., J. Avise, C. Wiedinmyer, D.P. Edwards, L.K. Emmons, G.D. Diskin, J. Podolske, A. Wisthaler. CO source contribution analysis for California during ARCTAS-CARB, *Atmospheric Chemistry and Physics*, 11(15), 7515-7532, 2011.

Wiedinmyer, C., S. K. Akagi, R. J. Yokelson, L. K. Emmons, J. A. Al-Saadi, J. J. Orlando, A. J. Soja. The Fire INventory from NCAR (FINN): A high resolution global model to estimate the emissions from open burning, *Geoscientific Model Development*, 4(3), 625-641, 2011.

Yokelson, R. J., I. R. Burling, J.B. Gilman, C. Warneke, C.E. Stockwell, J. de Gouw, S.K. Akagi, S.P. Urbanski, P. Veres, J. M. Roberts, W. C., Kuster, J. Reardon, D.W.T. Griffith, T.J. Johnson, S. Hosseini, J. W. Miller, D. R. Cocker III, H. Jung, D.R. Weise. Coupling field and laboratory measurements to estimate the emission factors of identified and unidentified trace gases for prescribed fires, Atmospheric Chemistry and Physics, 13, 89-116, 2013.

3. Targeted Improvements in Burned Area Characterization and Emission Factors

Improvements were undertaken in the core FINN algorithms and default data inputs to better reflect the state of the science and knowledge that had been gained about FINN performance since the release of earlier versions. These improvements will form the basis of the public release of FINN v.2. A primary objective was to develop a new algorithm and ArcGIS-based tool to assign more reasonable estimates of assumed area burned. Improvements in the area burned estimation were accompanied by better spatial resolution in the characterization of land cover, new fuel loading data with greater spatial resolution for the United States, and incorporation of the newly released, year-specific VCF Collection 5 product for estimating bare and vegetative cover. Emission factors and fuel loadings specific to various crop types were also incorporated. These model developments and their effects on FINN emission estimates are described in detail below.

3.1 Burned Area Characterization

3.1.1. Fire Identification

Fire identification, including location and timing, is clearly a critical foundation of any biomass burning emissions model. However, uncertainties in this input variable are associated with many factors, including, for example, the use and reconciliation of disparate data sources (e.g., varying satellite sensors and associated products; ground incident reports). As described in Section 2.1, FINN has relied on a MODIS product for fire detection. In the course of this project, several other products for fire detection were reviewed:

- The *Monitoring Trends in Burn Severity (MTBS)* database supports analysis of burn severity trends (http://www.mtbs.gov/nationalregional/burnedarea.html) in the western United States, which includes Texas. However, in the Western US, it only identifies fires with burned areas that exceed 1,000 acres. During 2012, only 20 fires (with a total of 106,350 acres burned) met this criterion in Texas and were included in the MTBS. Limitations of this database are that smaller fires associated with prescribed burning are likely to be missed, and it is not suitable as a U.S. national or global resource for fire detection.
- The *Wildland Fire Emissions Information System (WFEIS)* from the Michigan Tech Research Institute is a web interface that includes burned area maps, fuel loadings, and fuel consumption models to estimate fire fuel consumption and emissions for the continental United States and Alaska (http://wfeis.mtri.org/calculator). Data options for burned area include the MODIS MCD64A1, MTBS, Landsat Daily, and SmartFire 2011 National Emissions Inventory (NEI) and Agricultural NEI products. At the time our project was initiated, WFEIS only had data available for 2000-2011; this resource is promising for future efforts in the United States but not for global estimates.
- The *Western Regional Air Partnership Fire Emissions Tracking System (FETS)* includes information about fire location, timing, and size for the western United States but not Texas (http://wrapfets.org/).
- The *Visible Infrared Imaging Radiometer Suite (VIIRS*) sensor was launched aboard the Suomi National Polar-orbiting Partnership (NPP) satellite on October 28th, 2011; fire detections began on January 18th, 2012. VIIRS active fire and night fire global products

are available as the sensor includes a day/night band. As described by NASA, the VIIRS instrument was designed for the needs of the operational weather community, but retained much of the MODIS capability for land science (http://npp.gsfc.nasa.gov/viirs.html). Comparisons between MODIS and VIIRS are available at http://viirsfire.geog.umd.edu/pages/viirsvsmodis.php and elsewhere. The VIIRS active fire product has been declared provisional back to October 16th, 2012. Interest in and use of VIIRS data products are rapidly growing, and these will likely replace the MODIS product in the future. The lack of a full year of data for 2012 was not sufficient to meet TCEQ's request for this project, but the VIIRS products should considered as a promising resource for global fire detection in the future.

- *SMARTFIRE* (Larkin et al; 2014; Raffuse et al, 2012) is a system that provides an inventory of fires for the contiguous US based on a compilation of remote sensing observations and incident reports. Although this is a useful product, complete results for 2012 were unavailable to us for this project (*personal communications with S. Raffuse of Sonoma Technology, Inc.,* September 2, 2014).
- The *NOAA Hazard Mapping System (HMS)* provides a clearing house for MODIS, GOES and AVHRR fire detections as well as smoke plumes determined from visible satellite observations. This is only available for North America, but is a useful source of information for model evaluation.
- The *National Interagency Fire Center (NIFC)* reports annual area burned for each state in the US (e.g., (http://www.predictiveservices.nifc.gov/intelligence/2012_statssumm/2012Stats&Summ.html). However, fire locations are not included. This product is not sufficient for the needs of FINN, but it could be useful for cross-comparison purposes.

At this time, FINN v.2 will continue to rely solely on the MODIS Active Fire product for fire detection. These data have the high spatial and temporal resolution needed for regional air quality modeling, as well as a long time record; the data are continually quality-assured and easy to obtain. Annual total MODIS Active Fire record counts during 2012, shown in Figure 4, were obtained from the United States Forest Service (USFS) Remote Sensing Applications Center (RSAC) (http://activefiremaps.fs.fed.us/data/fireptdata/modisfire_2012_na.htm). [These data are also available via the NASA website: https://firms.modaps.eosdis.nasa.gov/download/] Moving forward, we will follow the evolution of the VIIRS algorithms and products as well as any other potentially valuable satellite detection datasets.

Figure 4. Annual total MODIS Rapid Response fire detection counts in 2012 (detection confidence estimate ≥ 20%).

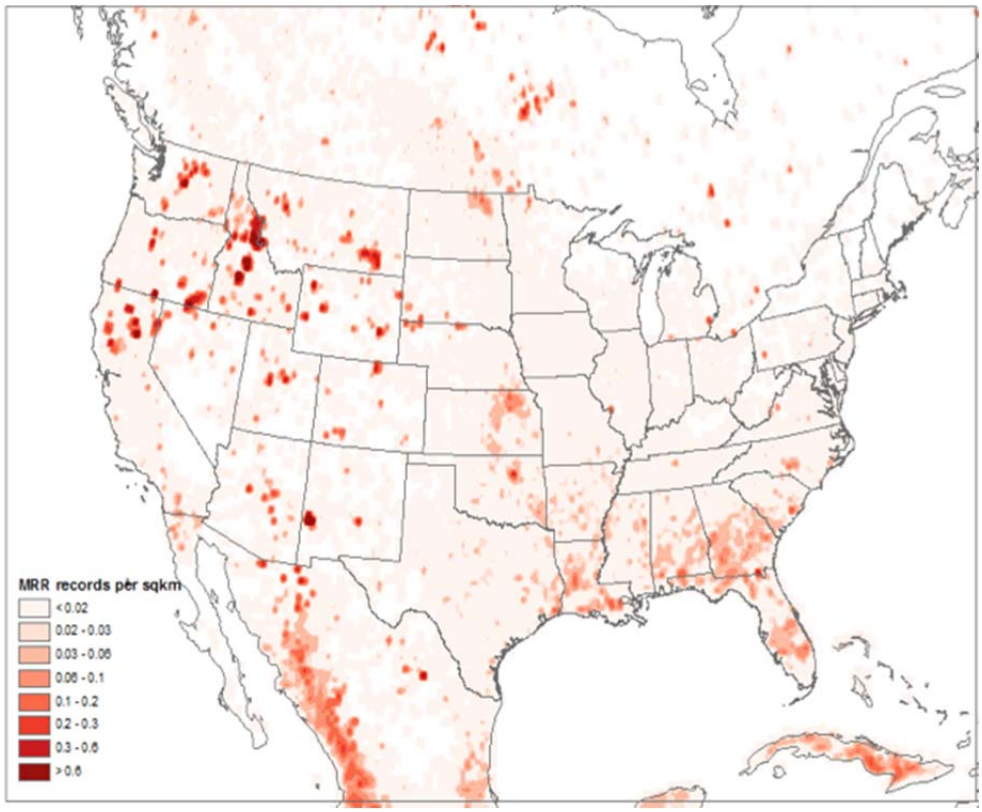

3.1.2 Estimation of Burned Area

The new approach developed as part of this project to estimate the burned area of each fire event on a given day was to assume a 1-km^2 area per MODIS Active Fire records, join neighboring detections through a convex hull based on the estimated scan and track sizes of the satellite pixel, and dissolve neighboring polygons to estimate a total daily burned area. The algorithm included the following steps (as illustrated for a specific fire in Figure 5):

1. MODIS Active Fire records (detection confidence estimate ≥ 20%) for a wildfire in southern Montana that occurred on June 27, 2012 are shown in Figure 5a. Each fire detection was assumed to cover an area of 1 km^2, which we referred to as a "fire square" (shown in Figure 5b). Note that Figure 5b provides an indication of the potential for underestimation of burned area because it is likely that these detections actually represent a contiguous fire region. Earlier versions of the FINN algorithm would rely only on the sum of the fire squares to represent total burned area.
2. In our revised approach, nearby fire detections were joined to form a "fire polygon", according to the following:
    a. The "scan" and "track" sizes of the satellite pixel for each MODIS Active Fire record were utilized to identify groups of records that represented contiguous detections. This was accomplished by generating a rectangle with easterly and northerly sizes equal to 110% of the scan and track sizes, respectively, for each detection. Note that because the satellite path may not completely align with

the northerly or southerly directions, the nominal size of the rectangle was increased by 10% to ensure detection of contiguous satellite pixel pairs. We refer to this rectangle as a "detection rectangle" (Figure 5c).

b. When two Active Fire records had intersecting detection rectangles, these two records were either (1) the detection of a single fire event by two contiguous satellite sensors or (2) the detection of a fire in a nearby location by another satellite overpass. In either case, these overlapping records were assumed to be detections of the same fire event stretching across the area. Fire records for a given day were grouped into clusters of records whose detection rectangles intersected directly or indirectly through other records in the cluster. We refer to this cluster as a "detection cluster".

c. Fire squares that belong to a given detection cluster were merged into one contiguous polygon according to the following approach. For all pairs of fire squares whose detection rectangles directly intersected, a convex hull was generated. Convex hulls from a cluster were dissolved into one contiguous polygon. Small spatial "holes", with an area less than 0.5 arcminute x 0.5 arcminute (~ 1km^2) were eliminated. This resulting "fire polygon" was an estimate of the burned area for a single fire event for the day (Figure 5d).

3. Bare ground, assumed to have no vegetation to burn, was removed from the total burned area using the VCF version 051 Product (Figure 6) recently released on February 11, 2015 (https://lpdaac.usgs.gov/version_51_vegetation_continuous_fields_release). In this work, we applied year-specific (2012) VCF data, which was a substantial change from the older VCF data applied in the previous FINN versions. The VCF map for the fraction of bare cover was overlaid onto the fire polygon and the final burned area was estimated as:

$$Burned\ Area = \begin{cases} Polygon\ Area & if\ LCT\ is\ forest/shrub \\ Polygon\ Area * 0.75 & if\ LCT\ is\ sanvanna/grass \\ 0 & if\ LCT\ is\ bare/water \end{cases}$$

3.1.3. Land Cover Analysis

The burned area was divided into "fire subdivisions" to analyze the underlying land cover. The algorithm used Voronoi tessellation with detection coordinates as seeds according to the following approach:

1. The distance between each detection point was determined for a given fire polygon that was shorter than 0.5 arcminute (~1 km). A graph was generated with detection points as nodes and edges weighted by the inverse distance.
2. Each of the connected components was evaluated, and nodes were iteratively eliminated until no edges remained. For each node within the connected component, the sum of the weights of the edges (i.e., the inverse distance to neighboring nodes) was calculated. Nodes with the largest values were eliminated first; when this criterion included more than one node, all nodes were replaced by the midpoint of the directly connected group.
3. The fire polygon was divided into Voronoi tessellations using a subset of the fire detection coordinates, as shown in Figure 5e. For fires occurring during North and

Central America during 2012, 95% of the divisions were between 0.98 km^2 to 2.6 km^2, with a minimum of 0.59 km^2 and maximum of 7.65 km^2.

The fire polygon was converted into a raster using the ArcGIS "Polygon to Raster" tool and processed with the land cover raster datasets described in Chapter 4.

Figure 5. Illustration of the FINN burned area estimation algorithm. (a) MODIS Active Fire detections on June 27, 2012 in southern Montana, (b) corresponding 1km^2 "fire squares, (c) "detection rectangles" determined from the scan and track sizes of the pixel, (d) "fire polygon" used with the MODIS VCF product as the basis for the burned area estimate and (e) fire subdivisions for land cover analysis within the burned area.

(a)

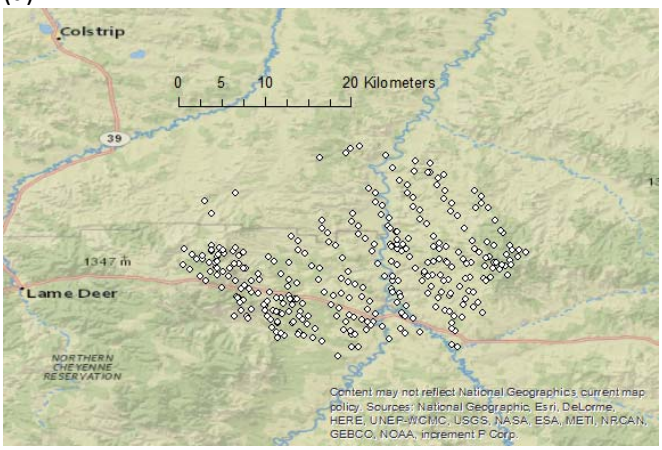

(b)

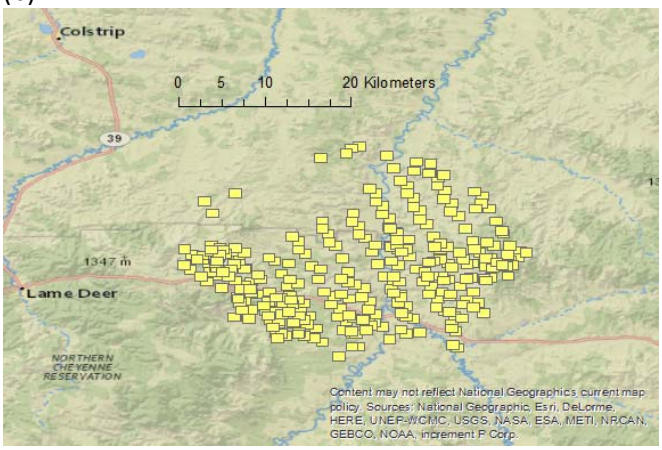

(c)

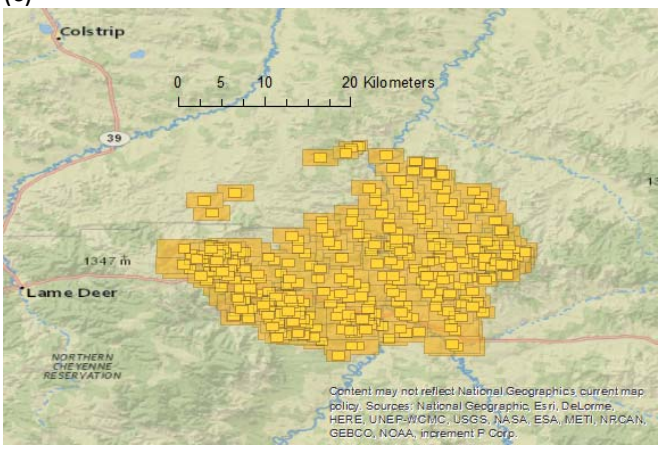
Colstrip
0 5 10 20 Kilometers
39
1347 m
Lame Deer
NORTHERN CHEYENNE RESERVATION
Content may not reflect National Geographics current map policy. Sources: National Geographic, Esri, DeLorme, HERE, UNEP-WCMC, USGS, NASA, ESA, METI, NRCAN, GEBCO, NOAA, increment P Corp.

(d)

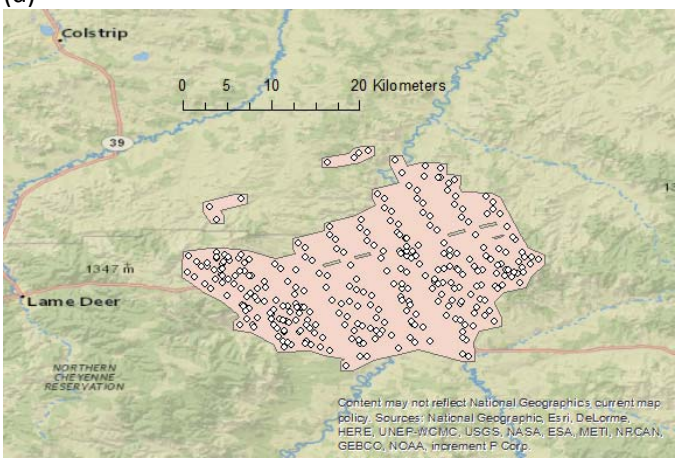
Colstrip
0 5 10 20 Kilometers
39
1347 m
Lame Deer
NORTHERN CHEYENNE RESERVATION
Content may not reflect National Geographics current map policy. Sources: National Geographic, Esri, DeLorme, HERE, UNEP-WCMC, USGS, NASA, ESA, METI, NRCAN, GEBCO, NOAA, increment P Corp.

(e)

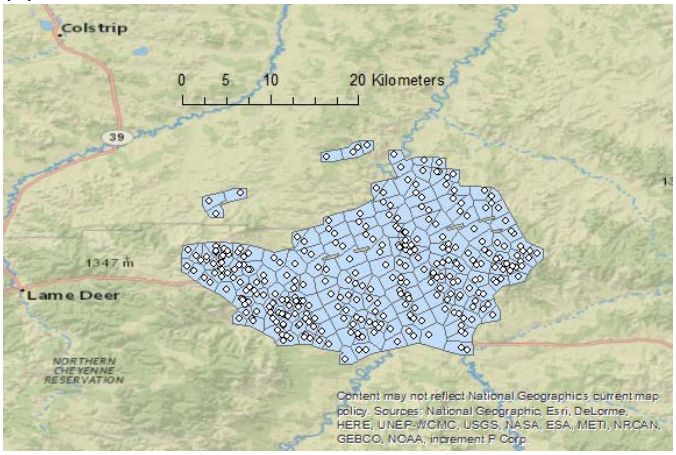
Colstrip
0 5 10 20 Kilometers
39
1347 m
Lame Deer
NORTHERN CHEYENNE RESERVATION
Content may not reflect National Geographics current map policy. Sources: National Geographic, Esri, DeLorme, HERE, UNEP-WCMC, USGS, NASA, ESA, METI, NRCAN, GEBCO, NOAA, increment P Corp.

Figure 6. MODIS VCF version 051 percent cover for year 2012 (a) tree cover (b) non-tree vegetation, and (c) non-vegetated.

(a)

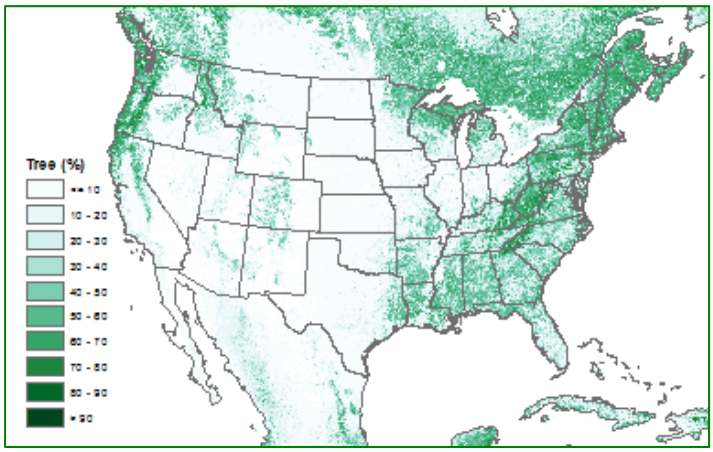

(b)

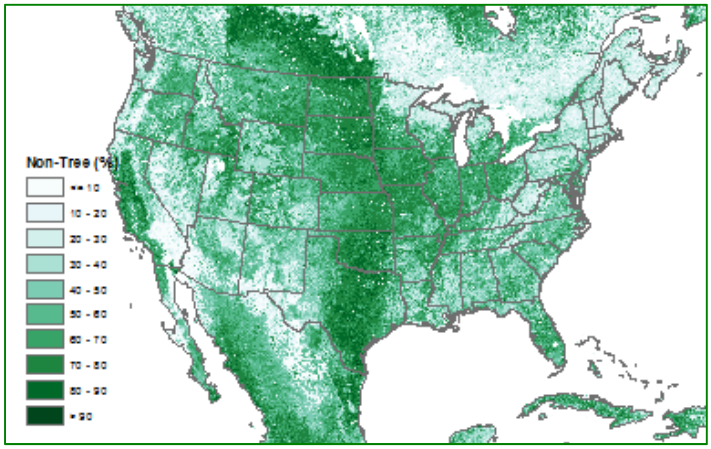

(c)

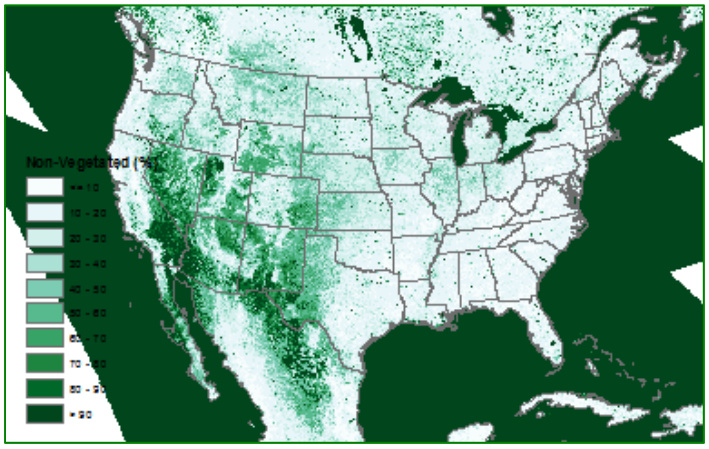

3.2 Emission Factors

Emission factors assigned in the FINN model were updated to incorporate recent results from the literature and additional land cover types that are available in the model (see Chapter 4). Crop-specific emission factors and fuel loadings developed by McCarty (2011) have been added to FINN v.2 as an option for users that have a land cover data resource that distinguishes major crop types typically found in the United States. McCarty (2011) specified emission factors for eight major crop types, including bluegrass, corn, cotton, rice, soy, sugarcane, wheat, as well as an "other" category. Emission factors assigned for sorghum were based on the "other" category. A summary of emission factors for all land cover types in FINN v.2 (with associated references) is shown in Table 4.

Table 4. Summary of FINN v.2 emission factors (g/m^2) by land cover type. *Note that the Akagi et al reference refers to the emission factors reported by Akagi et al (2011) and all updates (from May 2014 and February 2015) posted at http://bai.acom.ucar.edu/Data/fire/. Note that a land cover code of "7" is not used in FINNv2.*

FINN Land Cover (ID)	FINN Code	Emissions Factor (g/m^2)								
		CO	NO_x	NMOC	NH_3	SO_2	$PM_{2.5}$	PM_{10}	OC	BC
Savanna and Grassland[a]	1	63	3.90	12.4	0.52	0.48	7.17	15.8	2.62	0.37
Shrubland and Woody Savanna[b]	2	67	3.65	17.4	1.2	0.68	12.6	15.4	3.7	1.31
Tropical Forest[c]	3	93	2.55	26	1.33	0.4	9.1	18.5	4.71	0.52
Temperate Forest[d, f,g]	4	88	1.91	23.5	0.84	1.1	12.6	13	7.6	0.56
Boreal Forest [c, e, f, g]	5	127	0.90	29.3	2.72	0.4	15.3	18.5	7.6	0.56
Temperate Evergreen Forest[c,f, g]	6	88	1.92	23.5	0.84	1.1	12.9	18.5	7.6	0.56
Cropland (generic)[h, i]	9	64	1.83	25.7	2.17	1.2	6.2	8.5	2.3	0.75
Rice[j,k,l]	8	53	2.04	35	1.24	1.4	5.8	5.8	2.3	0.75
Wheat[i,j,m]	10	55	1.30	33.8	0.64	0.44	4	6.6	2.3	0.75
Cotton[i,j]	11	73	2.24	25.7	2.17	1.6	6.2	8.9	2.3	0.75
Soy[i,j]	12	69	2.06	25.7	2.17	1.6	6.2	8.9	2.3	0.75
Corn[i,j]	13	53	1.50	25.7	2.17	1.2	5	10.7	2.3	0.75
Sorghum[h,i]	14	64	1.83	25.7	2.17	1.2	6.2	8.5	2.3	0.75
Sugar Cane[i,j,n]	15	59	1.98	57.7	1.14	1.7	4.4	4.9	2.3	0.75

[a] From Akagi et al Table S1 average of all savanna (NMOC is a sum of all individual NMOC EFs); PM_{10} emission factor for bluegrass from McCarty et al. (2011).
[b]From Akagi et al. $PM_{2.5}$ based on PM_2 average for chaparral; TSP value applied for PM_{10}.
[c]From Akagi et al. Final average of tropical forest (Table S3). Source for SO_2 for boreal forest and PM_{10} for boreal and temperate evergreen forests.
[d]From Akagi et al. Final emission factor for temperate forest (Table S4); PM_{10} based on $PM_{3.5}$.
[e]From Akagi et al. Average of all boreal forest (Table S2); SO_2 based on value for temperate forest.
[f]From Akagi et al. OC=OA based temperate evergreen values from extratropical update May 2014.xlsx
[g]Emission factor for black carbon based on FINN v.1 for mixed forests
[h]From McCarty et al (2011). "Other" crop emission factors for CO, NO_x, SO_2, $PM_{2.5}$, PM_{10},
[i]From Stockwell et al. (2015) Emission factors for NMOC, NH_3, OC, and BC based on average for crop residue (S13)

[j]From McCarty et al. (2011); Emission factors for CO, NO_x, SO_2, $PM_{2.5}$, PM_{10} (with the exception of rice)
[k]From Stockwell et al. (2015); Emission factors for NMOC and NH_3 based on Asian rice straw adjusted (D)
[l]From McCarty et al. (2011); Emission factor for PM_{10} same as $PM_{2.5}$ for rice, since in the literature $PM_{10} < PM_{2.5}$
[m]From Stockwell et al. (2015); Emission factors for NMOC and NH_3 based on wheat straw adjusted (D)
[n]From Stockwell et al. (2015); Emission factors for NMOC and NH_3 based on sugar cane adjusted (D)

3.3 Implications for Emissions Estimates

Figure 7 shows the effects of the FINN modifications described above (burned area estimation, updated VCF product application, and emission factors) on total CO emission estimates in the CAMx photochemical modeling domain relative to FINN v1.5. Use of the new VCF 051 data resulted in a 39% decrease in CO emissions, while the new algorithm for burned area led to a 125% increase in emissions. The emission factor updates resulted in a 12% decrease in CO emissions. Overall, the 2012 CO emissions for the entire CAMx modeling domain increased by 42% with the modifications relative to the earlier version of FINN.

The directionality and magnitudes of the effects of the modifications were similar across the six regions shown in Figure 1: the updated VCF collection decreased CO emissions by 23% to 47%, while the new burned area algorithm increased emissions by 80% to 166%. The emission factor updates resulted in decreases in emissions ranging from 3% to 19%. The overall changes in the six regions ranged from 6% to 74%. The Western US and Mexico experienced relatively larger increases in emissions, driven primarily by the change in the burned area algorithm. The response of NO_x emission to the modifications was similar to that of CO, with slightly greater effects from the updates to the emission factors.

Figure 7. Effects of FINN modifications on CO emissions estimates for the entire CAMx modeling domain.

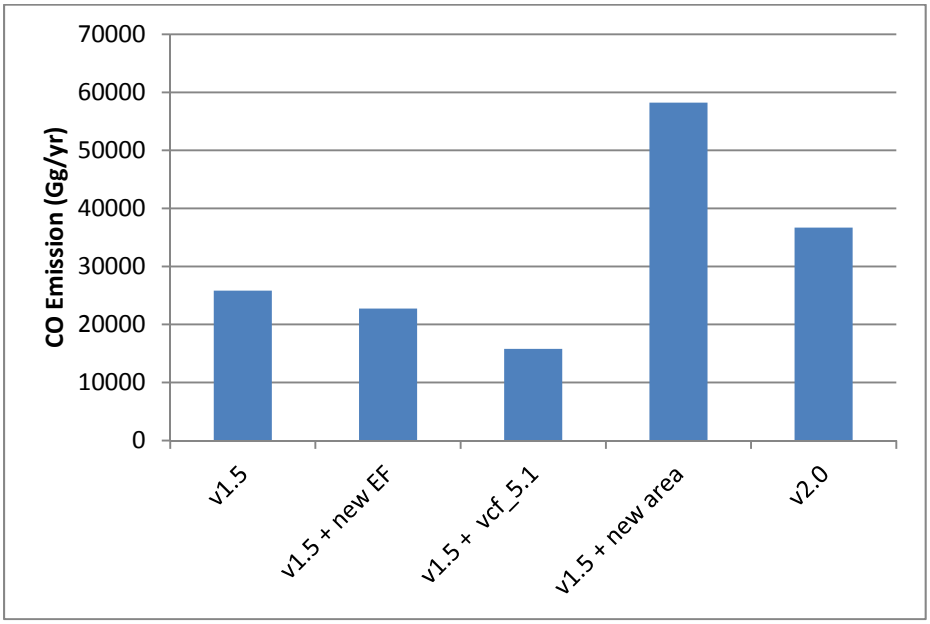

3.4 References

Akagi, S. K., R. J. Yokelson, C. Wiedinmyer, M. J. Alvarado, J. S. Reid, T. Karl, J. D. Crounse, P. O. Wennberg. Emission factors for open and domestic biomass burning for use in atmospheric models, *Atmospheric Chemistry and Physics*, 11(9), 4039-4072, 2011.

Larkin N.K., Raffuse S.M., and Strand T.M. Wildland fire emissions, carbon, and climate: U.S. emissions inventories. *Forest Ecology and Management*, 317, 61-69, April 1, 2014. Available at http://www.sciencedirect.com/science/article/pii/S0378112713006269.

McCarty, J. Remote sensing-based estimates of annual and seasonal emissions from crop residue burning in the contiguous United States, Journal of the Air & Waste Management Association, 61(1), 22-34, 2011.

Raffuse S., Du Y., Larkin S., and Lahm P. Development of the 2008 Wildland Fire National Emissions Inventory. Paper presented at the *20th International Emissions Inventory Conference, Tampa, FL, August 13-16,* by Sonoma Technology, Inc., Petaluma, CA. STI-912012-4340, 2012. Available at http://www.epa.gov/ttn/chief/conference/ei20/session2/sraffuse.pdf.

Stockwell, C.E., P. R. Veres, J. Williams, R. J. Yokelson. Characterization of biomass burning emissions from cooking fires, peat, crop residue, and other fuels with high-resolution proton-transfer-reaction time-of-flight mass spectrometry, Atmospheric Chemistry and Physics, 15, 845-865, 2015.

4. Land Cover and Fuel Loading Data Resources: Emissions Estimates and Regional Air Quality

In the FINN emissions model, land cover and land use are used to assign emission factors and fuel loadings and, consequently, these input data are critical for the estimation of fire emissions. Advances in the characterization of these model components should ideally occur in concert. For example, greater specificity in emission factors for croplands must be accompanied by an ability to distinguish these land use types. Ideally, a global dataset with sufficient regional specificity, validation, and temporal resolution is preferable, but that has and will continue to be an evolving objective as resources are limited in many regions of the world. The MODIS LCT product has been used as the default resource for land cover characterization in FINN, but emerging global databases from other sources, such as the United Nations (UN) and European Space Agency (ESA), are now available alternatives. In addition, U.S. national and Texas regional products that offer greater spatial resolution and specificity in land cover types are available. For this project, we examined the availability of various land cover and land use data and explored the effects of these different land cover representations on FINN v.2 emission estimates and regional air quality predictions in Texas.

4.1 Global Land Use/Land Cover Data Resources

4.1.1 Global Land Cover-SHARE (GLC-SHARE)

GLC-SHARE is a new global-level land cover database developed by the Food and Agriculture Organization (FAO) of the United Nations, Land and Water Division with partners (http://www.glcn.org/databases/lc_glcshare_en.jsp). The GLC-SHARE 2012 Beta Release 1.0 was published in 2014. Its overall objective has been to synthesize and harmonize global, national, and sub-national land cover data resources. It has a resolution of 30 arc-second^2 (~1 km^2) and eleven land cover classes: artificial surfaces, croplands, grasslands, tree-covered areas, shrub-covered areas, herbaceous vegetation (aquatic or regularly flooded), mangroves, sparse vegetation, bare soil, snow and glaciers, and water bodies. The mapping of GLC-SHARE categories to FINN categories (see Table 4) is shown in Table 5 and depicted in Figure 8. Note that GLC-SHARE does not distinguish between different types of forested land cover classes (e.g., evergreen/deciduous, broadleaf/needleleaf).

Table 5. Mapping between GLC-SHARE and FINN (ref. Table 4) for selected land cover categories.

GLC-SHARE Description	GLC-Code	FINN Code
Grasslands	3	1
Tree-covered Areas	4	3,4,5, (depending on latitude)
Shrub-covered Areas	5	2

4.1.2 ESA Climate Change Initiative (ESA-CCI)

ESA initiated the Climate Change Initiative (CCI) to respond to the needs of the UN Framework Convention on Climate Change (UNFCCC). Land cover is among the Essential Climate Variables (ECVs). Phase 1 of the development of the land cover product occurred during August 1st-

October 1st, 2014, and its products are available to the external scientific community (http://www.esa-landcover-cci.org/?q=overview). Phase 2 was initiated on March 1st, 2014 and is planned to span three years. The database has a spatial resolution of 300-m, includes 36 land cover classes, and has primarily been developed based on observation from the MERIS and SPOT VEGETATION programs (data from ESA SAR sensors are applied for land cover discrimination). The 2010 database representing the 2008-2012 epoch was used in this work. The mapping of ESA-CCI categories to FINN categories (see Table 4) is shown in Table 6 and depicted in Figure 8.

Table 6. Mapping between ESA-CCI and FINN (ref. Table 4) for selected land cover categories.

ESA Description	ESA Code	FINN Code
Mosaic cropland (>50%) / natural vegetation (tree, shrub, herbaceous cover) (<50%)	30	9
Mosaic natural vegetation (tree, shrub, herbaceous cover) (>50%) / cropland (<50%)	40	2
Tree cover, broadleaved, evergreen, closed to open (>15%)	50	3,3,3
Tree cover, broadleaved, deciduous, closed to open (>15%)	60	3,4,5
Tree cover, broadleaved, deciduous, closed (>40%)	61	3,4,5
Tree cover, broadleaved, deciduous, open (15-40%)	62	3,4,5
Tree cover, needleleaved, evergreen, closed to open (>15%)	70	6,6,5
Tree cover, needleleaved, evergreen, closed (>40%)	71	6,6,5
Tree cover, needleleaved, evergreen, open (15-40%)	72	6,6,5
Tree cover, needleleaved, deciduous, closed to open (>15%)	80	6,6,5
Tree cover, needleleaved, deciduous, closed (>40%)	81	6,6,5
Tree cover, needleleaved, deciduous, open (15-40%)	82	6,6,5
Tree cover, mixed leaf type (broadleaved and needleleaved)	90	3,4,5
Mosaic tree and shrub (>50%) / herbaceous cover (<50%)	100	3,4,5
Mosaic herbaceous cover (>50%) / tree and shrub (<50%)	110	1
Shrubland	120	2
Deciduous shrubland	122	2
Grassland	130	1
Lichens and mosses	140	1
Sparse vegetation (tree, shrub, herbaceous cover) (<15%)	150	1
Sparse shrub (<15%)	152	2
Sparse herbaceous cover (<15%)	153	1
Tree cover, flooded, fresh or brakish water	160	3,4,5
Tree cover, flooded, saline water	170	3,4,5
Shrub or herbaceous cover, flooded, fresh/saline/brakish water	180	2

Figure 8. Land cover representations in the (a) MODIS LCT, (b) GLC-SHARE, and (c) ESA-CCI global products mapped to FINN categories. Note that these databases do not specify crop types.

(a)

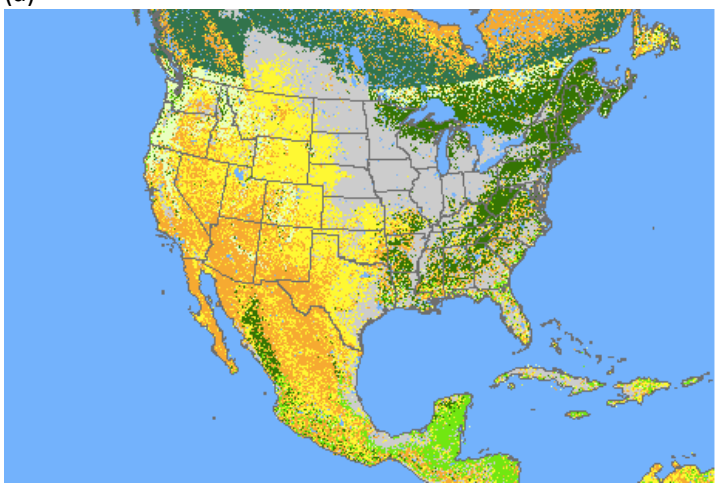

(b)

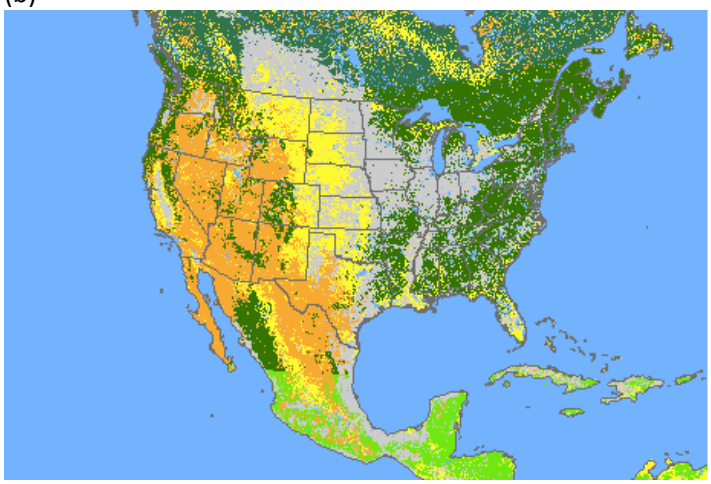

(c)

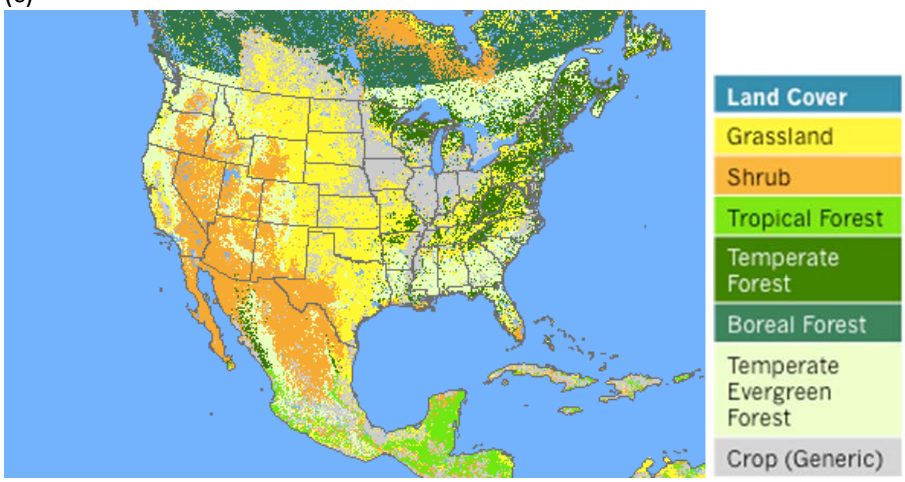

4.2 U.S. National Products

4.2.1 U.S. Forest Service Fuel Characteristic Classification System (FCCS)

The FCCS database (http://www.landfire.gov/NationalProductDescriptions25.php) was developed to characterize wildland fuels and capture the diversity of fuelbeds throughout much of North America for fire behavior, fire effects, and dynamic vegetation models (http://www.fs.fed.us/pnw/fera/publications/factsheets/factsheet_fccs.pdf; http://www.fs.fed.us/pnw/fera/fft/fccsmodule.shtml; http://www.fs.usda.gov/ccrc/tools/fccs). It provides the fire hazard of each fuelbed, including its surface fire behavior potential, crown fire potential, and available fuel potential, surface fire behavior, and combustible carbon. The FCCS classified fuels into six horizontal fuelbed strata including canopy, shrubs, herb, woody fuels, litter-lichen-moss, and ground fuels. Strata are further divided into categories and subcategories with common combustion characteristics. The spatial resolution of the data applied here was 1 km. The mapping of FCCS categories to FINN categories (see Table 4) is shown the Appendix and depicted in Figure 9.

4.2.2 USDA National Agricultural Statistical Service Cropland Data Layer (CDL)

Data for the identification and characterization of croplands were obtained from the U. S. Department of Agriculture National Agricultural Statistical Service (NASS) Cropland Data Layer (CDL; http://nassgeodata.gmu.edu/CropScape/). The CDL is an annual product providing crop-specific land cover data using satellite imagery and extensive agricultural ground truth collected during the growing season (http://www.nass.usda.gov/research/Cropland/SARS1a.htm). The 2012 product with 30-m spatial resolution was used in this work. The product included 121 total land cover classes for the continental United States, 107 of which were agricultural with the remaining associated with the 2001 U.S. Geological Survey (USGS) National Land Cover Dataset (NLCD). The CDL was not used as a stand-alone product for our work but was mapped to croplands in the FCCS or TCEQ datasets, respectively. Only crops for which emission factors were available (see Table 4) replaced generic croplands in the FCCS or TCEQ data; all other agricultural classes continued to be identified as generic croplands. The mapping of the FCCS_CDL dataset is depicted in Figure 9.

Figure 9. Land cover representations in the (a) FCCS and (b) FCCS_CDL products mapped to FINN categories.

(a)

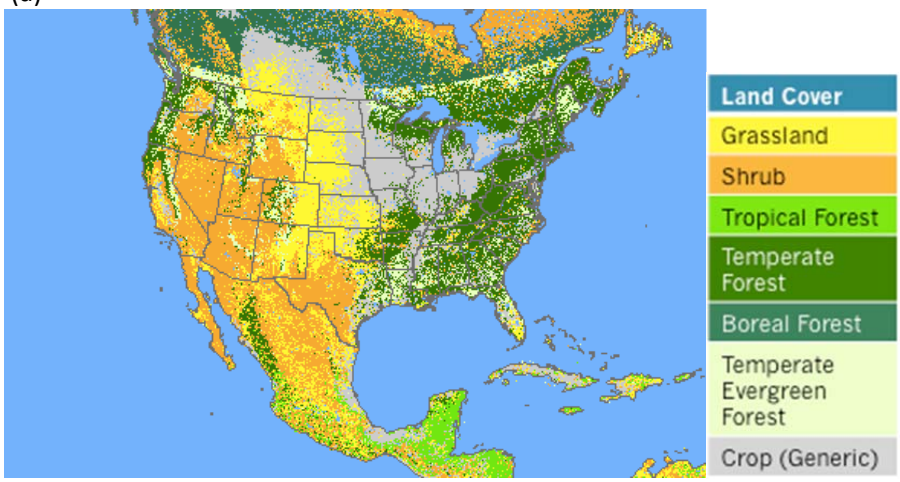

(b)

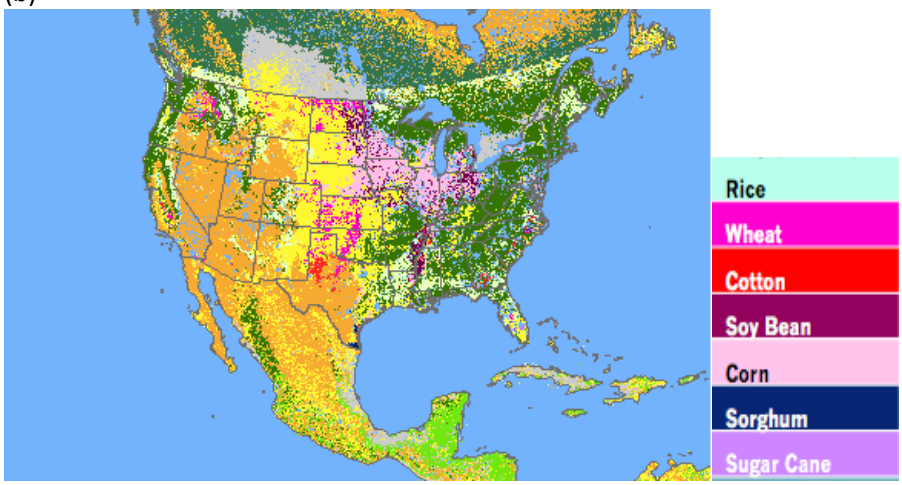

4.3 TCEQ Regional Land Cover Product

A regional land cover product for air quality modeling in Texas was developed by Popescu et al. (2011) for the Texas Commission on Environmental Quality (TCEQ) by combining three existing databases: LANDFIRE (previously known as the Landscape Fire and Resources Management Planning Tools Project from 2004 to 2009), the 2001 National Land Cover Dataset (NCLD) and the Texas Parks and Wildlife Department (TPWD) Texas Ecological System Classification Project. The LANDFIRE and 2001 NLCD products were derived from Landsat imagery (Rollins et al., 2009; Homer et al., 2007); the TPWD Texas Ecological System Classification Project relied on field data collection and aerial photography to provide a land classification map at 10-m resolution for Texas (http://tpwd.texas.gov/landwater/land/maps/gis/tescp/index.phtml). As shown in Figure 10a, this regional land cover product consisted of 36 land cover categories with 30-m spatial resolution. Similar to the approach with the FCCS product, the TCEQ dataset was considered with and without the CDL data for specific crop types in this work; these datasets are shown in Figure 10b mapped to the FINN categories.

Figure 10. (a) The TCEQ dataset developed by Popescu et al. (2011) and (b) the TCEQ and (c) TCEQ_CDL data product mapped to FINN categories.

(a)

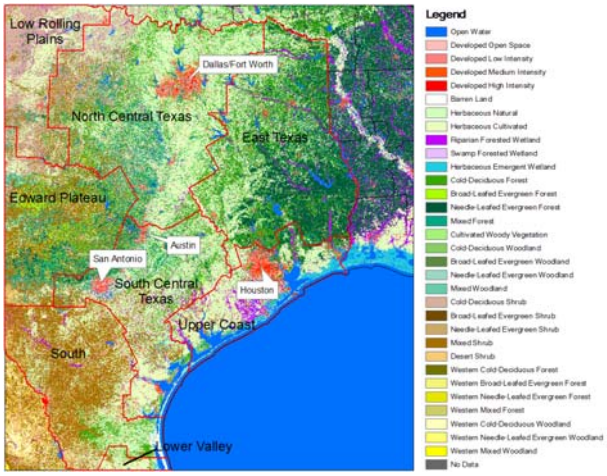

(b)

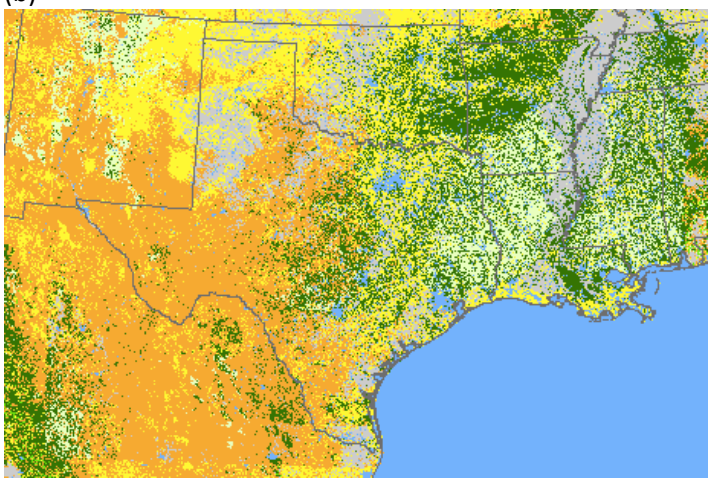

(c)

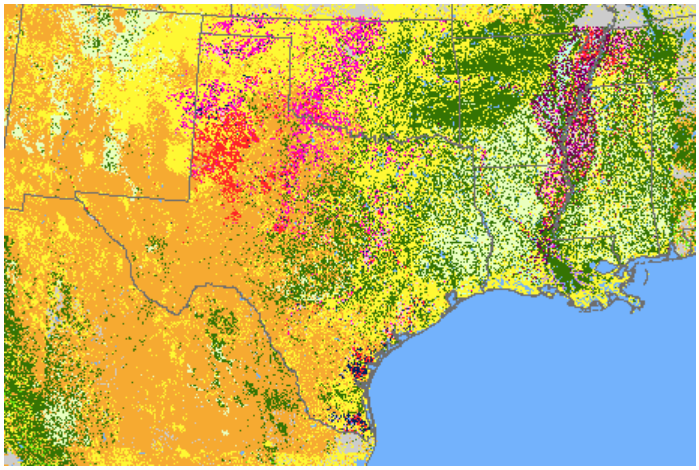

4.4 Intercomparison of Fuel Loading Estimates

Fuel loadings for forest and herbaceous vegetation were assigned for the aforementioned land cover datasets. The FCCS dataset includes not only land cover classification, but also fuel loading information associated with each FCCS land cover classification. Fuel loadings for each fuel component (including duff, herb, various woody fuels) are included in this dataset. The sum of canopy and downed wood fuel were designated as the "TREE" fuel class for our purposes, and the sum of shrub, herb, litter-lichen-moss, and ground fuels (duff etc.) were designated as the "HERB" fuel class (http://www.fs.fed.us/pnw/fera/products/tutorials/fccs/fccs_tutorial_html/index.htm). For each land cover type within each land cover product described in Sections 4.1 and 4.2, these two values were determined from the co-located FCCS values. .

In the case of croplands, fuel loadings from Akagi et al. (2011), McCarty et al. (2012), and Wiedinmyer et al. (2011) were applied to the specific and generic crop classes. Croplands were assumed to have only herbaceous cover. As described in Section 3.1, fuel loadings were estimated by taking the weighted average of the spatially overlapping fuel loadings of the FCCS class for each land cover class. With the exception of land cover in urban areas, all FCCS land cover types were represented within CONUS, including water, barren, and agriculture, at a spatial resolution of 30 meters. Fuel loadings of each land cover dataset are provided in the Appendix. Figure 11 shows weighted averages of fuel loadings for all fire events during 2012 for selected land cover products (MODIS LCT, ESA, and TCEQ) within each of the six geographic regions (ref. Figure 1) for illustrative purposes. It shows that fuel loadings may vary considerably even for identical FINN generic land cover types, because the underlying land cover type differs by land cover product.

4.4 References

Akagi, S. K., R. J. Yokelson, C. Wiedinmyer, M. J. Alvarado, J. S. Reid, T. Karl, J. D. Crounse, P. O. Wennberg. Emission factors for open and domestic biomass burning for use in atmospheric models, *Atmospheric Chemistry and Physics*, 11(9), 4039-4072, 2011.

McCarty, JL, G. Pouliot, S.M. Raffuse, M. Ruminski, J.J. Szykman, Amber J. Soja. Using Satellite data to Quantify Cropland Burning and Related Emissions in the Contiguous United States: Lessons Learned. Presented at the US EPA Emissions Inventory Conference, August 2012, Tampa Florida. http://www.epa.gov/ttnchie1/conference/ei20/session2/jmccarty.pdf

Popescu, S. C., Stukey, J., Mutlu, M., Zhao, K., Sheridan, R., Ku, N. W. (2011). Expansion of Texas Land Use/Land Cover through Class Crosswalking and Lidar Parameterization of Arboreal Vegetation Secondary Investigators. Retrieved June 8, 2015 from https://www.tceq.texas.gov/assets/public/implementation/air/am/contracts/reports/oth/582056459 3FY0925-20110419-tamu-expension_tx_lulc_arboreal_vegetation.pdf.

Wiedinmyer, C., S. K. Akagi, R. J. Yokelson, L. K. Emmons, J. A. Al-Saadi, J. J. Orlando, A. J. Soja. The Fire INventory from NCAR (FINN): A high resolution global model to estimate the emissions from open burning, *Geoscientific Model Development*, 4(3), 625-641, 2011.

Figure 11. Fuel loadings for tree and herbaceous fuels by land cover product (MODIS LCT, ESA, TCEQ); values are averaged for 2012 fire events by FINN land cover class within six geographic regions shown in Figure 1.

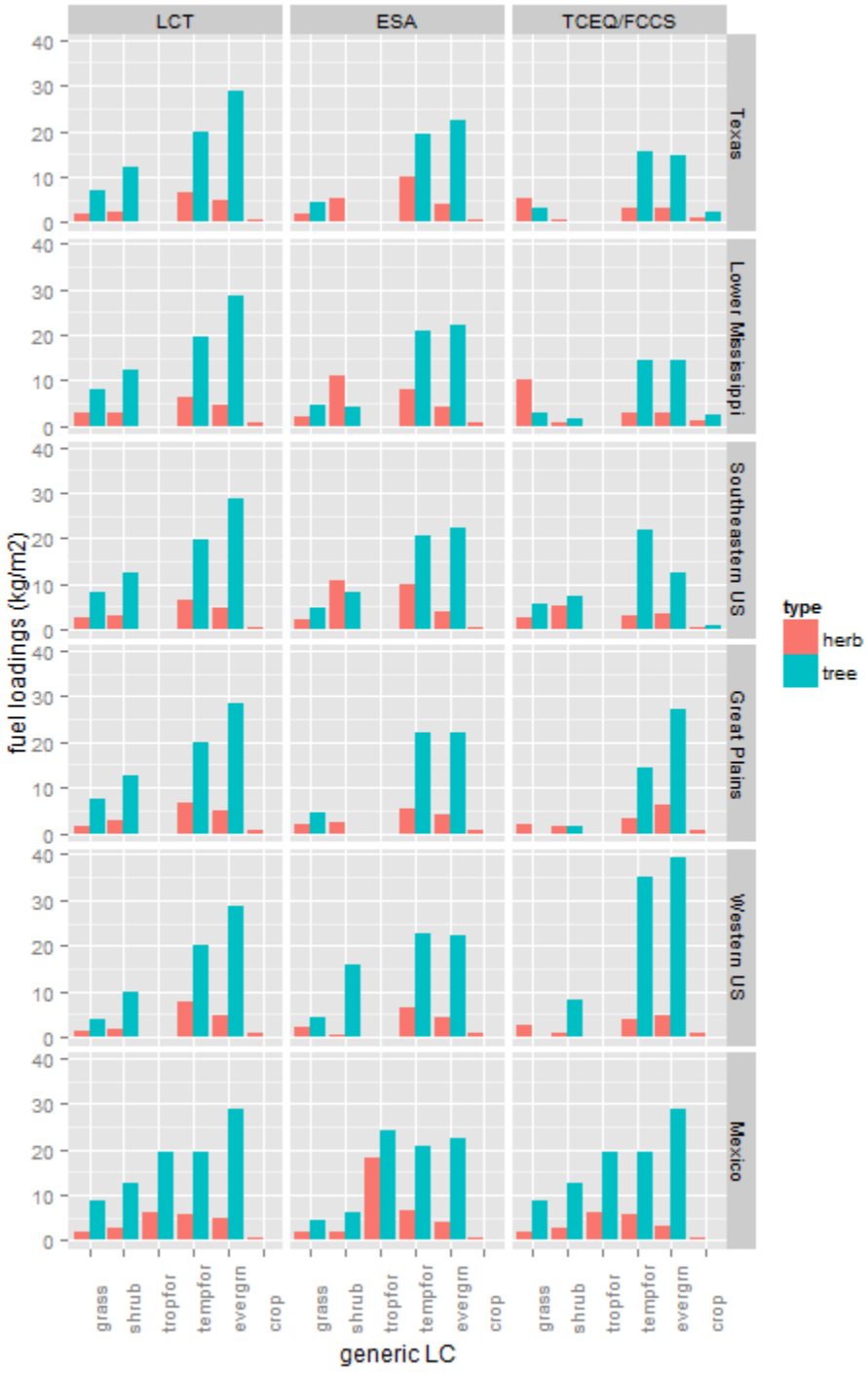

5. Fire Emissions Estimates and Implications for Air Quality Predictions

5.1 Scenarios

Simulations with the updated version of FINN were conducted to examine the effects of using the different land cover data products on estimated emissions. Seven scenarios were investigated:

Global:
Scenario 1 = MODIS LCT ONLY
Scenario 2 = GLC-SHARE ONLY
Scenario 3 = ESA ONLY

U.S. National:
Scenario 4 = FCCS in the continental US and MODIS LCT elsewhere
Scenario 5 = FCCS_CDL in the continental US and MODIS LCT elsewhere

Texas Regional:
Scenario 6 = TCEQ in the Texas regional domain, FCCS in the continental US, and MODIS LCT elsewhere
Scenario 7 = TCEQ_CDL in the Texas regional domain, FCCS in the continental US, and MODIS LCT elsewhere

The scenarios were designed with several objectives in mind. FINN is ultimately a global model. As such, a global land cover data product provides a consistent default for global-scale climate and air quality models and in the absence of regional data. Thus, one objective was to evaluate alternatives to the MODIS global LCT product. Another objective was to evaluate the use of available regional datasets in place of the global land cover information. For example, the FCCS was a resource for fuelbed information that could be related to FINN land cover classes as an alternative to the MODIS LCT for the United States. Simulations with and without the identification of key U.S. crop types were conducted to determine the spatial and seasonal effects of crop identification on FINN emission estimates. Finally, a key goal was to produce FINN simulations that could be used by the TCEQ in its 2012 air quality modeling, leveraging the regional land cover data available.

5.2 Annual Emissions Estimates

Annual emission estimates for CO, NO_X, and $PM_{2.5}$ by region and land cover product are presented in Figure 12. For the purposes of this study, the MODIS LCT served as the reference case for comparisons between data products, as it has served as the FINN default. Emissions estimates for the three pollutants were approximately -5% to -10% lower with the ESA product than the MODIS LCT in the western U.S.; however, the ESA product generally produced higher emissions estimates (1% to 76%, e.g., contribution to the highest estimate was associated with the ground duff fuel loading of mangroves within Mexico's tropical forests) than the MODIS LCT for all other regions. The GLC product produced higher emission estimates (2% to 27%) than the MODIS LCT product in Texas, the southeastern U.S., and the Great Plains, but lower emissions estimates in Mexico and the western U.S. (-6% to -24%).

The FCCS and FCCS_CDL products produced greater emissions estimates in the Great Plains, most notably for CO and $PM_{2.5}$ (25%-35%), than the MODIS LCT product. Estimates of CO and $PM_{2.5}$ were within 10% of the MODIS LCT product in the southeastern U.S., but estimates of NO_x

were considerably lower (-25% to -30%). Annual emissions estimates were within ±10% in the western U.S.

Use of the TCEQ or TCEQ_CDL products for Texas produced emission estimates that were 10% to 19% higher than the MODIS LCT product; differences between the TCEQ and TCEQ_CDL were negligible statewide during 2012. Similarly in the Lower Mississippi Valley, NO_x emission estimates were higher (15%) with the TCEQ and TCEQ CDL products than the MODIS LCT product; in contrast CO and $PM_{2.5}$ emissions were approximately -10% to -20% lower. Differences between the TCEQ and TCEQ_CDL datasets in the Lower Mississippi Valley were within 3%.

Changes in emissions due to change in land cover products often had similar relative effects with respect to magnitude and directionality for each of the three pollutants. Occasional exceptions were evident though, including differences in the response of NO_x emissions relative to CO and $PM_{2.5}$ for the Lower Mississippi Valley. This may be triggered by combination of factors. In this particular case, grasslands had a relatively greater NO_x emission factor than shrub or forest land cover classes, but the opposite was true for CO emission factors. In addition, grassland in the Lower Mississippi Valley had relatively greater herbaceous fuel loadings for the TCEQ (10.3 kg/m^2) than the MODIS product (2.9 kg/m^2). In contrast, forest fuel was less prominent in the TCEQ product than the MODIS product (e.g., 14.6 kg/m2 for TCEQ evergreen forest "TREE" fuels and 28.6 kg/m2 for MODIS). Collectively these factors combined to predict differential trends in emissions changes between NO_x and CO.

Figure 12. Annual emissions estimates for (a) CO, (b) NOx, (c) $PM_{2.5}$ by region (see Figure 1). Estimates are shown for the MODIS LCT, GLC-SHARE, ESA, and TCEQ and TCEQ_CDL (Texas and Lower Mississippi Valley) or FCCS and FCCS_CDL data products (Southeastern U.S. and Western U.S.). Note difference in scale for the Western U.S and Mexico, and emissions for Mexico reflect those for the entire country, i.e., beyond the boundaries of the CAMx photochemical modeling domain described in Section 5.5.1.

(a)

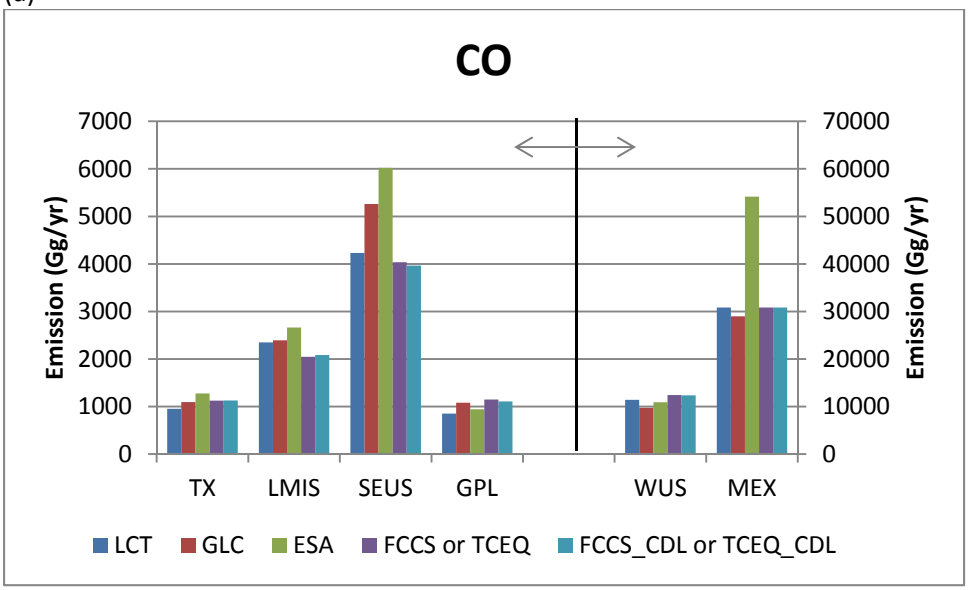

(b)

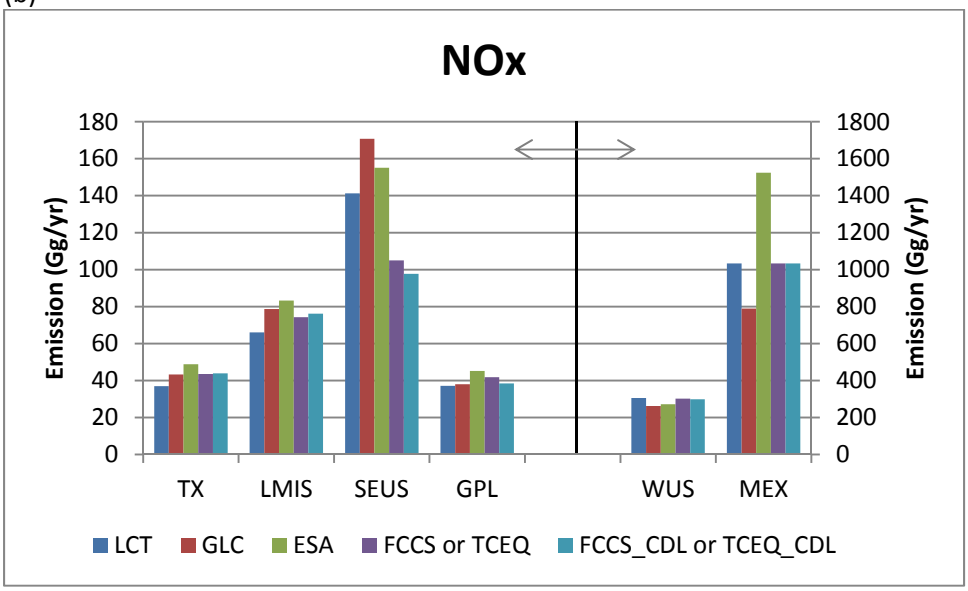

(c)

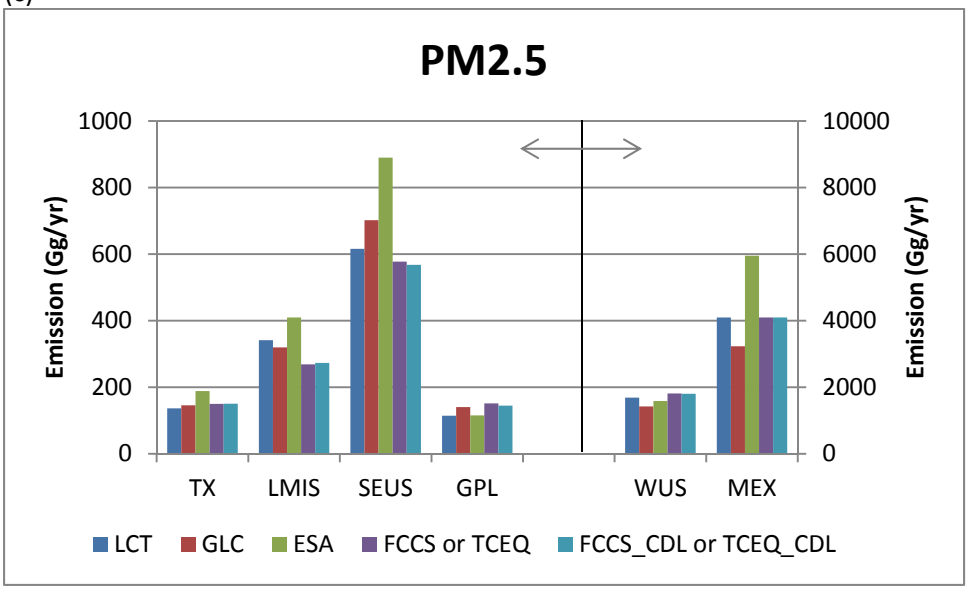
PM2.5
1000
800
600
400
200
0
10000
8000
6000
4000
2000
0
Emission (Gg/yr)
Emission (Gg/yr)
TX
LMIS
SEUS
GPL
WUS
MEX
LCT
GLC
ESA
FCCS or TCEQ
FCCS_CDL or TCEQ_CDL

5.3 CO Emissions by Land Cover Class

Figure 13 shows annual CO emissions estimates by land cover class for each data product in each geographic region. Differences between simulations highlighted the sensitivity of emissions estimates from the FINN model to various land cover inputs and associated fuel loadings and emission factors. Variations were not uniform geographically. Although emissions totals could be similar (for example between the results for the LCT and GLC simulations for Mexico), driving factors and their effects on emissions estimates may not be the same; therefore the ratios between emitted pollutants may not be consistent across simulations with different land cover products.

Land cover products from different sources do not necessarily identify the same land cover type at a given geographic location, as shown in Chapter 4. As an example, the land cover type for a specific fire event could be identified as forest in one product and shrub in another, resulting in different sets of parameters as the basis for emissions estimates. Furthermore, even for a case when the FINN vegetation type classification for a fire event is identical between two land cover products, the underlying land cover types of the original datasets may have different fuel loading values.

Because of the difficulties in attempting to generalize trends across different land cover scenarios, we focused on specific illustrative examples of the nature of changes across scenarios using Texas as a case study. The ESA product produced higher CO emissions estimates in Texas than the other products; large contributions to these estimates were from fires in evergreen forest. Table 7 shows a contingency table of FINN GIS preprocessor output records in Texas between the MODIS and ESA products; a total of 5,985 emission records were grouped by FINN land cover type. Land cover for many burned areas was identified as evergreen forest by the ESA dataset, but as another type by MODIS (blue column, Table 7a). Note that this was not the case for the evergreen forest class in the MODIS product (pink row, Table 7a). The orange cells in Table 7b show changes in CO emissions for burned areas that were identified as either of two types of forest by both land cover products. Areas identified as evergreen forest by ESA were estimated to have lower CO emissions than those similarly classified by MODIS (i.e., lower by 14.2 Gg for areas that were identified as evergreen forest by both inventories and by 59.4 Gg for areas identified as temperate forest by MODIS and evergreen forest by ESA). Thus, the CO emission estimate from FINN is smaller for the ESA inventory for individual fires. However increases in the number of fires occurring in evergreen forest leads to the overall greater estimate of CO emission with the ESA product relative to the MODIS product.

A second example was the relatively smaller contribution of shrub lands to CO emissions when the TCEQ land cover product was utilized as an alternative to the MODIS product. Table 8a is the contingency table between land cover types for the MODIS and TCEQ products. Purple cells in Table 8a shows the count of burned area polygons identified as shrub. Despite the smaller CO emissions estimate by the TCEQ product, the record count was actually greater for the TCEQ product (1318) than the MODIS product (1188). Two factors contributed to the smaller CO emissions estimate for shrubs from the TCEQ product. Fuel loadings were smaller for the TCEQ products: herbaceous fuel loadings were 2.49 kg/m^2 for the MODIS product and 0.61 kg/m^2 for the TCEQ product. Tree fuel loadings for the MODIS product were 12.2 kg/m^2, and no report for the TCEQ product. As described in Section 2.4, for polygons that had tree cover of less than 40%, it was assumed that no tree fuel was consumed. None of the 1,318 shrub records for the TCEQ

had tree coverage greater than 40%. Smaller fuel loadings contributed to lower FINN CO emission estimates for shrub lands in the TCEQ dataset than in the MODIS dataset.

Figure 13. Annual CO emissions estimates by land cover class in each data product for (a) Texas, (b) the Lower Mississippi Valley, (c) Southeastern U.S., (d) Great Plains, (e) Western U.S, and (f) Mexico. Note difference in scale in each plot.

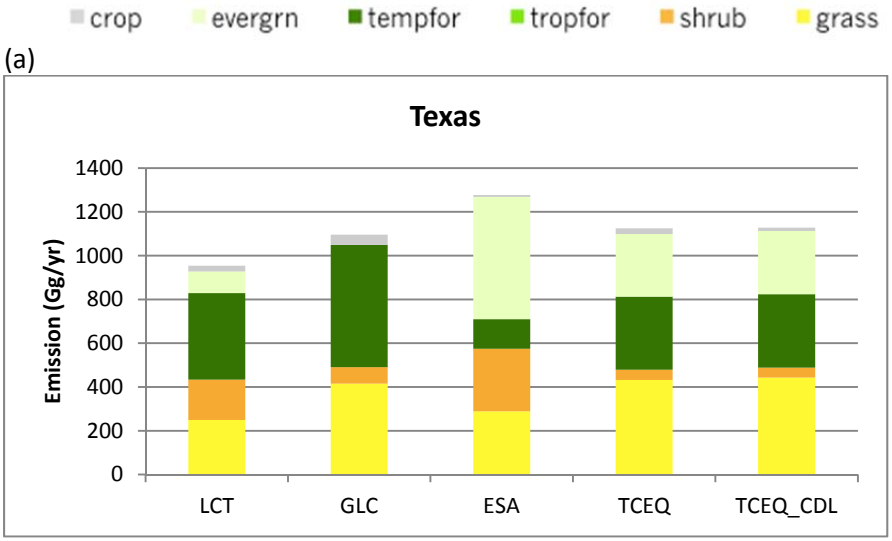

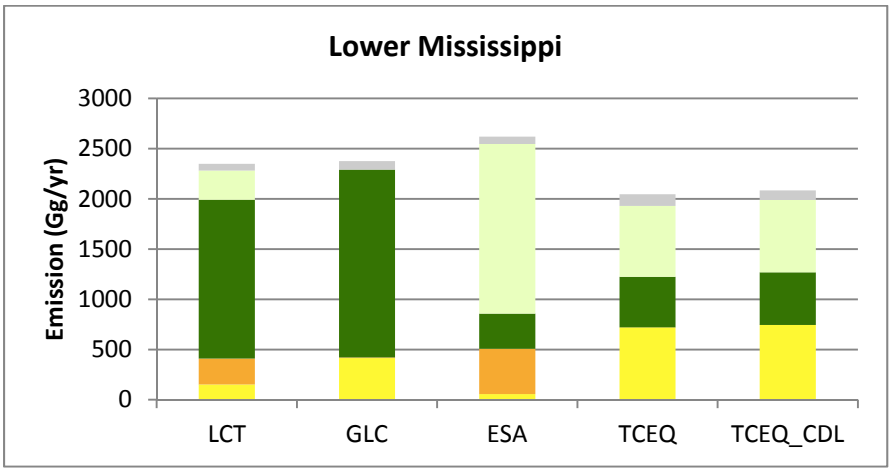

(c)

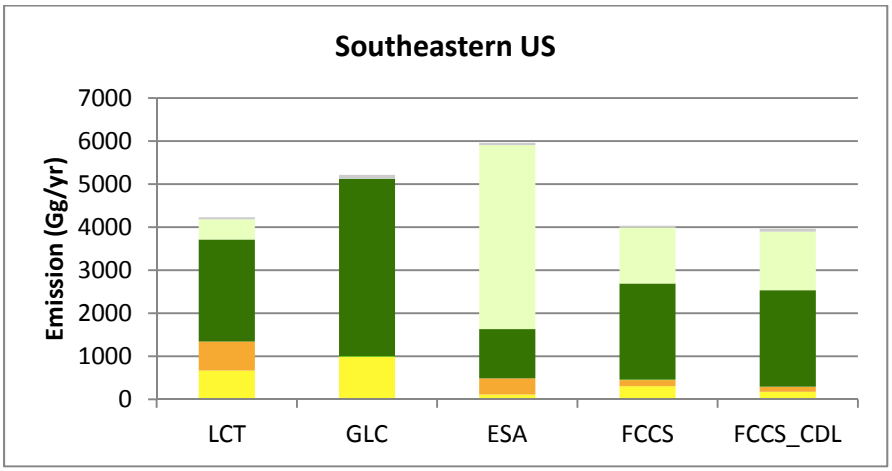
Southeastern US
Emission (Gg/yr)
7000
6000
5000
4000
3000
2000
1000
0
LCT
GLC
ESA
FCCS
FCCS_CDL

(d)

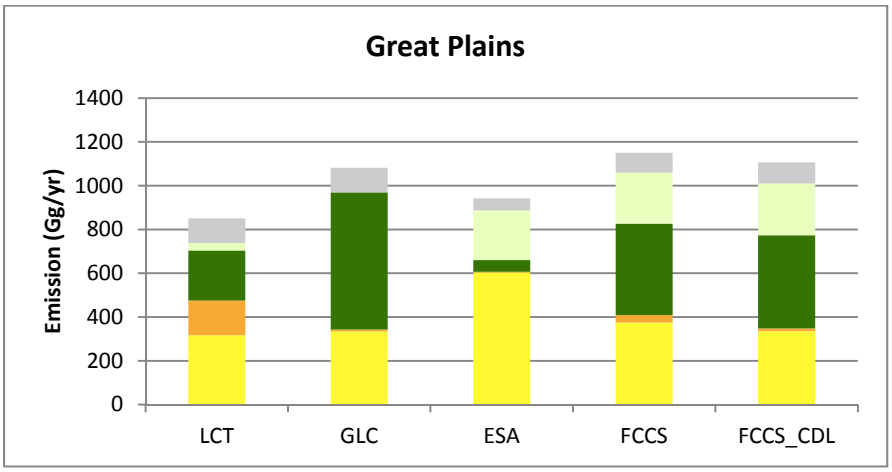
Great Plains
Emission (Gg/yr)
1400
1200
1000
800
600
400
200
0
LCT
GLC
ESA
FCCS
FCCS_CDL

(e)

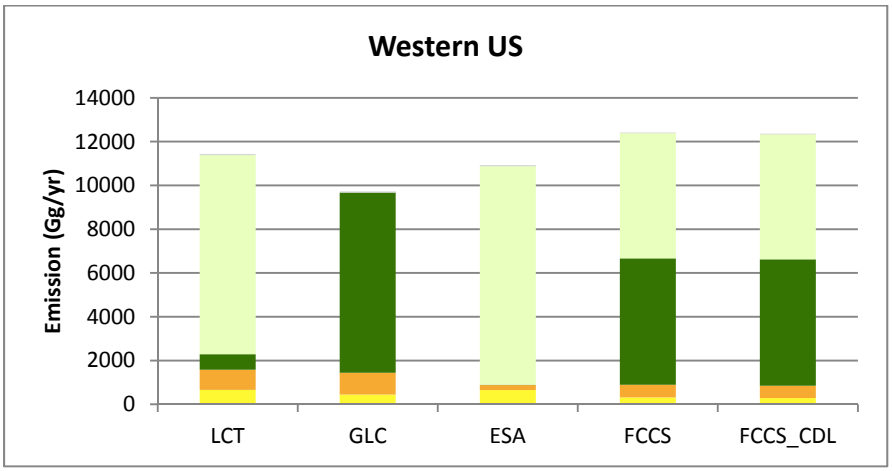
Western US
Emission (Gg/yr)
14000
12000
10000
8000
6000
4000
2000
0
LCT
GLC
ESA
FCCS
FCCS_CDL

(f)

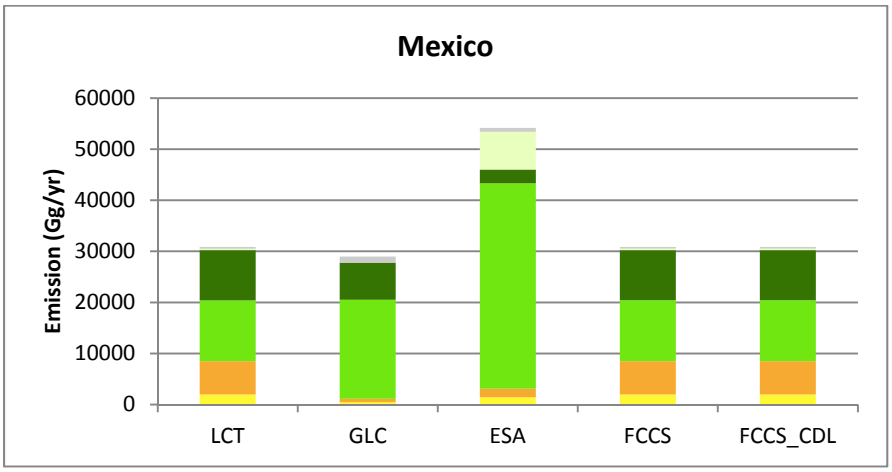
Mexico
Emission (Gg/yr)
60000
50000
40000
30000
20000
10000
0
LCT
GLC
ESA
FCCS
FCCS_CDL

Table 7. Contingency table of fire records between the MODIS LCT and ESA land cover products: (a) count of subdivided burned area polygons and (b) differences in CO emission estimated ($E_{ESA} - E_{MODIS}$) in Gg/yr. Land cover is identified according to FINN categories.

(a)

		ESA Land Cover					Count by MODIS
		Grass	Shrub	Temperate Forest	Evergreen Forest	Crop	
MODIS Land Cover	Grass	2074	490	24	344	160	3092
	Shrub	444	220	29	420	75	1188
	Temperate Forest	78	66	96	383	8	631
	Evergreen Forest	18	16	7	128	0	169
	Crop	710	71	3	33	88	905
Count by ESA		3324	863	159	1308	331	Total = 5985

(b)

		ESA Land Cover					CO Emissions Difference by MODIS
		Grass	Shrub	Temperate Forest	Evergreen Forest	Crop	
MODIS Land Cover	Grass	19.5	46.3	16.5	99.9	-5.5	176.8
	Shrub	-23.8	46.3	16.0	84.2	-3.5	119.2
	Temperate Forest	-31.8	11.4	23.2	-59.4	-6.9	-63.5
	Evergreen Forest	-5.5	5.4	2.8	-14.2	0.0	-11.5
	Crop	41.8	46.0	2.2	11.9	0.0	102.0
CO Emissions Difference by ESA		0.2	155.4	60.8	122.4	-15.9	Total = 323.0

Table 8. Contingency table of fire records between the MODIS LCT and TCEQ land cover products: (a) count of subdivided burned area polygons and (b) differences in CO emission estimated ($E_{TCEQ} - E_{MODIS}$) in Gg/yr. Land cover is identified according to FINN categories.

(a)

		TCEQ land cover					
		Grass	Shrub	Temperate Forest	Evergreen Forest	Crop	Count by MODIS
MODIS Land Cover	Grass	1079	935	631	144	303	3092
	Shrub	258	280	295	243	112	1188
	Temperate Forest	110	20	155	343	3	631
	Evergreen Forest	28	0	18	123	0	169
	Crop	450	83	154	18	200	905
Count by TCEQ		1925	1318	1253	871	618	Total = 5985

(b)

		TCEQ land cover					CO Emissions Difference by MODIS
		Grass	Shrub	Temperate Forest	Evergreen Forest	Crop	
MODIS Land Cover	Grass	65.6	-26.6	101.1	29.1	-7.5	161.8
	Shrub	36.6	-13.8	23.9	20.0	-3.6	63.1
	Temperate Forest	10.3	-5.8	-43.3	-94.8	-1.2	-134.7
	Evergreen Forest	6.6	0.0	-3.1	-32.4	0.0	-29.0
	Crop	65.7	0.6	33.9	6.0	3.1	109.3
CO Emissions Difference by TCEQ		184.8	-45.5	112.5	-72.1	-9.2	Total = 170.5

5.4 Contributions of Croplands to Monthly CO Emissions Estimates

Figure 14 shows monthly CO emission estimate by FINN land cover class for the TCEQ_CDL scenario for the Lower Mississippi region and the FCCS_CDL scenario for the Great Plains, respectively. These regions had the largest signals from crop emissions of the six regions that were evaluated in the study. Emissions from croplands exhibited seasonality that differed by crop type and also from natural vegetation. For the Lower Mississippi Valley, emissions from agricultural fires in the spring were on lands used for wheat and soy farming; in the summer from corn farming, and then in the fall from sugarcane fields. In the Great Plains, spring had contributions from lands used for corn farming, whereas summer and fall had emissions from wheat fields. Contributions from these agricultural burnings activities were a minor contribution to regional total emissions, which were primarily from fires from natural vegetation.

Figure 14. Monthly CO emissions estimates by land cover class for selected land cover scenarios: (a) TCEQ_CDL scenario for the Lower Mississippi Valley and (b) FCCS_CDL scenario for the Great Plains. The top plot in each shows all FINN land cover types whereas the bottom plot shows only crops.

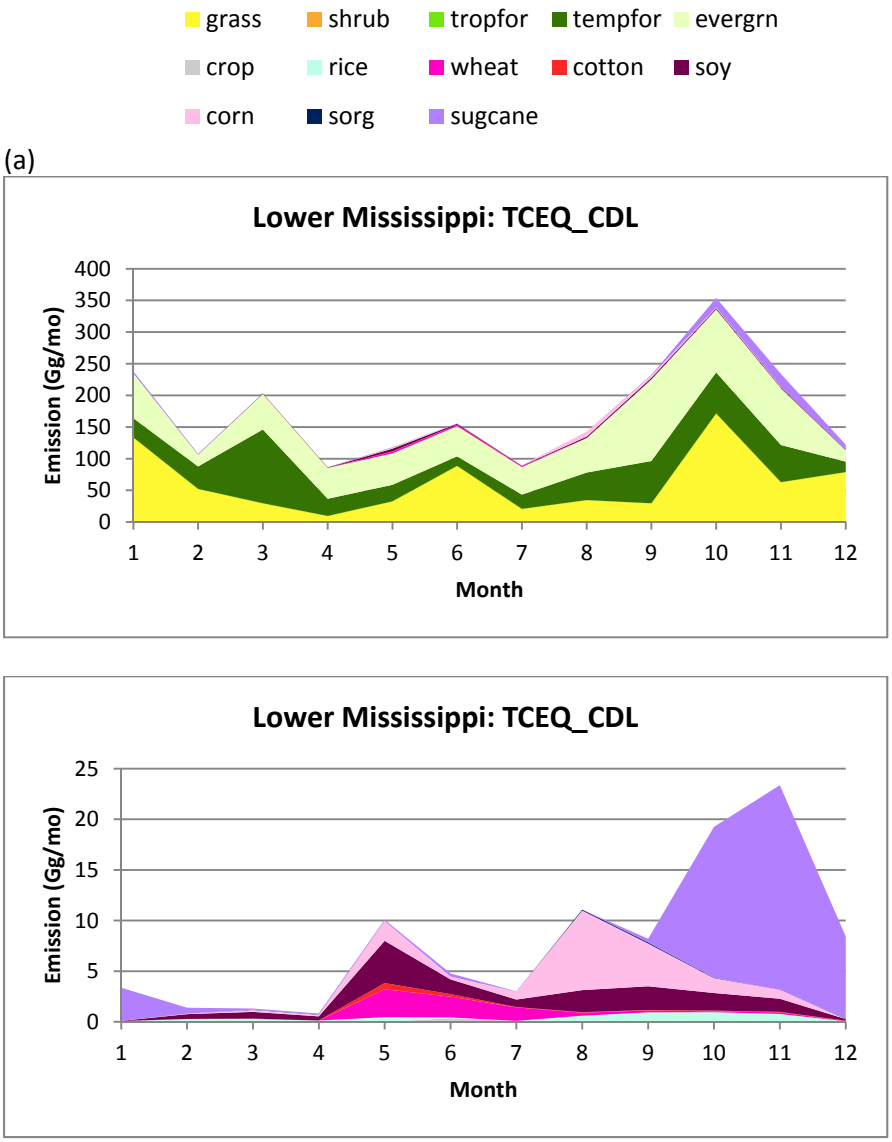

(b)

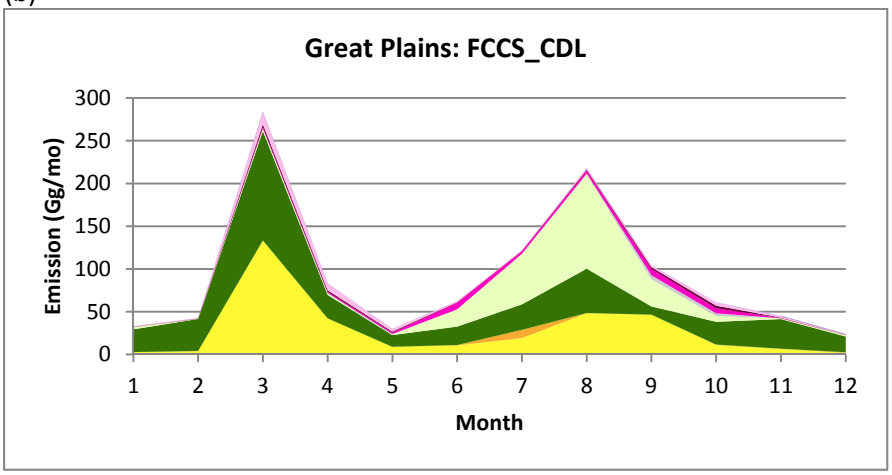
Great Plains: FCCS_CDL
Emission (Gg/mo)
300
250
200
150
100
50
0
1
2
3
4
5
6
7
8
9
10
11
12
Month

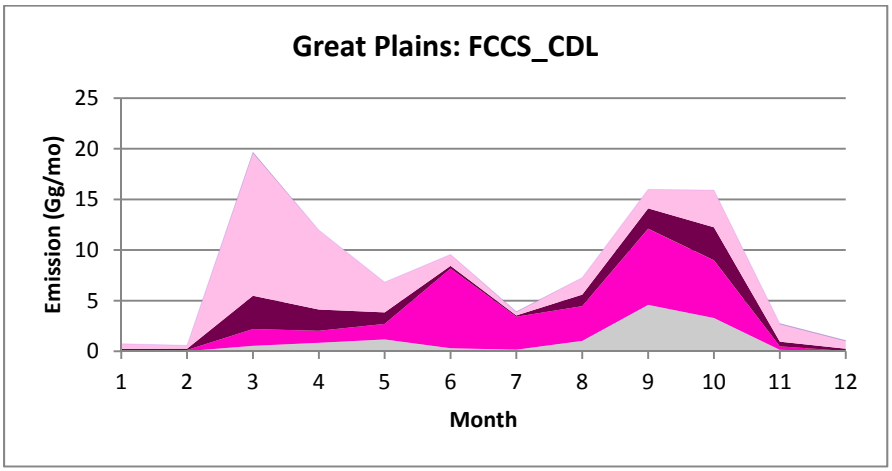
Great Plains: FCCS_CDL
Emission (Gg/mo)
25
20
15
10
5
0
1
2
3
4
5
6
7
8
9
10
11
12
Month

5.5 Implications for Regional Air Quality

5.5.1 CAMx Configuration

CAMx v6.20 (Ramboll Environ, 2015) was run for several FINN emission scenarios using a photochemical modeling dataset developed by the TCEQ spanning May 16 – June 30, 2012 (https://www.tceq.texas.gov/airquality/airmod/data/results?2012). The model configuration and default input data are summarized in Table 9. The modeling domain is shown in Figure 15 and includes a 36-km grid over the continental US, a 12 km grid over the south-central US, and a 4-km grid over eastern Texas. The vertical grid consists of 28 layers spanning from the surface to approximately 14 km (Table 10). Modeling did not include explicit top boundary conditions that can now be developed for CAMx v6.20 from GEOS-Chem or MOZART global chemistry model output (Kemball-Cook et al., 2014).

Daily FINNv2 fire emissions speciated to MOZART-4 were developed for the entirety of 2012. Several FINNv2 scenarios were prepared for the May-June 2012 modeling episode by speciating to the CB6r2 chemistry mechanism and converting to the CAMx input point source format using a suite of processors developed by Ramboll Environ. These processors are compatible with an updated version of the Emission Processing System (EPS v3.22) recently developed for the TCEQ (Jimenez and Yarwood, 2015). EPS3 was run using the following modules and associated pre/post-processors:

Name	Purpose
FIRESPEC	Windows and maps fire coordinates (latitude/longitude) to model domain projection, maps MOZART-4 species to CAMx CB6r2 compounds
GROUPPTS	Groups individual FINN pixel records into larger fire complexes according to a "Fire ID" now available in FINNv2 files
PREFIR	Reads pre-processed fire data and converts to EPS3 EMBR formats
CHMSPL	Speciates emissions (since this is already done in FIRESPEC, this just involves units conversion from tons/day to moles or grams/day)
TMPRL	Allocates emissions temporally to each hour of the day
PSTFIR	Allocates emissions vertically and outputs results in binary point source files
PTSMRG	Merges FINN fire point sources with TCEQ-developed anthropogenic point sources

A FINN emissions file consists of daily emission estimates for each ~1 km^2 fire pixel. Chemical species include NOx, CO, SO_2, NH_3, various PM components, and NMOC allocated to MOZART-4 species (Table 3). All gases are given in units of mol/day, while PM components are given in kg/day. Additional pertinent information includes the coordinates of each fire pixel (latitude/longitude), a "Fire ID" that indicates whether a particular fire pixel is part of a larger fire complex polygon, land cover type, and area burned (m^2). The FIRESPEC preprocessor removes fires outside of the CAMx 36 km domain and remaps the MOZART-4 species to CAMx CB6r2 species listed in Table 11. GROUPPTS uses new information available in the FINNv2 files (Fire ID) to group individual fire points into a larger fire complex (see Section 3.1.2). This approach replaces the old GROUPPTS methodology used with FINNv1 that was based simply on finding fire points within 5 km of each other. PREFIR then formats the FINN data into emission binary record (EMBR) files for EPS3 processing. PREFIR includes an option to combine individual fires if: (1) they are in the same grid cell; (2) share the same "county" designation and SCC code

(to determine local time zone); and (3) share the same fire class assignment of a common fire complex.

Table 9. Model configuration and default input data developed by TCEQ for the 2012 CAMx modeling episode (Source: http://www.tceq.texas.gov/airquality/airmod/data/tx2012).

Model Component	Description
Modeling Period	May 16 – June 30, 2012
CAMx Version	6.20
Horizontal Domain	36km/12km/4km (Figure 15)
Vertical Structure	28 Vertical Layers (Table 10)
Meteorological Model	WRF v3.6.1 “p2a/i2”, Kv using CMAQ method, “kv100” patch
Chemical Mechanism	CB6r2
Boundary Conditions	GEOS-Chem
Emissions	TCEQ 2012 “reg3a”

Figure 15. CAMx 36km/12km/4km nested modeling grids. (Source: http://www.tceq.texas.gov/airquality/airmod/data).

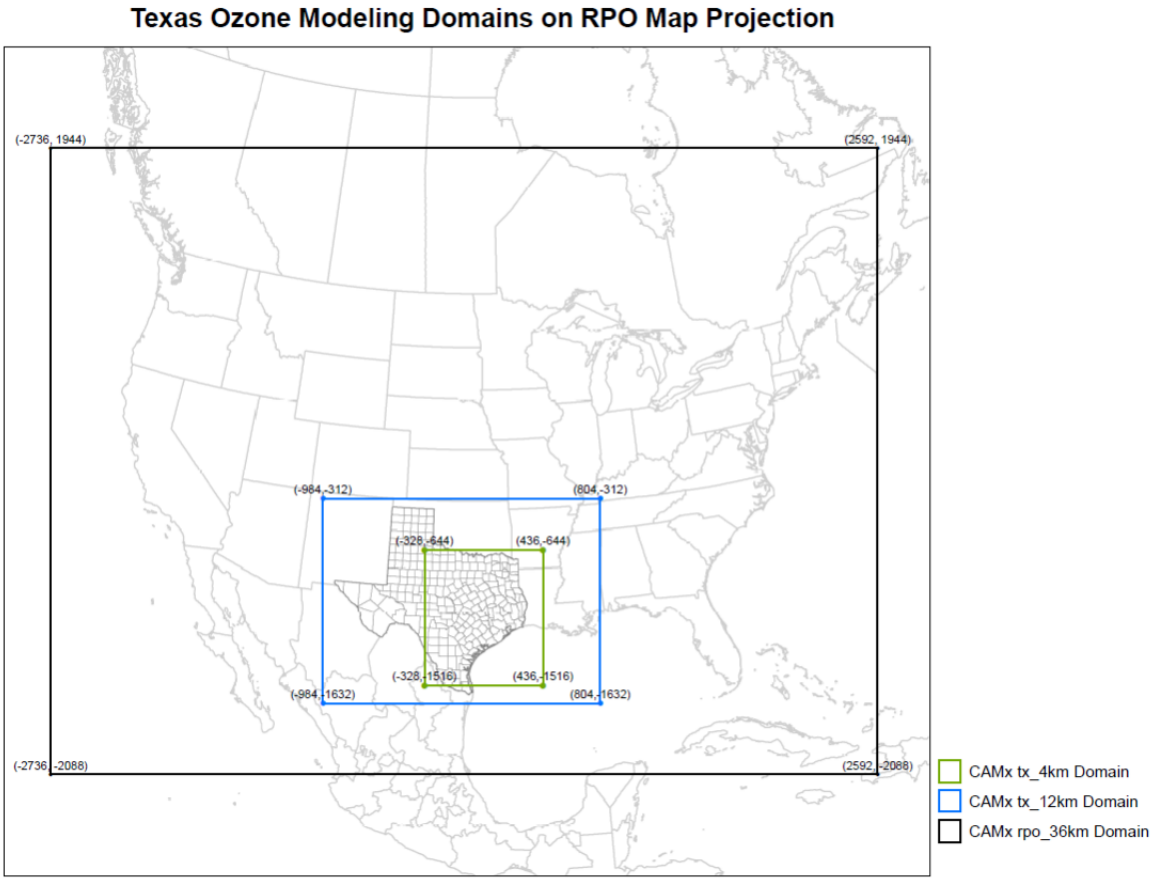

Table 10. Mapping between WRF and CAMx model vertical layer structures for the May-June 2012 modeling database. The WRF domain extends to ~20 km (50 hPa) with 43 layers. http://www.tceq.texas.gov/airquality/airmod/rider8/modeling/domain.

Corresponding WRF Layer	Layer Top (m AGL)	CAMx Layer	Layer Center (m AGL)	Thickness (m)
38	15179.1	28	13637.9	3082.5
36	12096.6	27	10631.6	2930.0
32	9166.6	26	8063.8	2205.7
29	6960.9	25	6398.4	1125.0
27	5835.9	24	5367.0	937.9
25	4898.0	23	4502.2	791.6
23	4106.4	22	3739.9	733.0
21	3373.5	21	3199.9	347.2
20	3026.3	20	2858.3	335.9
19	2690.4	19	2528.3	324.3
18	2366.1	18	2234.7	262.8
17	2103.3	17	1975.2	256.2
16	1847.2	16	1722.2	249.9
15	1597.3	15	1475.3	243.9
14	1353.4	14	1281.6	143.6
13	1209.8	13	1139.0	141.6
12	1068.2	12	998.3	139.7
11	928.5	11	859.5	137.8
10	790.6	10	745.2	90.9
9	699.7	9	654.7	90.1
8	609.7	8	565.0	89.3
7	520.3	7	476.1	88.5
6	431.8	6	387.9	87.8
5	344.0	5	300.5	87.1
4	256.9	4	213.8	86.3
3	170.6	3	127.8	85.6
2	85.0	2	59.4	51.0
1	33.9	1	17.0	33.9

Table 11. Mapping of MOZART-4 species to CAMx CB6r2 species. Note that FPRM, PSO4, and PNO3 are allocated using default WRAP profiles for agricultural burning (applied to shrubs, grasslands, and agricultural burning) and for wildfires (applied to all forest fires).

CAMx	MOZART4	Scale	MW(g/mol)	Gas or Aerosol
NO	NOx	0	46	G
NO2	NOx	1	46	G
CO	CO	1	28	G
FORM	CH2O	1	30	G
ALD2	CH3CHO	1	44	G
ALDX	GLYALD	1	44	G
ETOH	C2H5OH	1	46	G
MEOH	CH3OH	1	32	G
ETHA	C2H6	1	30	G
PAR	C3H6	1	14.5	G
PAR	BIGENE	1.7	14.5	G
PAR	BIGALK	5	14.5	G
PAR	C3H8	1.5	14.5	G
PAR	MEK	3	14.5	G
PAR	C2H2	1	14.5	G
PAR	HYAC	3	14.5	G
ETH	C2H4	1	28	G
OLE	C3H6	1	28	G
OLE	BIGENE	1	28	G
ISOP	ISOP	1	68	G
TERP	C10H16	1	136	G
TOL	TOLUENE	0.3	92	G
XYL	TOLUENE	0.1	106	G
BENZ	TOLUENE	0.6	78	G
ACET	CH3COCH3	3	58	G
KET	MEK	1	28	G
ISPD	MACR	1	64	G
ISPD	MVK	1	64	G
CRES	CRESOL	1	112	G
OPEN	BIGALD	1	80	G
MGLY	CH3COCHO	1	72	G
AACD	CH3COOH	1	60	G
FACD	HCOOH	1	46	G
SO2	SO2	1	64	G
NH3	NH3	1	17	G
TOLA	TOLUENE	0.3	92	G
XYLA	TOLUENE	0.1	106	G
ISP	ISOP	1	68	G
TRP	C10H16	1	136	G
NR	C2H2	1	16	G
NR	C3H8	1.5	16	G
NR	TOLUENE	0.5	16	G
NR	BIGENE	0.3	16	G
CH3CN	CH3CN	1	41	G
HCN	HCN	1	27	G

CH4	CH4	1	16	G
POA	OC	1.7	1	A
PEC	BC	1	1	A
CPRM[1]	PM10	1	1	A
CPRM[1]	PM25	-1	1	A
FPRM[2]	PM25	1	1	A
FPRM[2]	OC	-1.7	1	A
FPRM[2]	BC	-1	1	A
PSO4[3]	PM25	0	1	A
PNO3[3]	PM25	0	1	A

[1] CPRM contains coarse-mode PM mass between 2.5-10 microns.

[2] FPRM contains non-carbon fine-mode PM mass.

[3] Sulfate (PSO4) and nitrate (PNO3) are allocated from FPRM inside the FIRESPEC module.

The EPS3 TMPRL module applies a single diurnal profile in local time to all fires such that emissions are highest in the early afternoon and lowest at night (Figure 16). The time zone of each fire is assigned based on its longitude relative to 15-degree longitudinal zones. Any emissions allocated to the next date due to a time zone shift are assigned to the same hour of the current date to conserve daily total emissions mass per daily emissions file. The emissions are then shifted to the CAMx time zone to coincide with the other model inputs.

Figure 16. Diurnal distribution of fire emissions applied in the EPS3/TMPRL module.

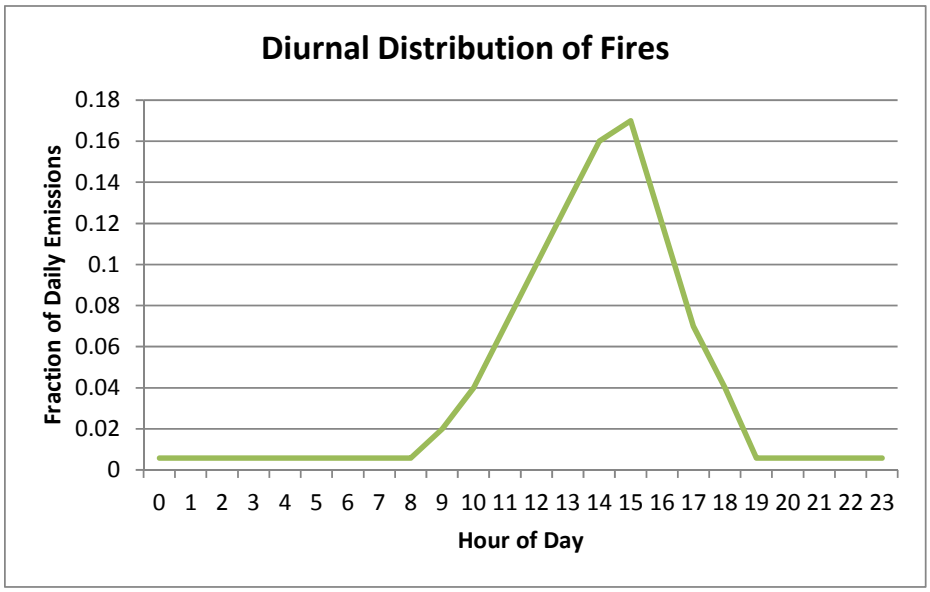

PSTFIR incorporates the WRAP methodology (http://www.wrapair.org/forums/fejf/documents/WRAP_2002_PhII_EI_Report_20050722.pdf) to vertically allocate fire emissions each hour. The aggregated daily area burned for each fire complex (determined in GROUPPTS) is used to classify each fire complex into one of five size bins. This approach replaces the old PSTFIRE methodology used with FINNv1 that classified fire size according to a linear regression between NOx emissions and area burned. The fire size classification determines the fraction of emissions allocated to the CAMx surface layer and to the elevated plume, and defines the top and bottom heights of the elevated plume, for each hour of the day (Figure 17). A single point source is used to represent elevated emissions from each fire complex using the new EPS3/CAMx capability to define initial plume depth. This approach replaces the old methodology where multiple point sources were defined to inject elevated fire emissions into each CAMx layer spanning the plume depth.

Figure 17. Diurnal profile of the vertical distribution of the fire plumes (red) and the fraction of hourly emissions allocated to CAMx vertical layer 1 (green) in each of the five fire classes defined by daily area burned within each fire complex.

Class 1: < 10 acres	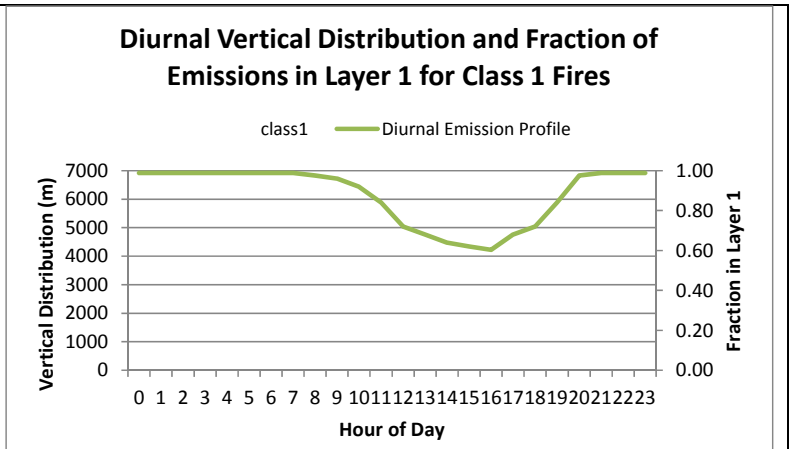
Class 2: 10-100 acres	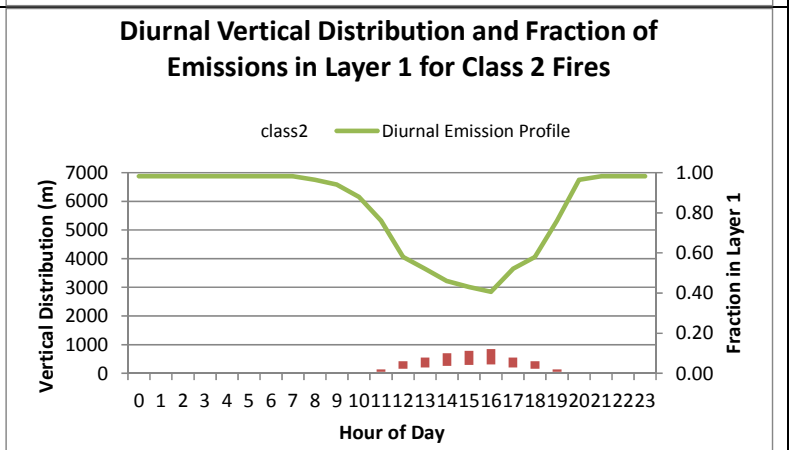
Class 3: 100 – 1000 acres	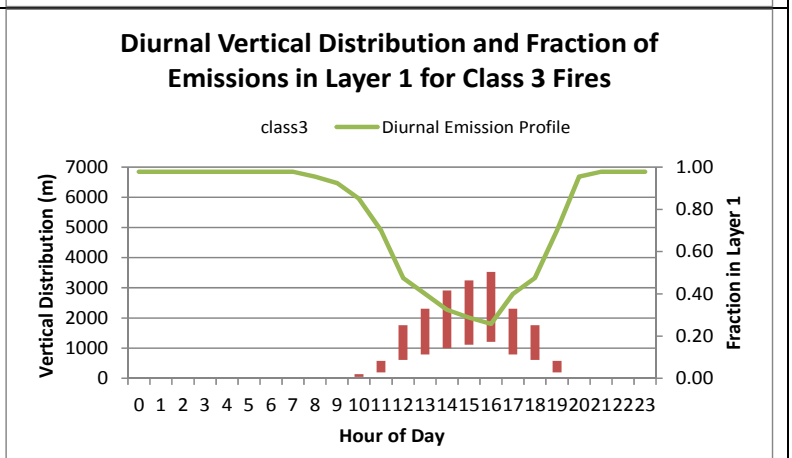

Class 4: 1000 – 5000 acres	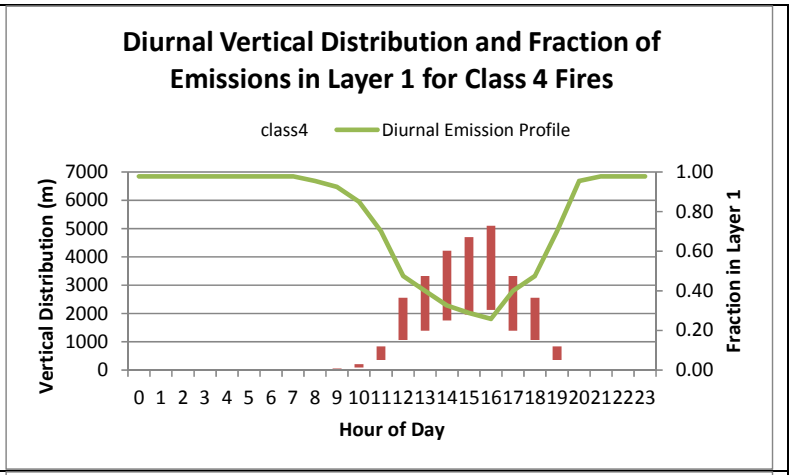
Class 5: > 5000 acres	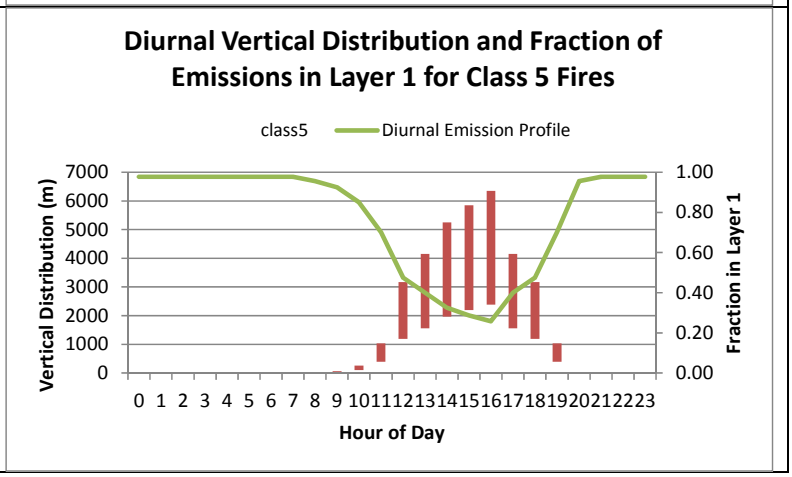

5.5.2 Regional Air Quality Predictions

CAMx simulations were performed using three different land cover products: MODIS LCT, ESA and TCEQ_CDL. In addition, an emissions inventory for which all fire emissions were removed ("No Fire" case) was also conducted for comparison purposes. Predicted maximum daily 8-hour (MDA8) ozone concentrations were determined for each day of June for each grid cell within the modeling domain. Differences in MDA8 O3 between each of three cases and the "No Fire" case indicated the contributions of fire events to regional air quality and are shown in Figure 18 for selected days. In the first part of June (ref. June 4th in Figure 18), northwestern Mexico (Sierra Madre Occidental) exhibited high fire activity, which affected ozone levels in the region as well as within downwind areas of the U.S. Fire activity in western U.S. (Rocky Mountains) became pronounced later in the month (ref. June 28th in Figure 18).

Figure 19 shows the distribution of the contributions of all fires within the entire modeling domain to MDA8 ozone concentrations in each of the geographic regions. The statistics are based on predicted values for 36-km resolution grid cells regardless of location. The contributions of fire events to predicted MDA8 ozone concentrations can be substantial on specific days and geographic locations; for example, the maximum contribution of fire events to MDA8 ozone is 119 ppb for the TCEQ_CDL scenario in the western U.S., and 47 ppb in Texas for MODIS LCT scenario. Another notable feature of Figure 19 is that medians and the boxes (i.e., middle two quartiles) have positive values, with the 25th percentile for the western US as the

only exception. These results suggested that during the month of June, fire events, which may be local or remote, are always contributing positively to MDA8 ozone concentrations. This was likely associated with the contribution of fires in northwestern Mexico that occurred every day for the initial two-thirds of the month. Texas and the Lower Mississippi Valley had the largest deviations from zero, with median values of 1.8 to 2.2 ppb for Texas and 0.9 to 1.3 ppb for the lower Mississippi Valley, than other regions the U.S., due to their proximity to Mexico.

Figure 18. Contribution of fire events to predicted MDA8 ozone concentration for selected days (a) June 4th and (b) June 28th, 2012. The contribution was determined as the difference in predicted MDA8 ozone concentrations between the MODIS LCT and "No Fire" scenarios by grid cell.

(a)

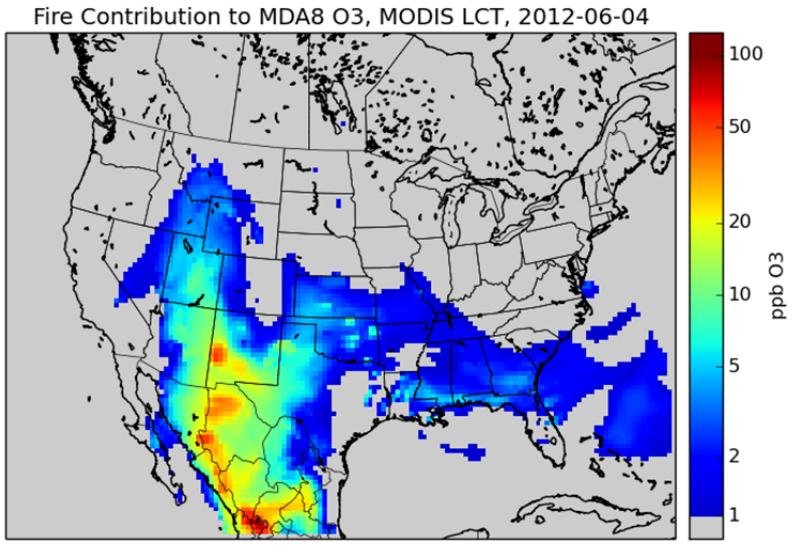

(b)

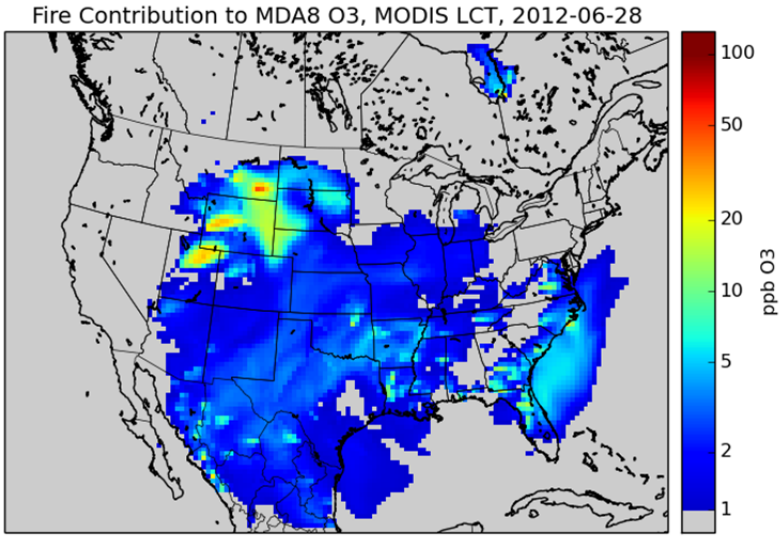

Figure 19. Contribution of all fire events to MDA8 ozone concentrations in each geographic region during June 2012. The box represents 25th to 75th percentiles with a vertical line showing the median. Whisker stretches to the minimum and maximum values. Values represent predictions for 36-km resolution grid cells regardless of location. The concentration axis uses inverse hyperbolic sine transformation ($\sinh^{-1} x \equiv \ln(x + \sqrt{1 + x^2})$) to facilitate interpretation.

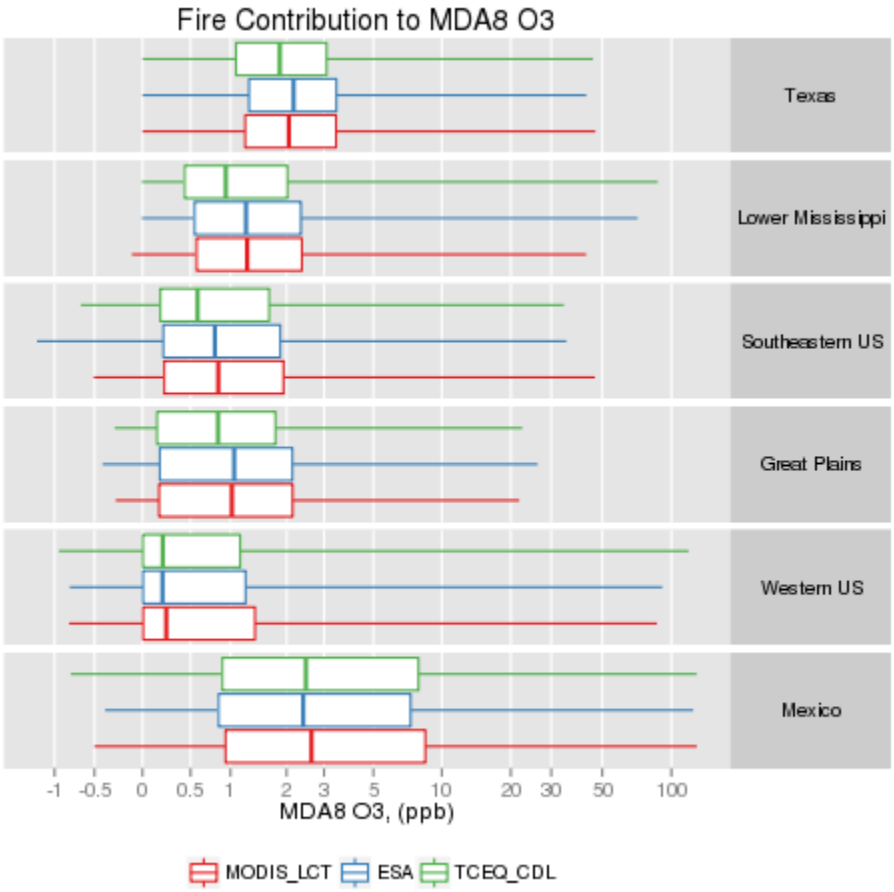

Simulations were conducted with the ESA, TCEQ CDL scenarios, and MODIS LCT scenarios to examine the effects of differing land cover products on predictions of MDA8 ozone concentrations. Figure 20 shows differences in MDA8 ozone concentrations for the ESA and TCEQ CDL scenarios relative to the MODIS LCT scenario for two selected days. On June 4th, the ESA scenario shows decreased MDA8 ozone in northeastern Mexico in comparison to the MODIS LCT case. On the same day, both the ESA and TCEQ_CDL cases exhibited higher MDA8 ozone levels in the southeastern US in comparison to the MODIS LCT case, likely caused by elevated emissions in coastal Louisiana during June 1st through 3rd. The MODIS LCT product did not assign permanent wetland in contrast to other products (e.g. ESA's category 180: flooded shrub or herbaceous cover), resulting in smaller FINN emission estimates with the MODIS LCT product.

Figure 21 shows differences in predicted MDA8 ozone concentrations between the land cover scenarios. At selected times and geographic locations, predictions may vary considerably when different land cover products are used. For example, differences in predicted MDA8 ozone in

Texas range from -10 ppb to +21 ppb between the ESA and MODIS LCT products and from -18 ppb to +33 ppb between the TCEQ_CDL and MODIS LCT products.

Fire emissions exhibit strong seasonality as exemplified in Figure 2, and monthly emissions estimates may differ considerably from annual estimates. Figure 22 shows NO_x emission by region of interest (Figure 1) during June 2012; note that the extent of emissions is limited to be within the boundaries of the photochemical modeling domain, which crosses central Mexico. Emissions from Mexico were relatively large during the month and had long-range effects on air quality in downwind areas of much of the U.S. As a monthly total during June, emissions from Mexico were lower for the ESA product, in contrast to annual total emissions shown in Figure 12. This was the likely cause of the lower central tendency of MDA8 ozone for the ESA scenario than the MODIS LCT case, as seen in Figure 21. Emissions estimates for Mexico for the TCEQ_CDL scenario were identical to that of the MODIS LCT scenario because the TCEQ_CDL product focuses only on U.S. national and regional modifications. In contrast, the TCEQ_CDL product produced lower emission estimates than the MODIS LCT in the western U.S. and in domain total emissions, leading to predictions of lower MDA8 ozone concentrations.

MDA8 ozone concentrations at specific locations affected by local fire events may differ from broader regional trends. Figure 23 shows scatter plots of the fire contribution to MDA8 ozone concentrations with varying land cover data products. Large contributions to MDA8 ozone concentrations were likely to be associated with local fire events, and therefore were relatively consistent with region specific emissions. For example, the ESA scenario in the western U.S. produced greater NO_x emissions during June; Figure 23 shows a series of points with a slope greater than the 1:1 line for the ESA scenario, which likely reflects the effect of local fire events that had larger estimates of NO_x emissions than the MODIS LCT product.

Figure 20. Predicted difference in MDA8 ozone concentrations between the ESA and MODIS LCT products (left) and TCEQ_CDL and MODIS LCT products (right) on (a) June 4, 2012 and (b) June 28, 2012.

(a)

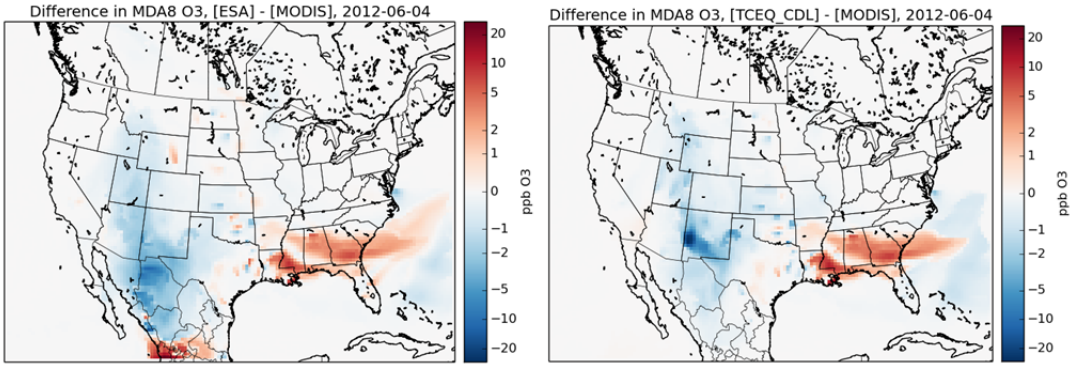

(b)

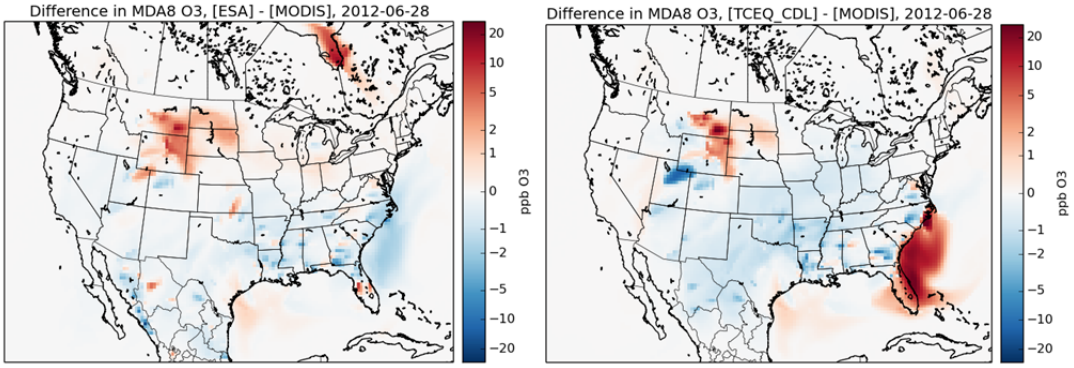

Figure 21. Differences in MDA8 ozone concentrations between the ESA or TCEQ_CDL scenarios and the MODIS LCT scenario. The box represents 25th to 75th percentiles with a vertical line showing the median. Whisker stretches to the minimum and maximum values. The concentration axis uses inverse hyperbolic sine transformation ($\sinh^{-1} x \equiv \ln(x + \sqrt{1 + x^2})$ to facilitate interpretation.

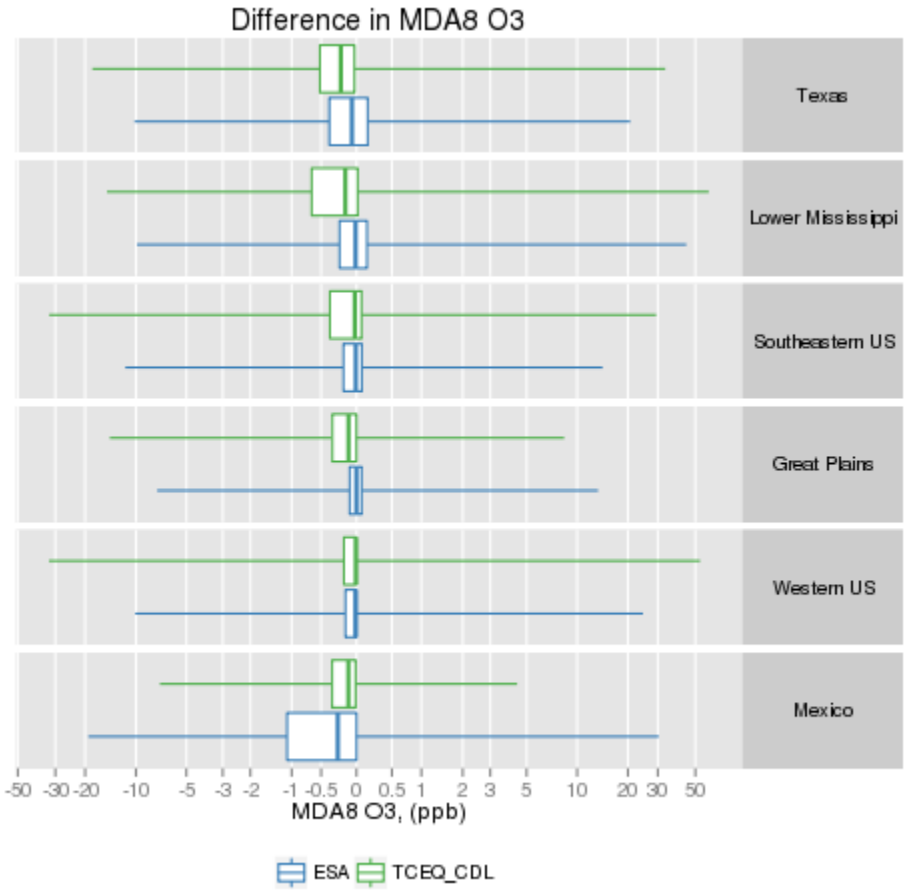

Figure 22. NO_x emissions estimates for June 2012 within the CAMx modeling domain: (a) by region of interest and (b) the 36-km photochemical modeling domain total.

(a)

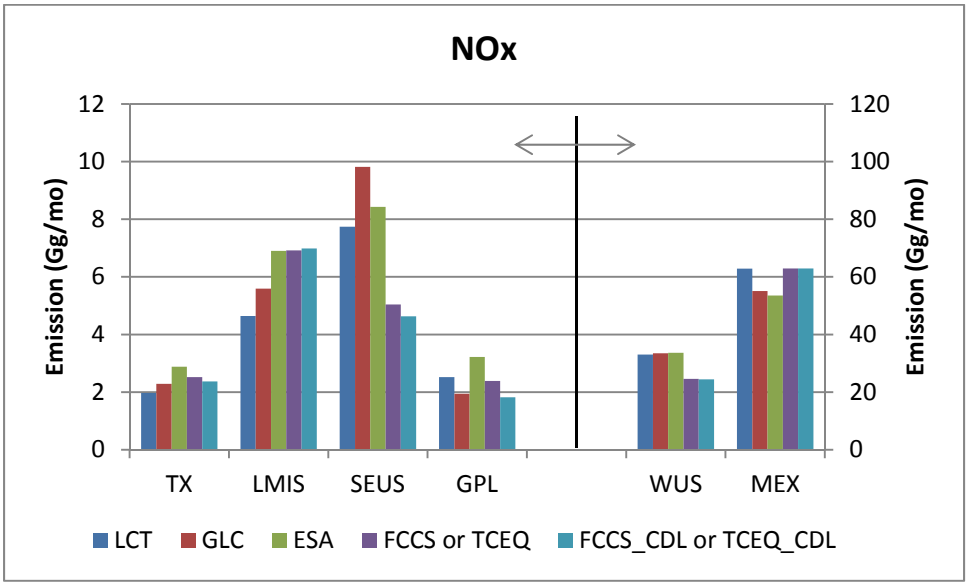

(b)

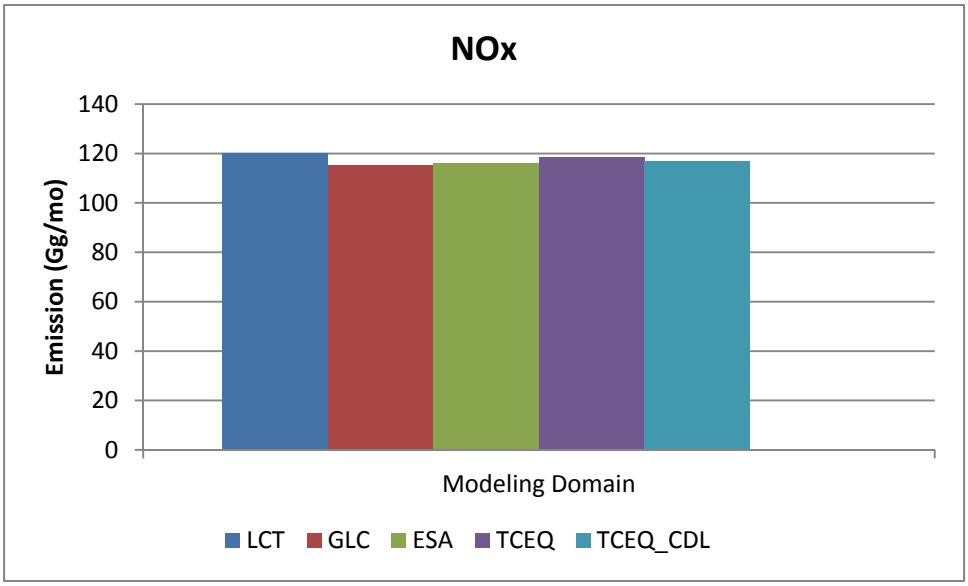

Figure 23. Scatter plot of MDA8 O3 concentration between the (a) ESA versus MODIS LCT scenarios and (b) TCEQ_CDL versus MODIS LCT scenarios. Values represent predictions for 36-km resolution grid cells regardless of location.

(a)

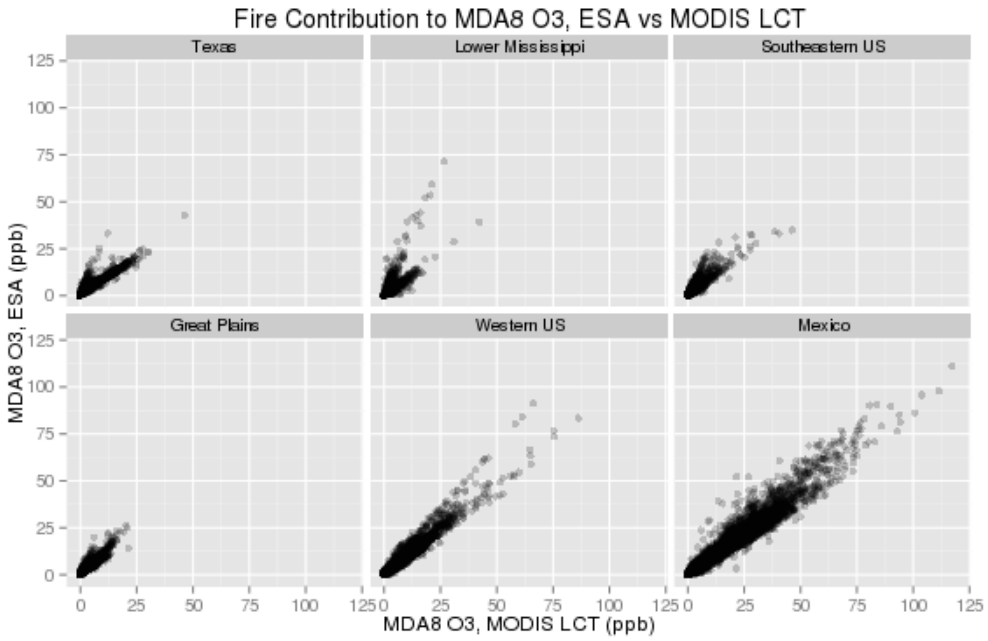

(b)

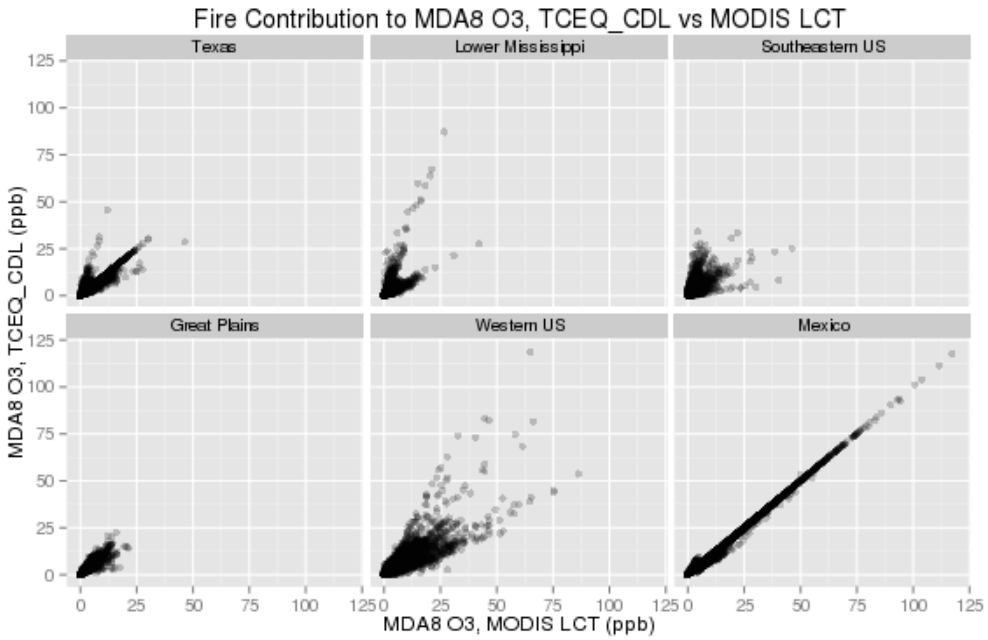

5.6 References

Jimenez, M., G. Yarwood. EPS v3.22 Enhancements to Support CAMx Plume Rise Distribution Override Feature. Final report for WO582-15-53711-08-FY15-35, prepared for the Texas Commission on Environmental Quality, Austin, TX, by Ramboll Environ, Novato, CA (July 2015).

Kemball-Cook, S., T. Pavlovic, J. Johnson, L. Parker, D.J. Rasmussen, J. Zagunis, L. Ma, G. Yarwood. Analysis of Wildfire Impacts on High Ozone Days in Houston, Beaumont, and Dallas-Fort Worth during 2012 and 2013. Final report for WO582-11-10365-FY14-19, prepared for the Texas Commission on Environmental Quality, Austin, TX, by ENVIRON International Corporation, Novato, CA (July 2014).

Ramboll Environ, 2015. User's Guide: Comprehensive Air quality Model with extensions, version 6.20. Prepared by Ramboll Environ, Novato, CA, March 2015 (www.camx.com).

6. Partitioning of NO_x Emissions to NO_z in Fire Plumes

Fires produce large quantities of NO_x and reactive VOC that would be expected to generate locally high ozone concentrations. The early chemical environment within hot turbulent smoke plumes is highly complex and not well understood. Observational research from surface and aircraft monitoring indicate mixed ozone impacts from fires (Jaffe and Wigder, 2012). Singh et al. (2012) find little evidence for surface ozone enhancements in the immediate area of California wildfires except possibly when mixed with urban pollution. Yet chemical transport models such as CAMx (and others) consistently show large surface ozone impacts from fire sources (McKeen et al., 2002; Mueller and Mallard, 2011; Emery et al., 2012, Pfister et al. 2011).

The immediate dilution of fresh fire emissions into large grid volumes, and the poor representation of chemical processing that result, may be factors that contribute to discrepancies between modeled and observed ozone impacts. Similar issues arise in modeling the non-linear chemical impacts from large anthropogenic point source plumes, which are best addressed by applying Plume-in-Grid treatments at sub-grid scales (Yarwood et al., 2012; Emery et al., 2013). In some global modeling applications (e.g., Alvarado et al., 2010) fresh fire NO_x emissions have been partitioned to oxidized forms ("NO_z" such as nitrates) prior to their injection to the grid to account for rapid NO_x chemistry as fire plumes disperse to grid scale. Such approaches have been shown to be effective in reducing ozone production from fires. An approach following Alvarado et al. (2010) was recently employed in regulatory modeling conducted for the State of Louisiana (ENVIRON and ERG, 2013), which helped to reduce ozone over-predictions related to ubiquitous agricultural burning in the region.

In this project we considered numerous approaches to partition fire NO_x emissions to NO_z compounds, such as simply applying constant proportions to a few NO_z species across all fire types and sizes, considering fire/fuel type to account for different relative levels of NO_x and VOC emissions, and considering fire size to account for time scales for plume rise and dispersion to grid scale. On the basis of an extensive literature review with these considerations in mind, we developed a diurnally-varying, fuel-dependent fire plume NOz speciation technique based on recent Lagrangian chemical plume modeling performed by Lonsdale et al. (2014).

Our approach partitions NO_x reported in FINNv2 files into NO_2, nitric acid (HNO_3), peroxyacetyl nitrate (PAN), C3 and higher peroxyacyl nitrates (PANX) and organic nitrates (NTR) in a manner that conserves total moles of reactive nitrogen ($NO_y = NO_2 + HNO_3 + PAN + PANX + NTR$). Note that we assume that all NO is rapidly processed to NO_2 in early stages of the plume so that zero NO is emitted, consistent with Table 11. Organic nitrates for chemical mechanisms prior to CB6r2 are assigned to "NTR", whereas for CB6r2 they are assigned to "NTR2".

The breakout of NO_x into these five NO_y species is based on results from the Aerosol Simulation Program v2.1 (Alvarado and Prinn, 2009) run by Lonsdale et al. (2014) for a matrix of simulations over multiple zenith angles, temperatures, total ozone column, and four vegetation types (tropical forest, temperate forest, boreal forest, and savannah/grasslands). Lonsdale et al. (2014) present a limited set of graphics depicting the hourly evolution of NO_y species during 5-hour simulations for each vegetation type with initial plume releases at zero zenith angle (local noon). The largest NO_y sensitivity occurs for vegetation type, but little sensitivity to initial zenith angle is evident over the range 0-60 degrees. We selected results from the first simulation hour to define the midday maximum NO_z breakout by vegetation type, assuming that 1 hour is

representative of the time scale for plume rise and initial plume dispersion to grid scale in most cases. We set the fractions of PAN and PANX at night to half their midday values, which is approximated from the results of Lonsdale et al (2014). Fractions for PAN and PANX are linearly interpolated during morning hours (06-11) and afternoon hours (13-18). HNO_3 and NTR/NTR2 fractions are assumed to remain constant in time. NO_2 fractions are adjusted each hour to make up the balance of total NO_y. Table 12 shows the specified midday and nighttime NO_y fractions by vegetation type, along with the resultant daily average fractions.

Table 12. Noontime, nighttime and daily average partition of total NO_x into five NO_y compounds based on the Aerosol Simulation Program (ASP) modeling results of Lonsdale et al. (2014) for four vegetation types. Also shown is the mapping between ASP and CB6 species.

ASP species	CB species	Tropical Forest	Temperate Forest	Savannah/ Grasslands	Boreal Forest
Local Noon					
NOx	NO2	36%	40%	72%	3%
PAN	PAN	18%	16%	7%	41%
Peroxy nitrates	PANX	13%	9%	1%	17%
Alkyl nitrates	NTR/NTR2	5%	5%	2%	19%
NO3	HNO3	28%	30%	18%	20%
Night (hours 00-05 and 19-23)					
NOx	NO2	51.5%	53%	76%	32%
PAN	PAN	9%	8%	3.5%	20.5%
Peroxy nitrates	PANX	6.5%	4.5%	0.5%	8.5%
Alkyl nitrates	NTR/NTR2	5%	5%	2%	19%
NO3	HNO3	28%	30%	18%	20%
Daily Average					
NOx	NO2	42.1%	45.1%	73.6%	14.4%
PAN	PAN	14.4%	12.8%	5.6%	32.9%
Peroxy nitrates	PANX	10.4%	7.2%	0.8%	13.6%
Alkyl nitrates	NTR/NTR2	5%	5%	2%	19%
NO3	HNO3	28%	30%	18%	20%

The FINNv2 emissions files contain a land cover code for each individual subdivided polygon (see Section 3.1.3). The four vegetation types listed in Table 12 are mapped to the nine FINNv2 land cover types (Table 13) so that the FIRESPEC pre-processor can apply the appropriate daily average NO_y factors from Table 12 to the daily NO_x emissions for each subdivided polygon.

Hourly temporal profiles for each of the five NO_y species are derived by combining hourly NO_y fractions by vegetation type with the diurnal fire temporal profile shown in Figure 16. The resulting five temporal profiles are applied in the EPS3 TMPRL module to allocate daily emissions of NO_2, PAN, PANX, HNO_3 and NTR/NTR2 from each fire to each hour of the day. These hourly profiles are shown in Figure 24 for each of the four vegetation types.

Table 13. Mapping of 4 ASP vegetation types of Lonsdale et al. (2014) to the 9 FINNv2 land cover types to support the speciation of daily NOx emissions in the FIRESPEC pre-processor.

FINN Index	FINNv2 Landcover Type	ASP Vegetation Type
0	Un-vegetated	Grassland
1	Grassland	Grassland
2	Shrub	Grassland
3	Tropical Forest	Tropical Forest
4	Temperate Forest	Temperate Forest
5	Boreal Forest	Boreal Forest
6	Temperate Evergreen Forest	Temperate Forest
7	Pasture	Grassland
8	Rice	Grassland
9	Crop (Generic)	Grassland
10	Wheat	Grassland
11	Cotton	Grassland
12	Soy Bean	Grassland
13	Corn	Grassland
14	Sorghum	Grassland
15	Sugar Cane	Grassland

Figure 24. Hourly temporal profiles used in the EPS3 TMPRL module to partition total daily NO_x from each fire into hourly NO_2, PAN, PANX, HNO_3 and NTR/NTR2 as a function of four vegetation types: (a) tropical forest; (b) temperate forest; (c) savannah/grassland; (d) boreal forest.

(a)

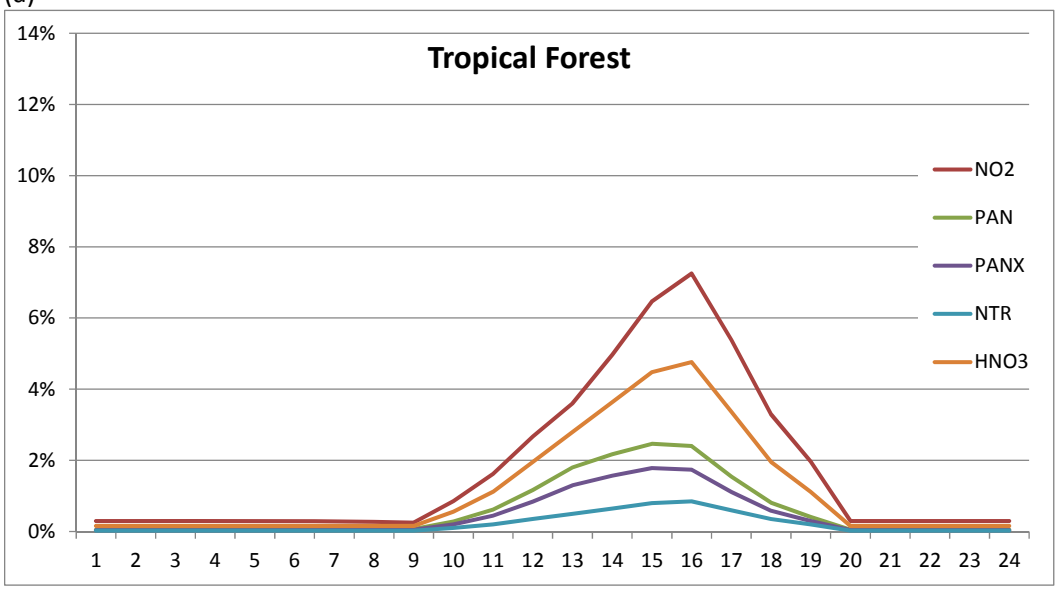

(b)

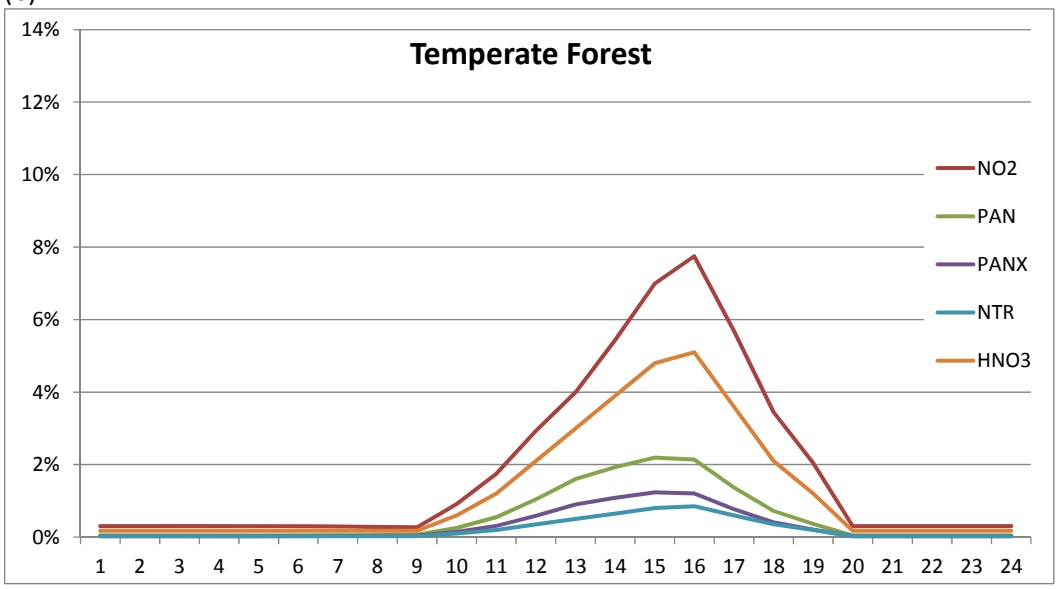

(c)

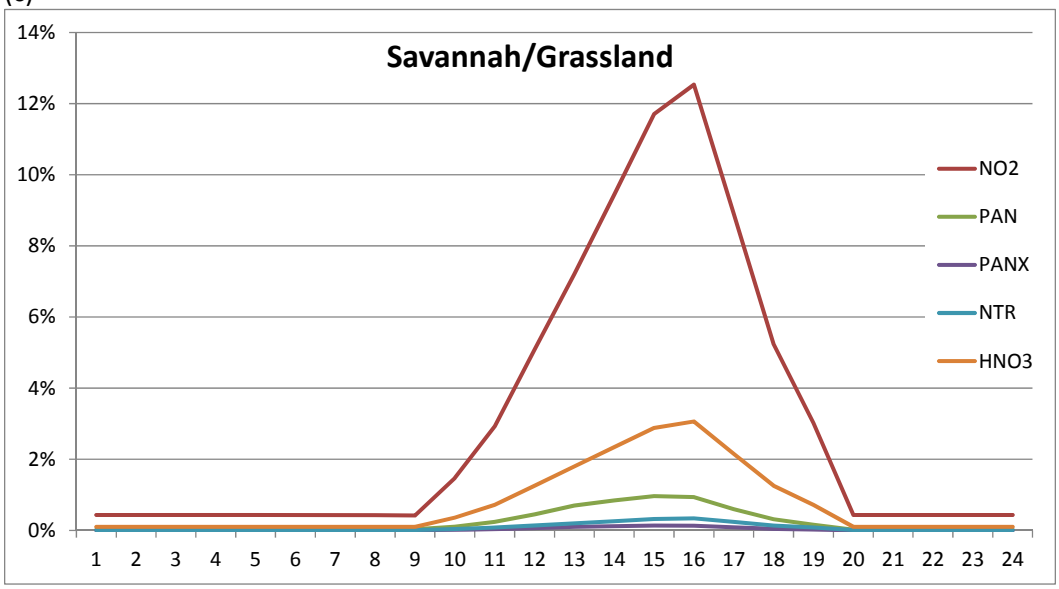

(d)

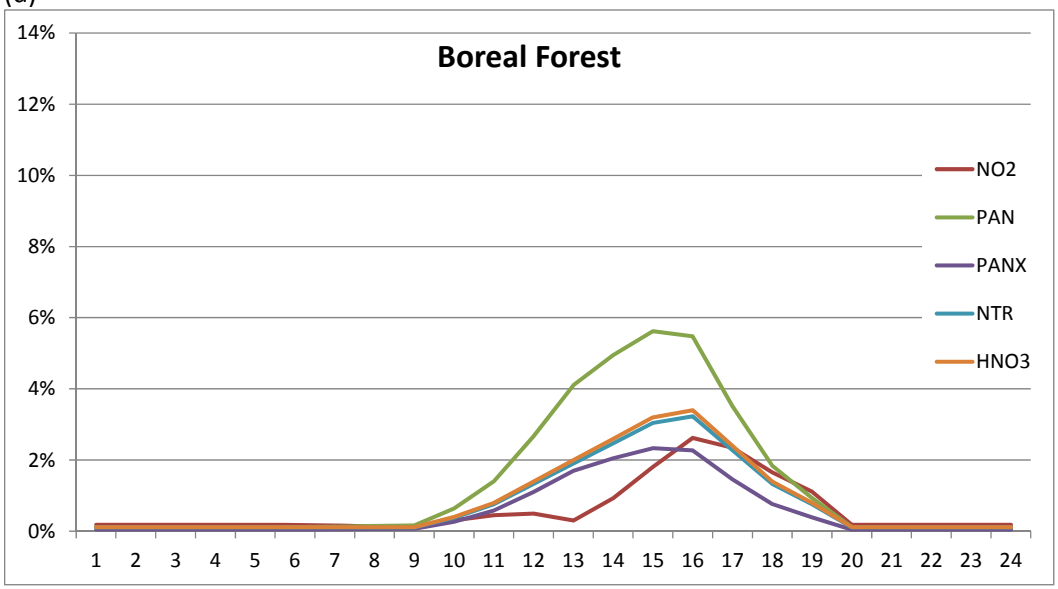

6.1 Predicted Effects on Air Quality

A CAMx simulation was conducted based on FINN emissions estimates from the TCEQ_CDL land cover scenario with NO_x partitioning implemented in the preprocessing for CAMx as described above. Results from this simulation were compared to a similar CAMx simulation also based on the FINN emissions estimates from the TCEQ_CDL land cover scenario but without NO_x partitioning implemented (described in Section 5.5.2).

Figure 25 shows the statistical distributions of the contributions of all fire events to MDA8 ozone concentrations in each of the geographic regions for the two cases (i.e., concentration change of each simulation relative to the "No Fire" simulation). Figure 26 is a direct comparison of the

differences between the two cases. Differences in MDA8 ozone concentrations between the two cases were the greatest in Mexico, which had high fire activity during the month. For Texas, the median difference between the two cases was 0.30 ppb with the TCEQ_CDL_NOy case resulting in lower ozone concentrations.

Figure 25. Fire contribution to MDA8 ozone in each region for the TCEQ_CDL cases with and without NO_x to NO_z partitioning. The box represents 25th to 75th percentiles with a vertical line showing the median. Whisker stretches to the minimum and maximum values. The concentration axis uses inverse hyperbolic sine transformation ($\sinh^{-1} x \equiv \ln(x + \sqrt{1 + x^2})$ to facilitate interpretation.

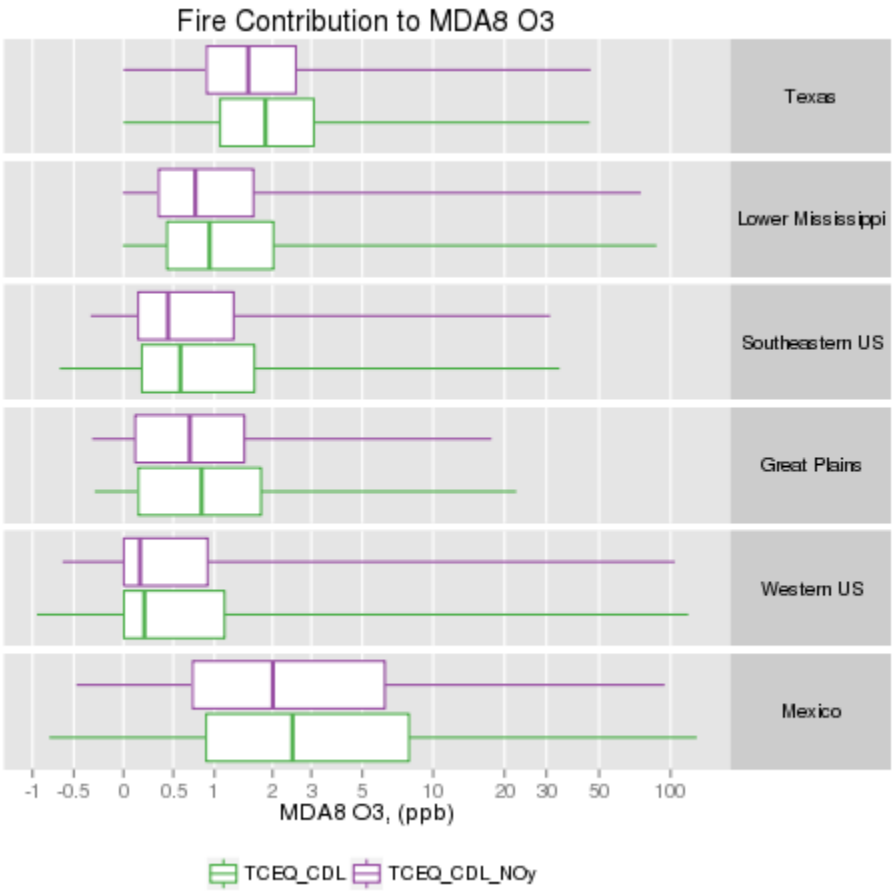

Figure 26. Distributions of differences in MDA8 ozone concentrations in Texas between the TCEQ CDL simulations with and without NOx partitioning by geographic region during June 2012. The box represents 25th to 75th percentiles with a vertical line showing the median. Whisker stretches to the minimum and maximum values. The concentration axis uses inverse hyperbolic sine transformation ($\sinh^{-1} x \equiv \ln(x + \sqrt{1 + x^2})$) to facilitate interpretation.

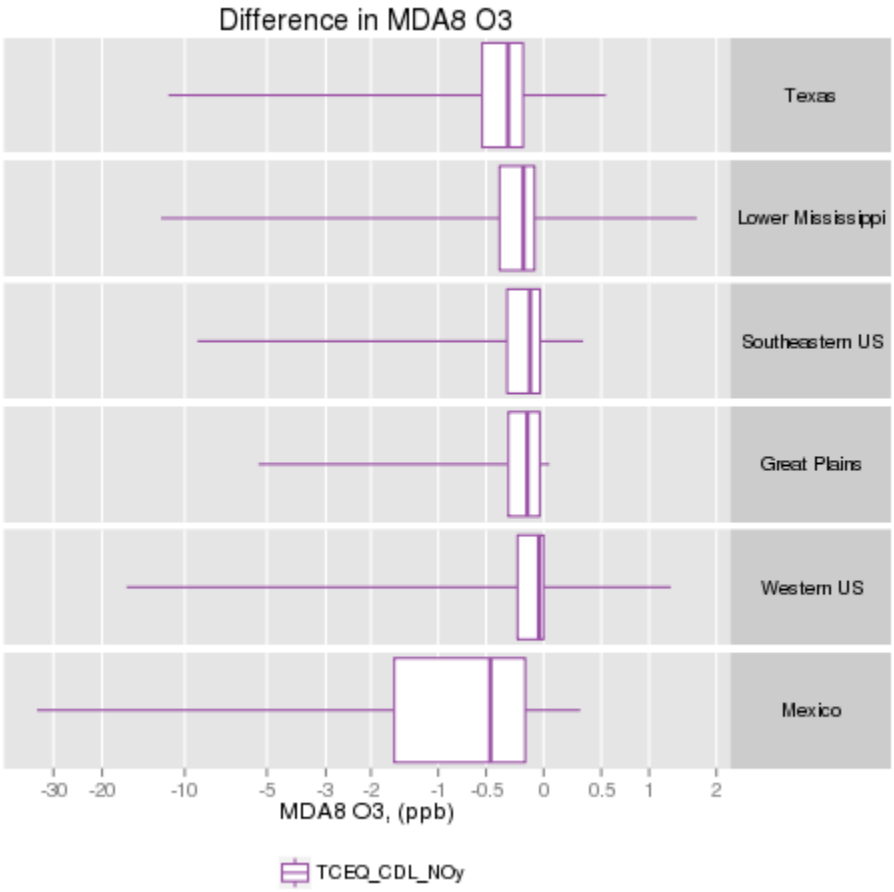

6.2 References

Alvarado, M.J., et al. Nitrogen oxides and PAN in plumes from boreal fires during ARCTAS-B and their impact on ozone: an integrated analysis of aircraft and satellite observations, Atmospheric Chemistry and Physics, 10, 9739-9760, 2010.

Alvarado, M.J., R.G. Prinn. Formation of ozone and growth of aerosols in young smoke plumes from biomass burning: 1. Lagrangian parcel studies. *Journal of Geophysical Research*, 114(D9), 2009.

Emery, C., J. Jung, N. Downey, J. Johnson, M. Jimenez, G. Yarwood, R. Morris. Regional and global modeling estimates of policy relevant background ozone over the United States. *Atmospheric Environment*, 47, 206-217, 2012.

Emery, C., B. Koo, T. Sakulyanontvittaya, G. Yarwood. Improving CAMx GREASD PiG Efficiency. Final report for WO 582-11-10365-FY13-09, prepared for the Texas Commission on Environmental Quality, Austin, TX, by ENVIRON International Corporation, Novato, CA, (November 2013).

ENVIRON and ERG, 2013. Technical Support Document: Photochemical Modeling for the Louisiana 8-Hour Ozone State Implementation Plan. Prepared for the Louisiana Department of Environmental Quality, Baton Rouge, LA, by ENVIRON International Corporation, Novato, CA and Eastern Research Group, Sacramento, CA (August 2013).

Jaffe, D. A., N. L. Wigder. Ozone production from wildfires: A critical review, *Atmospheric Environment*, 51, 1-10, 2012.

Lonsdale, C.R., M.J. Alvarado, R.J. Yokelson, K.R. Travis, E.V. Fischer. Parameterizing the Near-Source Chemistry of Biomass Burning Smoke Plumes. Presented at the 13th Annual Community Modeling and Analysis (CMAS) Conference, October 27-29, 2014, Chapel Hill, NC (https://www.cmascenter.org/conference/2014/agenda.cfm).

McKeen, S.A., G. Wotawa, D. D. Parrish, J. S. Holloway, M. P. Buhr, G. Hubler, F. C. Fehsenfeld, J. F. Meagher. Ozone production from Canadian wildfires during June and July of 1995, *Journal of Geophysical Research*, 107, D14, 4192, 2002.

Mueller, S.F., J.W. Mallard. Contributions of natural emissions to ozone and $PM_{2.5}$ as simulated by the Community Multiscale Air Quality (CMAQ) model. *Environmental Science & Technology*, 45, 4817-4823, 2011.

Pfister, G.G., J. Avise, C. Wiedinmyer, D.P. Edwards, L.K. Emmons, G.D. Diskin, J. Podolske, A. Wisthaler. CO source contribution analysis for California during ARCTAS-CARB, *Atmospheric Chemistry and Physics*, 11(15), 7515-7532, 2011.

Singh, H.B., C. Cai., A. Kaduwela, A. Weinheimer, A. Wisthaler. Interactions of fire emissions and urban pollution over California: Ozone formation and air quality simulations, *Atmospheric Environment*, 56, 45-51, 2012.

Yarwood, G., P. Karamchandani, C. Emery, S.-Y. Chen, S.S. Brown, D.D. Parrish. NOx Reactions and Transport in Nighttime Plumes and Impact on Next-Day Ozone. Final Report for Texas AQRP Project 10-020, prepared for the University of Texas, Austin, TX, by ENVIRON International Corporation, Novato, CA and NOAA/ESRL Chemical Sciences Division, Boulder, CO, 2012.

7. Data Quality Assurance and Audits of Data

Quality assurance was addressed throughout the project including FINN algorithm development and data processing activities.

7.1 FINN Code

The FINN code was developed by Dr. Christine Wiedinmyer at the National Center for Atmospheric Research. A thorough, independent review of the code was conducted by Dr. Yosuke Kimura of the University of Texas at Austin. The review process included all lines of Interactive Data Language (IDL) source code and a cross-comparison of model input files used for the project.

7.2 Land Cover Rasters and Fuel Loading

Land cover raster datasets for this project were obtained from official websites of each source and checked to be reasonable based on visual inspection of ArcGIS maps and counts of land cover types for respective polygons. Operations performed for this project included (1) resampling to 30-arcsecond resolution WGS84 projection and (2) merging of the CDL raster to TCEQ or FCCS raster datasets. The resampled datasets were again visually inspected by ArcGIS mapping and compared against the original source. For merging two raster datasets, auxiliary rasters showing the locations of agricultural lands based on two source raster datasets were made, and it was then confirmed that the land cover class from the appropriate source were selected for the merged product.

For estimating the fuel loadings of burned area polygons, cross-tabulated areas were determined using ArcGIS (http://resources.arcgis.com/en/help/main/10.2/index.html#/Tabulate_Area/009z000000w2000000/) and then MS Excel was used to determine a weight-average fuel loading. Resulting values were examined based on land cover characterization to ensure consistency. High fuel loadings were especially noted for white cedar/larch forests in the northern Great Plains, which have considerable understory vegetation, but the team did not feel supplemental data were available to warrant any changes at this time to the FCCS fuel loading values for these areas.

7.3 ArcGIS Preprocessor

As described in 3.1.2, a new tool for burned area estimation was developed for this project. The code was developed in the ESRI ArcGIS python environment. During the course of development, intermediate features were visually checked to identify extreme values and geometries. Polygon areas of all output features were repeatedly examined for unreasonably small or large values, which could indicate a defect in the algorithm, and appropriate corrections were made to the code. Upon completion of development, the subdivided burned area polygon's size ranged from 0.59 to 7.65 km^2, and selected small and large polygons were within the expected outcomes for the algorithm.

To determine the land cover types of burned area polygons, vector and raster intersections were considered. An initial version of code converted a land cover raster to a polygon to perform polygon versus polygon intersection to determine the land cover property. The results from this approach were used as a benchmark for the production code, which converted burned area polygons into raster formats to evaluate appropriate zonal statistics. The production code converted the burned area polygons into raster formats and performed raster operations to determine the land cover properties. This method required less computation time with reduced accuracy than the vector-based method but was not considered to affect the quality of the results. Both the raster dataset and the burned area polygon had spatial uncertainties of one kilometer or greater. The raster datasets had a resolution of 30 arcseconds and spatial heterogeneity existed inside ~1km^2 pixel. Fire detections in the MODIS Active Fire product had a spatial resolution limited by the pixel size of the MODIS detectors, i.e., one to a few kilometers. Therefore, the level of spatial precision that could be achieved by a vector operation was not useful in improving the overall accuracy of the analysis. The resolution of the raster that represented the burned area polygon determined the degree of speed enhancement and accuracy reduction. With several test runs, optimal resolution of the polygon to raster conversion was determined. The approach in this study converted burned area polygons into 6 arcsecond resolution pixels (~200m), which reduced the computation time to be 4% of the vector-based method. Mean and maximum differences in percent tree cover were 0.22% and 1.79% relative to the vector-based method, and only 0.89% of polygons identified different land cover types. This level of inaccuracy was considered acceptable for the purposes of this project.

7.4 FINN Output

FINN output was rigorously quality assured by summing CO, NO_x and $PM_{2.5}$ emissions, respectively, by geographic region (Figure 1) and FINN land cover type (Table 4). The primary objective of this exercise was to conduct analyses reported in Section 5.3, 5.4 and 5.3. To achieve these objectives, FINN output were closely examined for each record to confirm that the FINN algorithm was functioning properly in the code.

7.5 EPS3 Processors

Extensive QA of the updated EPS3 (and its associated pre- and post-processors) and the fire emissions data for the modeling episode were conducted at Ramboll Environ. Specifically: (1) the nitrogen speciation profiles and the temporal profiles developed for NO_y species were examined before being used for the emissions processing, to ensure their consistency with the information gathered from literature reviews; (2) the input and output for the preprocessors of EPS3 (FIRESPEC and GROUPPTS) were examined to ensure the validity of the results from the code, which had been updated to process the version 2 of FINN data and produce emissions of oxidized nitrogen species; (3) the USERIN file, input and output data for each of the EPS3 modules (PREFIR, CHMSPL, TMPRL, PSTFIR, PTSMRG), and the QA files were examined, and an extended QA summary was generated and examined for several individual fires. Upon completion of the emissions processing, mass consistency was verified for all four cases on a monthly and daily basis by comparing emissions of NO_x and CO in the FINN output files and the CAMx-ready binary emissions files for the entire domain and for the regions specified in Figure 1. The magnitude of the relative error ranged from 0.03% to 0.04% for the monthly domain

total emissions and was less than 0.17% (median value of 0.03%) for the monthly emissions in individual regions.

8. Conclusions and Recommendations

FINN is a global fire emissions model that estimates daily emissions of trace gases and particles from open biomass burning. It is widely used in global and regional modeling studies. The overall objective of this project was to conduct targeted improvements to the FINN model that would benefit the global and regional air quality management and research communities, with a special focus on needs for Texas. The project produced FINN emissions estimates for fire events in 2012 to support TCEQ air quality modeling efforts.

A new algorithm for estimating area burned from satellite-derived fire detections was developed and incorporated into FINN to address a known under prediction bias in the estimated area burned. Improvements in the area burned estimation were accompanied by better spatial resolution in the characterization of land cover, new fuel loading data with greater spatial resolution for the United States, and incorporation of the newly released, year-specific VCF Collection 5 product for estimating bare and vegetative cover. Crop-specific emission factors and fuel loadings developed by McCarty (2011) have been added to FINN as an option for users that have a land cover data resource that distinguishes major crop types typically found in the United States. Collectively, these modifications increased annual CO emissions estimates over the 36-km domain in TCEQ's CAMx configuration by 42% relative to the earlier default version of FINN, primarily due to increases in the area burned estimates. These modifications form the basis of the next generation of the FINN model, v.2.

In the FINN emissions model, land cover and land use are used to assign emission factors and fuel loadings and, consequently, these input data are critical for the estimation of fire emissions. The MODIS Land Cover Type product has been used as the default resource for land cover characterization in FINN, but new global, U.S. national, and Texas regional products are now available alternatives. Annual FINN emissions estimates during 2012 were generated for seven land cover data products alone or in combination:

- Three simulations were conducted with global databases: the MODIS Land Cover Type (LCT), United Nations Global Land Cover (GLC-SHARE), and European Space Agency (ESA) Climate Change Initiative.

- Two simulations utilized a combination of U.S. national databases, including the U.S. Forest Service Fuel Characteristic Classification System (FCCS) with and without the National Agricultural Statistical Service Cropland Data Layer (CDL), and MODIS LCT product outside of the U.S.

- Two simulations were conducted using a Texas (TCEQ) regional land cover product from Popescu et al. (2011) with and without the CDL, the FCCS in the remainder of the continental U.S., and MODIS LCT elsewhere.

Annual emissions estimates for CO, NO_x, and $PM_{2.5}$ were compared between the simulations for six geographic regions: Texas, the Lower Mississippi Valley, Southeastern U.S., Great Plains, Western U.S. and Mexico. Differences between simulations highlighted the complex sensitivity of emissions estimates from the FINN model to various land cover inputs and associated fuel loadings and emission factors. Within Texas, the global-scale ESA and GLC-SHARE products produced higher emissions estimates than the MODIS LCT product during 2012; the Texas regional product (with or without the CDL) produced emission estimates were 10% to 19%

greater than the MODIS Land Cover Type product. Characterization of croplands had minimal effects on annual emissions estimates in Texas.

The Emission Processing System underwent extensive updates to produce a new version (EPS v3.22) for the TCEQ as well as to accommodate use of the new area burned algorithm in FINN. CAMx simulations were performed with a June 2012 episode obtained from the TCEQ with three different land cover products, the MODIS LCT, ESA, and Texas regional product with the CDL. In addition, an emissions inventory for which all fire emissions were removed ("No Fire" case) was also conducted for comparison purposes.

In first part of June, northwestern Mexico (Sierra Madre Occidental) exhibited high fire activity, which affected ozone levels in the region as well as within downwind areas of the U.S. Fire activity in the Rocky Mountains of the western U.S. was pronounced later in the month. Regardless of the land cover product used for the fire emissions estimates, the median contribution of fire events to MDA8 ozone concentrations in Texas throughout the month of June was approximately 2 ppb. This contribution was likely associated with fires in northwestern Mexico that occurred every day for the initial two-thirds of the month. The maximum contribution of fires on predicted MDA8 ozone concentrations in Texas exceeded 40 ppb during the episode period. Differences in predicted MDA8 ozone concentrations in Texas ranged from -10 ppb to +21 ppb between the ESA and MODIS LCT products and from -18 ppb to +33 ppb between the TCEQ_CDL and MODIS LCT products.

The project developed and implemented an approach for partitioning NO_x emissions estimates from FINN into aged NO_z forms (i.e., NO_2, HNO_3, PAN, C3 and higher peroxyacyl nitrates, and organic nitrates) to account for rapid NO_x oxidation in fire plumes. A CAMx simulation was conducted based on FINN emissions estimates from the TCEQ_CDL land cover scenario with NO_x partitioning implemented in the preprocessing algorithm. Results from this simulation were compared to a similar CAMx simulation also based on the FINN emissions estimates from the TCEQ CDL land cover scenario but without NO_x partitioning implemented. Median differences in predicted MDA8 ozone concentrations between the simulations were within -0.5ppb for the six geographic regions, including Texas.

At this time, we recommend use of the following combination of land cover products in FINN to support Texas air quality modeling activities: the TCEQ_CDL regional product, the FCCS in the remainder of the continental U.S., and MODIS LCT elsewhere. This combination provides the greatest spatial resolution and specificity in land cover and fuel loadings for the Texas regional domain and continental U.S. However, we note the importance of understanding the range of FINN emissions estimates that can be obtained with different land cover products and the strong need for *in situ* evaluation of fuel loadings. Future work should focus on validation of land cover and in particular fuel loadings in the United States. The algorithm in EPS that partitions NO_x into aged NO_z forms should reflect the evolution of scientific understanding; our initial approach is implemented as an option in EPS v3.22. Reconciliation of fire detection between varying satellite and ground-based incident resources remains an on-going need; and evaluation of the VIIRS products should be considered in the future.

Appendix

A.1 MODIS LCT mapping and fuel loadings

MODIS Class Descriptions	MODIS Code	FINN Code*	Tree Loadings	Herb Loadings
Water	0	No Emission**		
Evergreen Needleleaf Forest	1	6,6,5	28.61	4.79
Evergreen Broadleaf Forest	2	6,6,5	19.45	5.17
Deciduous Needleleaf Forest	3	4,4,5	15.46	5.48
Deciduous Broadleaf Forest	4	4	19.50	4.73
Mixed Forests	5	3,4,5	19.98	7.93
Closed Shrublands	6	2	4.80	1.24
Open Shrublands	7	2	2.63	0.82
Woody Savannas	8	2	12.51	3.07
Savannas	9	1	10.51	2.89
Grasslands	10	1	2.62	1.40
Permanent Wetlands	11	1	8.34	10.14
Croplands	12	9	0.00	0.66
Urban and Built-Up	13	VCF Dependent***		
Cropland/Natural Vegetation	14	9	8.87	2.97
Snow and Ice	15	No Emission**		
Barren or Sparsely Vegetated	16	1	1.18	0.48

* When three numbers appear for FINN code they represents FINN code by latitude; they are <23.5N, 23.5N to 50N and >50N, respectively

** Assumes no emissions for water, snow and ice

*** Urban and Built-Up categories is changed to other categories based on VCF: grassland (code 10, if Tree < 40%), woody savanna (code 8, if 40% <= Tree < 60%) or mixed forest (code 5, if Tree >= 60%)

A.2 GLC mapping and fuel loadings

GLC Class Descriptions	GLC Code	FINN Code*	Tree Loadings	Herb Loadings
Artificial Surfaces	1	VCF Dependent**		
Cropland	2	9	0.00	0.66
Grassland	3	1	1.49	1.91
Tree Covered Areas	4	3,4,5	21.56	4.93
Shrubs Covered Areas	5	2	4.05	0.97
Herbaceous vegetation, aquatic or regularly flooded	6	1	15.43	9.28
Mangroves	7	3	15.78	45.18
Sparse vegetation	8	1	12.96	2.43
Baresoil	9	1	0.75	0.35
Snow and glaciers	10	VCF Dependent**		
Waterbodies	11	VCF Dependent**		

* When three numbers appear for FINN code they represents FINN code by latitude; they are <23.5N, 23.5N to 50N and >50N, respectively

** Artificial Surfaces, Snow and water are converted to other categories based on VCF: grassland (code 3, if Tree < 40%), shrubs (code 5, if 40% <= Tree < 60%) or tree (code 4, if Tree >= 60%)

A.3 ESA mapping and fuel loadings

ESA Class Desctiptions	ESA Code	FINN Code*	Tree Loadings	Herb Loadings
Cropland, rainfed	10	9	0.00	0.66
Cropland, rainfed, Herbaceous cover	11	9	0.00	0.66
Cropland, irrigated or post-flooding	20	9	0.00	0.66
Mosaic cropland (>50%) / natural vegetation (tree, shrub, herbaceous cover) (<50%)	30	9	0.00	0.66
Mosaic natural vegetation (tree, shrub, herbaceous cover) (>50%) / cropland (<50%)	40	2	6.25	2.25
Tree cover, broadleaved, evergreen, closed to open (>15%)	50	3	25.03	35.11
Tree cover, broadleaved, deciduous, closed to open (>15%)	60	3,4,5	21.27	6.62
Tree cover, broadleaved, deciduous, closed (>40%)	61	3,4,5	23.36	5.42
Tree cover, broadleaved, deciduous, open (15-40%)	62	3,4,5	15.84	12.33
Tree cover, needleleaved, evergreen, closed to open (>15%)	70	6,6,5	22.23	4.11
Tree cover, needleleaved, evergreen, closed (>40%)	71	6,6,5	26.01	10.71
Tree cover, needleleaved, evergreen, open (15-40%)	72	6,6,5	16.01	2.59
Tree cover, needleleaved, deciduous, closed to open (>15%)	80	6,6,5	21.55	14.42
Tree cover, needleleaved, deciduous, closed (>40%)	81	6,6,5	22.76	8.56
Tree cover, needleleaved, deciduous, open (15-40%)	82	6,6,5	16.94	12.25
Tree cover, mixed leaf type (broadleaved and needleleaved)	90	3,4,5	22.88	6.65
Mosaic tree and shrub (>50%) / herbaceous cover (<50%)	100	3,4,5	19.13	5.27

Mosaic herbaceous cover (>50%) / tree and shrub (<50%)	110	1	16.01	3.99
Shrubland	120	2	1.54	0.56
Deciduous shrubland	122	2	26.64	10.71
Grassland	130	1	4.44	2.03
Lichens and mosses	140	1	22.82	3.00
Sparse vegetation (tree, shrub, herbaceous cover) (<15%)	150	1	14.20	2.68
Sparse shrub (<15%)	152	2	4.16	1.72
Sparse herbaceous cover (<15%)	153	1	4.00	3.22
Tree cover, flooded, fresh or brakish water	160	3,4,5	18.80	11.00
Tree cover, flooded, saline water	170	3,4,5	15.62	58.49
Shrub or herbaceous cover, flooded, fresh/saline/brakish water	180	2	7.87	11.49
Urban areas	190	VCF Dependent**		
Bare areas	200	VCF Dependent**		
Water bodies	210	VCF Dependent**		
Permanent snow and ice	220	VCF Dependent**		

* Urban, bare, water and snow converted to other categories based on VCF: grassland (code 130, if Tree < 40%), mosaic herbaceous tree (code 110, if 40% <= Tree < 60%) or mixed tree (code 90, if Tree >= 60%)

A.4 FCCS mapping and fuel loadings

FCCS Class Desciptions	FCCS Code	FINN Code	Tree Loadings	Herb Loadings
No Natural Vegetation	0	Falls back to MODIS LCT*		
Black cottonwood-Douglas-fir-quaking aspen forest	1	4	27.05	9.30
Western hemlock-western redcedar-Douglas-fir forest	2	6	140.82	11.06
Douglas-fir forest	3	6	17.10	9.10
Douglas-fir/ceanothus forest	4	6	10.59	4.32
Douglas-fir-white fir forest	5	6	57.60	4.78
Oregon white oak-Douglas-fir forest	6	4	42.13	2.00
Douglas-fir-sugar pine-tanoak forest	7	4	49.73	4.79
Western hemlock-Douglas-fir-western redcedar/vine maple forest	8	4	124.93	16.48
Douglas-fir-western hemlock-western redcedar/vine maple forest	9	4	20.67	5.69
Western hemlock-Douglas-fir-Sitka spruce forest	10	6	151.62	13.73
Douglas-fir/western hemlock-Sitka spruce forest	11	6	40.45	3.39
Red fir-mountain hemlock-lodgepole pine-western white pine forest	12	6	61.84	4.98
Mountain hemlock-Pacific silver fir forest	13	6	15.67	4.21
California black oak woodland	14	4	29.80	1.10
Jeffrey pine-red fir-white fir/greenleaf-snowbrush forest	15	6	33.37	14.44
Jeffrey pine-ponderosa pine-Douglas-fir-California black oak forest	16	4	53.51	3.64
Red fir forest	17	6	44.40	13.20
Douglas-fir/oceanspray forest	18	4	24.83	2.63

White fir-giant sequoia-sugar pine forest	19	6	101.74	6.57
Western juniper/curl-leaf mountain mahogany woodland	20	4	8.19	1.39
Lodgepole pine forest	21	6	5.54	1.63
Lodgepole pine forest	22	6	6.96	3.13
Lodgepole pine forest	23	6	28.75	1.88
Pacific ponderosa pine-Douglas-fir forest	24	6	29.85	1.62
Pinyon-Utah juniper forest	25	6	13.43	1.68
Interior ponderosa pine-limber pine forest	26	6	15.67	2.18
Ponderosa pine-two needle pinyon-Utah juniper forest	27	6	15.63	0.58
Ponderosa pine savanna	28	2	8.87	1.31
Interior ponderosa pine-Engelmann spruce-Douglas-fir forest	29	6	9.57	4.21
Turbinella oak-alderleaf mountain mahogany shrubland	30	2	0.09	1.31
Ponderosa pine/pinyon pine-Utah juniper forest	32	6	15.07	0.79
Gambel oak/big sagebrush shrubland	33	2	0.99	1.06
Interior Douglas-fir-interior ponderosa pine/gambel oak forest	34	4	28.52	3.03
California live oak-blue oak woodland	36	2	8.96	1.90
Ponderosa pine-Jeffrey pine forest	37	6	39.58	5.30
Douglas-fir-madrone-tanoak forest	38	4	43.11	2.66
Sugar pine-Douglas-fir-oak forest	39	4	83.77	2.39
Tobosa-grama grassland	40	1	0.00	0.26
Idaho fescue-bluebunch wheatgrass grassland	41	1	0.00	0.18
Quaking aspen/Engelmann spruce forest	42	4	20.57	2.76
Arizona white-gray-Emory oak woodland	43	2	12.21	0.88

Scrub oak chaparral shrubland	44	2	0.22	3.38
Madrean pine-oak forest	45	4	9.12	1.79
Chamise chaparral shrubland	46	2	0.56	3.47
Redwood-tanoak forest	47	4	113.34	12.78
Douglas-fir-tanoak-madrone-bay forest	48	4	46.58	5.51
Creosote bush shrubland	49	2	0.07	0.28
Coastal sage shrubland	51	2	0.04	2.55
Douglas-fir-Pacific ponderosa pine/oceanspray forest	52	4	14.47	3.76
Pacific ponderosa pine forest	53	6	19.02	4.59
Douglas-fir-white fir-ponderosa pine forest	54	6	21.95	6.56
Western juniper/sagebrush savanna	55	2	0.91	0.52
Sagebrush shrubland	56	2	0.00	1.18
Wheatgrass-cheatgrass grassland	57	1	0.00	0.03
Western juniper/sagebrush savanna	58	2	0.63	0.07
Subalpine fir-Engelmann spruce-Douglas-fir-lodgepole pine forest	59	6	47.64	10.73
Sagebrush shrubland	60	2	0.00	0.29
Whitebark pine/subalpine fir forest	61	6	43.86	4.08
Huckleberry-heather shrublands	62	2	0.00	0.41
Showy sedge-alpine black sedge grassland	63	1	0.00	0.33
Tussock grass-oatgrass grassland	65	1	0.00	1.16
Bluebunch wheatgrass-bluegrass grassland	66	1	0.00	5.74
Interior ponderosa pine-Douglas-fir forest	67	6	33.23	6.20
Western juniper/sagebrush-bitterbrush shrubland	69	2	0.32	0.92
Subalpine fir-lodgepole pine-whitebark pine-Engelmann spruce forest	70	6	30.31	4.15

Ohia/Florida hopbush-kupaoa forest	71	4	8.40	1.55
Ohia/uluhe forest	72	4	18.13	2.70
Koa/pukiawe forest	73	4	18.45	1.92
Mamani-naio savanna	74	1	12.70	0.69
Slash pine/New Caledonia pine forest	75	6	20.04	12.76
Slash pine/molasses grass forest	76	6	13.46	13.36
Eucalyptus plantation forest	77	4	43.86	12.96
Florida hopbush-Mauna Loa beggarticks shrubland	78	2	0.94	1.99
Pili grass-broomsedge bluestem grassland	79	1	0.02	0.87
Fountain grass grassland	80	1	0.16	1.24
Pukiawe/Columbia bluestem grassland	81	1	0.04	1.30
White leadtree/Guinea grass shrubland	82	2	0.13	1.48
Molasses grass grassland	83	1	0.02	2.90
Ohia/Broomsedge bluestem savanna	84	1	0.51	2.52
Black spruce/lichen forest	85	6	2.54	12.53
Black spruce/feathermoss woodland	86	2	2.54	12.54
Black spruce/feathermoss forest	87	6	13.49	15.35
Black spruce/sphagnum moss forest	88	6	1.31	103.58
Black spruce/cottonsedge woodland	89	2	1.31	63.56
White oak-northern red oak forest	90	4	29.66	6.35
White spruce/prickly rose forest	91	6	8.48	11.87
Quaking aspen-paper birch-white spruce-black spruce forest	92	4	19.53	7.88
Paper birch-quaking aspen forest	93	4	20.79	9.77
Balsam poplar-quaking aspen forest	94	4	21.50	8.37
Willow-mountain alder shrubland	95	2	0.47	7.33

Cottongrass grassland	97	1	0.00	35.39
Marsh labrador tea-lingonberry tundra shrubland	98	2	0.00	2.93
Bluejoint reedgrass grassland	99	1	0.00	8.72
Altai fescue grassland	100	1	0.00	3.44
White spruce forest	101	6	16.09	11.77
White spruce forest	102	6	28.43	12.16
White spruce-paper birch forest	103	4	25.80	8.93
White spruce-paper birch forest	104	4	37.18	9.51
Paper birch-quaking aspen-white spruce forest	105	4	26.82	8.46
Red spruce-balsam fir forest	106	6	21.12	8.30
Pitch pine/scrub oak forest	107	4	37.52	8.78
Eastern white pine-northern red oak-red maple forest	109	4	17.70	4.40
American beech-yellow birch-sugar maple forest	110	4	31.50	4.14
Virginia pine-pitch pine-shortleaf pine forest	114	6	13.21	5.55
Rhododendron-blueberry-mountain laurel shrubland	115	2	0.76	13.58
Oak-pine/mountain laurel forest	120	4	25.71	8.04
Oak-pine/mountain laurel forest	121	4	28.03	8.64
White oak-northern red oak-black oak-hickory forest	123	4	36.46	7.06
Pitch pine-oak forest	124	4	6.32	5.59
Oak-hickory-pine-eastern hemlock forest	125	4	29.15	3.65
Green ash-American elm forest	129	4	22.77	0.91
Bluestem-Indian grass-switchgrass grassland	131	1	0.38	2.29
Tall fescue-foxtail-purple bluestem grassland	133	1	0.47	1.70
White oak-northern red oak-hickory forest	134	4	7.20	2.90

Eastern redcedar-oak/bluestem savanna	135	1	2.21	0.60
Red pine-eastern white pine forest	138	6	25.48	5.15
Jack pine/black spruce forest	140	6	7.14	4.91
Quaking aspen-paper birch forest	142	4	27.40	6.00
Quaking aspen-paper birch-white spruce-balsam fir forest	143	4	21.78	7.59
Jack pine forest	146	6	15.05	4.17
Jack pine savanna	147	2	2.61	1.31
Jack pine forest	148	6	14.84	1.78
Red pine-white pine forest	152	6	23.83	4.66
Bur oak savanna	154	2	13.20	1.94
Red spruce-balsam fir forest	155	6	21.02	10.73
Slash pine plantation forest	156	6	9.51	3.41
Loblolly-shortleaf pine-mixed hardwood forest	157	4	17.56	4.27
Loblolly-shortleaf pine-mixed hardwood forest	158	4	28.19	5.20
Loblolly-slash pine forest	161	6	14.46	3.67
Loblolly-slash pine forest	162	6	17.00	3.76
Sand pine forest	164	6	5.86	2.61
Longleaf pine/three-awned grass-pitcher plant savanna	165	2	1.73	0.94
Longleaf pine/three-awned grass-pitcher plant savanna	166	2	6.80	5.94
Gallberry-fetterbush shrubland	168	2	0.05	224.48
Pond pine/gallberry-fetterbush shrubland	170	2	0.97	51.97
Live oak/sea oats savanna	173	2	1.21	0.24
Live oak-sabal palm forest	174	4	33.38	3.49
Smooth cordgrass-black needlerush grassland	175	1	0.00	26.25
Smooth cordgrass-black needlerush grassland	176	1	0.00	69.26

Loblolly-shortleaf pine forest	178	6	12.32	4.39
Red maple-oak-hickory-sweetgum forest	180	4	26.55	6.44
Pond pine forest	181	6	15.14	14.39
Longleaf pine-slash pine/saw palmetto-gallberry forest	182	6	8.89	11.21
Loblolly-shortleaf pine forest	183	6	12.14	4.49
Longleaf pine/turkey oak forest	184	4	7.35	2.40
Longleaf pine/turkey oak forest	185	4	3.54	0.50
Turkey oak-bluejack oak forest	186	4	6.72	2.72
Longleaf pine/yaupon forest	187	6	7.21	3.41
Sand pine-oak forest	188	4	10.31	3.39
Sand pine-oak forest	189	4	12.21	5.37
Slash pine-longleaf pine/gallberry forest	190	6	9.75	6.96
Longleaf pine-slash pine/gallberry forest	191	6	8.92	2.66
Loblolly pine/bluestem forest	196	6	1.56	1.75
Sawgrass-Muhlenbergia grassland	203	1	0.00	1.70
Grand fir-Douglas-fir forest	208	6	65.64	5.94
Pinyon-Utah juniper woodland	210	2	9.67	0.58
Interior ponderosa pine forest	211	6	8.90	1.94
Pacific ponderosa pine forest	212	6	21.45	5.04
Wheatgrass-cheatgrass grassland	213	1	0.00	0.05
Giant sequoia-white fir-sugar pine forest	214	6	81.04	3.73
Douglas-fir-madrone/tanoak forest	215	4	42.69	0.65
Gambel oak-bigtooth maple forest	216	4	6.87	3.78
Gambel oak-bigtooth maple forest	217	4	5.50	2.35
Gambel oak/big sagebrush shrubland	218	2	0.89	1.46
Ponderosa pine-white fir/quaking aspen forest	219	4	25.46	6.21

Ponderosa pine-white fir/quaking aspen forest	220	4	34.80	2.08
Wheatgrass-ryegrass grassland	221	1	0.00	0.61
Interior ponderosa pine forest	222	6	8.92	0.87
Douglas-fir-white fir-interior ponderosa pine forest	223	6	34.22	0.65
Quaking aspen forest	224	4	15.07	3.33
Quaking aspen forest	225	4	12.74	0.73
White fir-gambel oak forest	226	4	20.59	5.55
White fir forest	227	6	19.51	4.74
Interior ponderosa pine-limber pine forest	228	6	9.27	2.08
Ponderosa pine/Utah juniper forest	229	6	14.65	0.55
Pinyon-Utah juniper forest	230	6	11.96	0.44
Gambel oak-Rocky Mountain juniper-ponderosa pine forest	231	4	11.41	1.96
Mesquite savanna	232	2	1.19	0.45
Sagebrush shrubland	233	2	0.00	0.81
Sagebrush shrubland	234	2	0.00	0.18
Idaho fescue-bluebunch wheatgrass grassland	235	1	0.00	0.47
Tobosa-grama grassland	236	1	0.00	0.04
Huckleberry-heather shrubland	237	2	0.00	1.34
Pacific silver fir-mountain hemlock forest	238	4	46.71	6.22
Douglas-fir-sugar pine-tanoak forest	239	4	66.67	2.19
Saw palmetto/three-awned grass shrubland	240	2	1.94	1.81
Longleaf-loblolly pine forest	241	6	21.54	2.90
Longleaf-loblolly pine forest	242	6	18.86	0.97
Pitch pine/scrub oak shrubland	243	2	9.72	2.11
Ohia/uluhe forest	260	4	2.70	2.63

Pili grass-broomsedge bluestem grassland	261	1	0.02	0.70
Molasses grass grassland	262	1	0.00	2.40
Ohia/broomsedge bluestem savanna	263	1	0.25	1.44
Post-blackjack oak forest	264	4	15.65	2.06
Balsam fir-white spruce-mixed hardwood forest	265	4	16.33	3.59
Sugar maple-basswood forest	266	4	27.27	3.46
American beech-yellow birch-sugar maple-red spruce forest	267	4	20.69	5.23
American beech-yellow birch-sugar maple-eastern hemlock forest	268	4	21.34	5.26
Sugar maple-yellow poplar-American beech-oak forest	269	4	16.58	6.81
Red spruce-Fraser fir/rhododendron forest	270	4	31.20	10.97
Mangrove forest	272	4	2.74	121.51
Engelmann spruce-Douglas-fir-white fir-ponderosa pine forest	273	6	46.58	4.11
American beech-sugar maple forest	274	4	28.46	3.53
Chestnut-white-northern red oak forest	275	4	25.18	5.17
Oak-pine-magnolia forest	276	4	37.77	3.11
Black spruce-northern white cedar-larch forest	279	6	14.99	79.02
Bluestem-Gulf cordgrass grassland	280	1	0.00	1.42
Shortleaf pine-post oak-black oak forest	281	4	11.13	3.99
Loblolly pine forest	282	6	21.68	6.45
Willow-laurel-water oak forest	283	4	18.88	1.18
Green ash-American elm-silver maple-cottonwood forest	284	4	39.37	0.68
Limber pine-ponderosa pine forest	286	6	24.15	3.57
Eastern white pine-eastern hemlock forest	287	6	19.90	3.27

Bald cypress-water tupelo forest	288	4	44.94	1.64
Pond cypress/Muhlenbergia-sawgrass savanna	289	1	0.37	8.39
Longleaf-slash pine/saw palmetto forest	291	6	8.87	6.10
Fremont cottonwood-California sycamore forest	301	4	9.88	1.09
Willow / sedge grassland	302	1	0.00	0.58
Cottonwood / willow savanna	303	2	8.82	1.16
Engelmann spruce-subalpine fir / horsetail forest	304	4	13.61	7.26
Red alder forest	305	4	7.62	4.35
Knobcone pine forest	306	6	28.45	3.57
Paloverde shrubland	307	2	0.00	0.16
Low sagebrush shrubland	308	2	0.02	0.81
Blackbrush shrubland	309	2	0.00	0.15
Greasewood shrubland	310	2	0.07	0.51
Saltbush shrubland	311	2	0.07	0.27
Gambel oak / sagebrush shrubland	312	2	5.02	0.85
Mountain mahogany shrubland	313	2	8.06	0.63
Limber pine-bristlecone pine forest	314	6	37.95	0.81
Showy sedge-Black alpine sedge grassland	315	1	0.00	0.78
Coyotebush-ceanothus shrubland	316	2	0.04	4.92
Bigtooth maple forest	317	4	3.33	1.41
Bluejoint reedgrass-water sedge grassland	318	1	0.00	0.87
Pacific silver fir-Sitka alder forest	319	4	3.56	0.52
Western larch forest	320	4	27.35	4.11
Western hemlock-Alaska cedar forest	321	6	22.89	10.95
Sitka spruce-western hemlock forest	322	6	42.58	14.04

Trembling aspen / sagebrush boreal woodland	323	2	0.35	0.86
White spruce woodland	324	2	6.58	24.43
White spruce-mountain hemlock forest	325	6	16.85	6.60
Willow- birch shrubland	326	2	0.27	2.32
Marsh Labrador tea / cottongrass grassland	327	1	0.00	31.81
Hemlock / sedge-cottongrass savanna	328	1	0.19	31.88
Mountain heath tundra shrubland	329	2	0.00	1.64
American dunegrass grassland	330	1	0.00	0.72
Sitka alder-salmonberry shrubland	331	2	0.27	5.76
Balsam poplar-paper birch forest	332	4	21.97	6.76
Dryas tundra shrubland	333	2	0.00	0.36
Mountain heather tundra shrubland	334	2	0.00	1.51
Sweetgale shrubland	335	2	0.00	17.88
Lyngbye's sedge-alkaligrass grassland	336	1	0.00	1.86
Softstem bulrush-needle spikerush grassland	337	1	0.00	3.47
Water sedge-tall cottongrass grassland	338	1	0.00	1.46
Nootka lupine-sedge grassland	339	1	0.00	1.14
Holly-privet shrubland	401	2	2.90	4.80
Pine / holly-privet forest	402	6	7.39	4.28
Post oak-blackjack oak-white oak forest	403	4	1.86	1.30
Yellow poplar-sugar maple-basswood forest	404	4	9.59	3.55
Northern red oak montane forest	405	4	1.84	2.09
American beech-southern magnolia-oak forest	406	4	29.57	3.04
Darlington oak forest	407	4	35.15	3.57
Quaking aspen-bur oak forest	408	4	5.60	0.94
Virginia pine-chestnut oak / little bluestem forest	409	4	0.40	0.73

Table Mountain pine-chestnut oak forest	410	4	2.37	3.84
Ashe juniper-oak savanna	411	2	2.04	0.57
Dwarf bilberry-bog blueberry shrubland	412	2	0.47	2.24
Pin oak / bluestem forest	413	4	4.32	1.29
Eastern redcedar / big bluestem savanna	414	2	1.82	0.59
Bluestem-forb grassland	415	1	0.03	0.68
Chinkapin oak-eastern redcedar / bluestem savanna	416	2	0.47	0.97
Little bluestem-blackseed speargrass grassland	417	1	0.04	0.51
White spruce / juniper / little bluestem savanna	418	2	0.30	0.98
Blackjack oak-post oak / bluestem savanna	419	2	2.50	0.63
Big bluestem-bluejoint grassland	420	1	0.00	2.37
Chinkapin oak-bur oak / giant cane forest	421	4	3.80	1.04
Post oak-shortleaf pine / bluestem-Indiangrass savanna	422	2	0.13	3.02
Oak / bluestem-Indiangrass savanna	423	2	0.24	3.01
Pondcypress / dahoon holly / sedge forest	424	4	27.47	6.23
Swamp tupelo-sweetbay magnolia forest	425	4	24.41	5.02
Sugarberry / acacia forest	426	4	3.19	0.31
Red spruce-northern white cedar-tamarack forest	427	4	12.93	10.87
Melaleuca forest	428	4	34.93	4.87
Black locust forest	429	4	11.25	2.89
White oak-southern red oak forest	430	4	32.91	3.29
Chinkapin oak-Shumard oak forest	431	4	2.99	3.69
Florida poisontree-West Indian mahogany forest	432	4	4.87	3.99
Pine-oak / American beachgrass savanna	433	2	0.69	0.67

Post oak-southern red oak / little bluestem-Indiangrass forest	434	4	4.09	1.69
Little bluestem-buffalograss grassland	435	1	0.00	0.69
Shore little bluestem-paspalum grassland	436	1	0.00	0.57
Saltmeadow cordgrass-switchgrass grassland	437	1	0.00	0.56
Pondcypress / pond apple forest	438	4	25.36	16.69
Pondcypress / swamp titi / maidencane savanna	439	2	1.30	1.04
Pondcypress-cabbage palm-strangler fig forest	440	4	67.82	5.13
Red maple-black ash / common winterberry forest	441	4	17.74	5.72
Bulrush grassland	442	1	0.00	3.35
Prairie cordgrass-bluejoint grassland	443	1	0.00	3.80
Woollyfruit sedge-yellow sedge grassland	445	1	0.00	9.78
Bald cypress-tupelo / swamp titi forest	448	4	47.64	5.58
Pin oak-white oak / buttonbush forest	449	4	32.00	4.39
Oak-Ashe juniper forest	450	4	2.37	1.89
Texas live oak / roughleaf dogwood forest	451	4	2.63	1.92
Bluestem-tall fescue-switchgrass grassland	453	1	0.16	1.40
American beech-maple / American red raspberry forest	454	4	18.14	3.99
Red pine forest	455	6	23.39	3.09
Chinese tallow tree forest	456	4	74.11	3.48
Florida strangler fig-gumbo limbo-cabbage palm forest	457	4	28.89	11.09
Berlandier's fiddlewood-Texas ebony shrubland	458	2	0.00	2.59
Inland and coastal water	900	Falls back to MODIS LCT*		

* Record with FCCS Code 0 (any non-natural vegetation surface) and 900 (water) uses MODIS LCT land cover to estimate emission

A.5 FCCS_CDL mappings and fuel loadings

FCCS_CDL Class Description	FCCS_CDL Class	FINN Class	Tree Loadings	Herb Loadings
	0-458, 900	Common with FCCS*		
Corn	1201	13	0.00	1.62
Cotton	1202	11	0.00	0.38
Rice	1203	8	0.00	0.67
Soybeans	1205	12	0.00	0.56
Wheat	1223	10	0.00	0.66
Other Small Grains	1225	9	0.00	0.66
Sugarbeets	1241	9	0.00	0.66
Beans	1242	9	0.00	0.66
Potatoes	1243	9	0.00	0.66
Other Crops	1244	9	0.00	0.66
Sugarcane	1245	15	0.00	1.50
Misc. Vegs. & Fruits	1247	9	0.00	0.66
Lentils	1252	9	0.00	0.66
Biofuels	1260	1	0.00	0.66
Fallow	1261	1	0.00	0.69
Pasture/Grass	1262	1	0.00	0.69
Other Tree Nuts	1271	4	0.00	0.69
Other Tree Fruits	1273	4	0.00	0.69
Bluegrass/Grass Seed	1280	1	0.00	0.69
Pasture/Hay/Alfalfa	1281	1	0.00	0.69
Dbl. Crop Win Wht/Corn	1290	10	0.00	1.62
Dbl. Crop Wheat/Soy	1291	10	0.00	0.66
Dbl. Crop Other Grain/Corn	1292	9	0.00	0.66

Dbl. Crop Lettuce/Durum Wheat	1293	9	0.00	0.66
Dbl. Crop Wht/Sorghum	1295	10	0.00	0.66
Dbl. Crop Wheat/Cotton	1296	10	0.00	0.66
Dbl. Crop Corn/Soybeans	1299	13	0.00	0.66
Dbl. Crop Barley/Soybeans	1300	0	0.00	0.00

* Code <= 900 are identical to FCCS scenario. Note also the special treatment of codes 0 and 900 by FCCS scenario.

A.6 TCEQ mapping and loadings

TCEQ Class Descriptions	TCEQ Code	FINN Code	Tree Loadings	Herb Loadings
Open Water	1	VCF Dependent*		
Developed Open Space	2	VCF Dependent*		
Developed Low Intensity	3	VCF Dependent *		
Developed Medium Intensity	4	VCF Dependent *		
Developed High Intensity	5	VCF Dependent *		
Barren Land (Rock/Sand/Clay/Unconsolidated Shore)	6	VCF Dependent *		
Herbaceous Natural	7	1	3.09	1.25
Herbaceous Cultivated	8	9	2.29	1.02
Riparian Forested Wetland	9	4	14.17	1.78
Swamp Forested Wetland	10	4	26.05	3.00
Shrub Wetland	11	2	0.23	8.83
Herbaceous Emergent Wetland	12	1	1.55	17.01
Cold-Deciduous Forest	13	4	15.77	3.40
Broad-Leafed Evergreen Forest	14	4	9.90	1.74
Needle-Leafed Evergreen Forest	15	6	14.61	3.09
Mixed Forest	16	4	12.47	3.06
Cultivated Woody Vegetation	17	4	1.20	0.53
Cold-Deciduous Woodland	18	4	8.74	2.12
Broad-Leafed Evergreen Woodland	19	4	2.23	0.69
Needle-Leafed Evergreen Woodland	20	6	13.11	2.90
Mixed Woodland	21	4	7.22	1.95
Cold-Deciduous Shrub	22	2	1.73	0.70
Broad-Leafed Evergreen Shrub	23	2	1.05	0.38
Needle-Leafed Evergreen Shrub	24	2	2.75	0.97

Mixed Shrub	25	2	1.45	0.59
Desert Shrub	26	2	0.62	0.39
Western Shrub Wetland	28	2	4.62	0.90
Western Cold-Deciduous Forest	29	4	22.32	2.93
Western Broad-Leafed Evergreen Forest	30	4	1.17	0.43
Western Needle-Leafed Evergreen Forest	31	6	13.73	1.79
Western Mixed Forest	32	4	17.44	2.19
Western Cold-Deciduous Woodland	33	4	11.49	1.86
Western Broad-Leafed Evergreen Woodland	34	4	1.40	0.43
Western Needle-Leafed Evergreen Woodland	35	6	9.19	1.23
Western Mixed Woodland	36	4	9.68	1.19

* Water, developed and barren categories is changed to other categories based on VCF: herbaceous natural (code 7, if Tree < 40%), mixed shrub (code 25, if 40% <= Tree < 60%) or mixed forest (code 16, if Tree >= 60%)

A.7 TCEQ_CDL mappings and fuel loadings

TCEQ_CDL Class Descriptions	TCEQ_CDL Code	FINN Code	Tree Loadings	Herb Loadings
Corn	1	13	0.00	1.62
Cotton	2	11	0.00	0.38
Rice	3	8	0.00	0.67
Sorghum	4	14	0.00	0.66
Soybeans	5	12	0.00	0.56
Sunflower	6	9	0.00	0.66
Peanuts	10	9	0.00	0.66
Tobacco	11	9	0.00	0.66
Sweet Corn	12	13	0.00	1.62
Pop or Orn Corn	13	13	0.00	1.62

Barley	21	9	0.00	0.66
Durum Wheat	22	10	0.00	0.66
Spring Wheat	23	10	0.00	0.66
Winter Wheat	24	10	0.00	0.66
Dbl Crop WinWht/Soybeans	26	10	0.00	0.66
Rye	27	9	0.00	0.66
Oats	28	9	0.00	0.66
Millet	29	9	0.00	0.66
Canola	31	9	0.00	0.66
Safflower	33	9	0.00	0.66
Alfalfa	36	1	0.00	0.66
Other Hay/Non Alfalfa	37	1	0.00	0.66
Dry Beans	42	9	0.00	0.66
Potatoes	43	9	0.00	0.66
Other Crops	44	9	0.00	0.66
Sugarcane	45	15	0.00	1.50
Sweet Potatoes	46	9	0.00	0.66
Watermelons	48	9	0.00	0.66
Onions	49	9	0.00	0.66
Cucumbers	50	9	0.00	0.66
Peas	53	9	0.00	0.66
Tomatoes	54	9	0.00	0.66
Herbs	57	9	0.00	0.66
Clover/Wildflowers	58	1	0.00	0.66
Sod/Grass Seed	59	1	0.00	0.66
Switchgrass	60	1	0.00	0.66
Fallow/Idle Cropland	61	1	0.00	0.66

Cherries	66	9	0.00	0.66
Peaches	67	9	0.00	0.66
Apples	68	9	0.00	0.66
Grapes	69	9	0.00	0.66
Christmas Trees	70	6	0.00	0.66
Citrus	72	4	0.00	0.66
Pecans	74	4	0.00	0.66
Walnuts	76	4	0.00	0.66
Aquaculture	92	VCF Depended*		
Open Water	101	VCF Depended*		
Developed Open Space	102	VCF Depended*		
Developed Low Intensity	103	VCF Depended*		
Developed Medium Intensity	104	VCF Depended*		
Developed High Intensity	105	VCF Depended*		
Barren Land (Rock/Sand/Clay/Unconsolidated Shore)	106	VCF Depended*		
Herbaceous Natural	107	1	3.20	1.26
Herbaceous Cultivated	108	9	0.90	0.86
Riparian Forested Wetland	109	4	14.12	1.78
Swamp Forested Wetland	110	4	25.99	3.00
Shrub Wetland	111	2	0.23	8.83
Herbaceous Emergent Wetland	112	1	1.55	17.26
Cold-Deciduous Forest	113	4	15.73	3.39
Broad-Leafed Evergreen Forest	114	4	9.94	1.75
Needle-Leafed Evergreen Forest	115	6	14.58	3.09
Mixed Forest	116	4	12.52	3.07
Cultivated Woody Vegetation	117	4	1.20	0.53

Cold-Deciduous Woodland	118	4	8.81	2.14
Broad-Leafed Evergreen Woodland	119	4	2.24	0.70
Needle-Leafed Evergreen Woodland	120	6	13.02	2.89
Mixed Woodland	121	4	7.33	1.98
Cold-Deciduous Shrub	122	2	1.75	0.70
Broad-Leafed Evergreen Shrub	123	2	1.05	0.38
Needle-Leafed Evergreen Shrub	124	2	2.75	0.97
Mixed Shrub	125	2	1.45	0.58
Desert Shrub	126	2	0.62	0.39
Western Shrub Wetland	128	2	4.65	0.90
Western Cold-Deciduous Forest	129	4	22.42	2.93
Western Broad-Leafed Evergreen Forest	130	4	1.17	0.43
Western Needle-Leafed Evergreen Forest	131	6	13.73	1.79
Western Mixed Forest	132	4	17.43	2.19
Western Cold-Deciduous Woodland	133	4	11.53	1.87
Western Broad-Leafed Evergreen Woodland	134	4	1.40	0.43
Western Needle-Leafed Evergreen Woodland	135	6	9.19	1.23
Western Mixed Woodland	136	4	9.68	1.19
Open Water	156	VCF Depended*		
Developed/Open Space	161	VCF Depended*		
Developed/Low Intensity	162	VCF Depended*		
Developed/Med Intensity	163	VCF Depended*		
Developed/High Intensity	164	VCF Depended*		
Barren	166	VCF Depended*		
Deciduous Forest	171	4	12.10	2.88

Evergreen Forest	172	6	10.61	2.26
Mixed Forest	173	4	10.61	2.09
Shrubland	177	2	3.22	1.14
Grassland/Pasture	186	1	4.25	1.42
Woody Wetlands	196	4	5.43	0.94
Herbaceous Wetlands	197	1	3.31	3.22
Pistachios	204	4	0.00	0.66
Triticale	205	9	0.00	0.66
Carrots	206	9	0.00	0.66
Cantaloupes	209	9	0.00	0.66
Olives	211	4	0.00	0.66
Oranges	212	4	0.00	0.66
Peppers	216	9	0.00	0.66
Greens	219	9	0.00	0.66
Squash	222	9	0.00	0.66
Vetch	224	9	0.00	0.66
Dbl Crop WinWht/Corn	225	10	0.00	1.62
Dbl Crop Oats/Corn	226	9	0.00	1.62
Lettuce	227	9	0.00	0.66
Pumpkins	229	9	0.00	0.66
Dbl Crop Lettuce/Cotton	232	9	0.00	0.66
Dbl Crop Barley/Sorghum	235	9	0.00	0.66
Dbl Crop WinWht/Sorghum	236	10	0.00	0.66
Dbl Crop Barley/Corn	237	9	0.00	0.66
Dbl Crop WinWht/Cotton	238	10	0.00	0.66
Dbl Crop Soybeans/Cotton	239	12	0.00	0.66
Dbl Crop Soybeans/Oats	240	12	0.00	0.66

Dbl Crop Corn/Soybeans	241	13	0.00	0.66
Blueberries	242	9	0.00	0.66
Cabbage	243	9	0.00	0.66
Turnips	247	9	0.00	0.66
Dbl Crop Barley/Soybeans	254	9	0.00	0.66

* Water, developed and barren categories is changed to other categories based on VCF: herbaceous natural (code 107, if Tree < 40%), mixed shrub (code 125, if 40% <= Tree < 60%) or mixed forest (code 116, if Tree >= 60%)